A Study of Stress Grading System of Medium Voltage Motor Fed by Adjustable Speed Drives

by

Alireza Naeini

A thesis
presented to the University of Waterloo
in fulfillment of the
thesis requirement for the degree of
Doctor of Philosophy
in
Electrical and Computer Engineering

Waterloo, Ontario, Canada, 2019

Examining Committee Membership

The following served on the Examining Committee for this thesis. The decision of the Examining Committee is by majority vote.

External Examiner   Gian Carlo Montanari
Professor

Supervisors   Shesha Jayaram
Professor
Edward A. Cherney
Adjunct Professor

Internal Members   Siva Sivoththaman
Professor
Omar Ramahi
Professor

Internal-external Member   Roydon Fraser
Professor

AUTHOR'S DECLARATION

I hereby declare that I am the sole author of this thesis. This is a true copy of the thesis, including any required final revisions, as accepted by my examiners.

I understand that my thesis may be made electronically available to the public.

Abstract

The demand for medium voltage (MV) induction motors with an adjustable speed drive (ASD) has grown significantly over the past decade for many industrial applications. This is mainly because the applications of adjustable speed drives have clear advantages of enhanced efficiency of using electric power and precise control of the speed of industrial processes. However, the high frequency components of the output voltages of an ASD produce complex transients that stress the motor insulation. The fast rise time of repetitive impulse voltage creates additional electrical and thermal stresses on the motor's insulation system. In addition, the overshoot voltage at the edge of the pulses, due to the impedance mismatch between the motor and the cable, increases the risk of insulation breakdown. The performance of the stress grading system under these fast-pulsed voltages is a critical issue for MV motors. The high electric field in the stress grading system and temperature rise due to Joule heat are the most important problems of a conventional form-wound coil stressed by an adjustable speed drive. Any local high electric field produces surface partial discharges (PD) on the stress grading system that may lead to immature insulation failure. Limiting the temperature rise and controlling the local electric field to avoid surface discharges and hot spots using an appropriate stress grading system is essential to prolong the life of MV motors.

The conductive armor tape (CAT) and stress grading tape (SGT) are the two main components of the stress grading system of a form wound motor coil. The material properties and builds of the CAT and SGT applied to the conventional form-wound coils have been designed for power frequency voltages. However, it is less effective under pulsed width modulation (PWM) voltage that are typical from ASDs, because they have high frequency components that lead to elevated electrical and thermal stresses and thus faster ageing. The distribution of voltage and electric field along the coil in the overhang region are changed by the material properties; therefore, the enhanced electric field in the CAT or the SGT may lead to PD and hot spots in these regions.

In this study, comprehensive electro-thermal coupled finite element method (FEM) using COMSOL® 5.3a has been developed in order to simulate the stress grading system with nonlinear field dependent materials. The actual dimensions of a 13.8 kV bar sample were applied in the simulation model along with the appropriate material parameters extracted from the experimental test results. The temperature rise associated with a one cycle of pulsed voltage is very small. However, a prolonged transient coupled electro-thermal FEM simulation, for example for one-hour, is impractical due to very long computation

time. The simulation was run for three cycles and the heat source was calculated. Then the average heat source of domains during these cycles was calculated by another time transient ordinary derivative equation (ODE) interface. This average was used in a stationary study of heat transfer to obtain the temperature profile at steady state. To validate the simulation results, the temperature profile along the stress grading system were measured and simulated under pulsed voltage (2.5 kHz, 11.3 kV peak pulsed voltage) which shows good agreement between the simulation and the measurement studies.

The electrical conductivity of CAT and SGT, which differs significantly by vacuum pressure impregnation (VPI), is the most important parameter affecting the voltage distribution, and it can change the temperature profile and the regions of hot spots along the stress grading system. This can also can be changed by temperature and tape builds. Therefore, the electrical conductivity of the tapes used was measured after VPI and under conditions of operation. The SGT works under high electric field, so, the conductivity of this tape must be measured under a high electrical field. However, it is impossible to measure the conductivity with DC voltage above 0.6 kV/mm, because of the excessive heat and temperature rise in the SGT material during the measurement. To reach higher electric fields, the measurement was carried out under pulse conditions. The conductivity of a one half-lap layer and a double half-lap layer of CAT and SGT at various temperatures was measured. Based on simulation and measurement results, this study presents the effect of conductivity of stress grading materials on the temperature profile and the electric field distribution along end winding region. One way of increasing the electrical conductivity of the tapes is to increase the number of layers of the tape. Therefore, simulation studies on various stress grading system builds on the electrical and thermal performances of the stress grading systems was done in this study.

Reducing the maximum surface electric field is essential for prolonging insulation life. Simulations on the effect of floating metal foils, applied to the stress grading tape, on the electric field and temperature distribution, was studied in this work, under repetitive impulse voltages. Additionally, the evaluation of the thermal and electrical characteristics of the stress grading system under a reduced length of CAT from the slot exit was carried out. The temperature profile of the stress grading system under pulsed voltage at room and at elevated room and near typical operating temperatures are measured and simulated for several CAT lengths. The partial discharge inception voltage was also measured for different CAT lengths. A lower temperature rise is desirable, as this leads to a longer life, in the absence of partial discharges.

The nonlinearity of SGT has an effect on the electric field distribution. Simulation studies on the effect of various SGT nonlinearities on the electrical and thermal performance of a stress grading system was evaluated in this study. The effect of using a stress grading system based on a micro-varistor characteristic on both temperature and electric field was also investigated. An optimization on the initial conductivity of the micro-varistor characteristic confirms that desired electric field and temperature rise are achievable by selecting an optimum conductivity. The effect of a proposed stress grading system, which is a combination of an optimized SGT conductivity and minimum CAT length, on the temperature and electrical performance under repetitive impulse voltage is evaluated. Finally, to practically evaluate the effect of micro-varistor type of stress grading system, the electrical and thermal performance of a cable termination based on a micro-varistor characteristic were evaluated by measurement and simulation.

Acknowledgements

I would like to thank my supervisors, Professor Shesha Jayaram and Professor Edward Cherney for their assistance, support, and guidance throughout this work. I also wish to express my appreciation to my PhD Committee (Prof. Roydon Fraser, Prof. Gian Carlo Montanari, Prof. Omar Ramahi, and Prof. Siva Sivoththaman), who have honored me by being on the committee of my final examination.

My special thanks go to Dr. Saeed Ul-Haq from General Electric Peterborough and all the laboratory engineers for their great support during this work.

My special thanks go to my colleagues and friends Mahdi, Mohana, Saleh, Amin, Anurag, Arathi, Satish, Khadijeh, Marcelo and Ibrahim, who all were there for me during my ups and downs. My thanks go to my all dear friends who have enriched my life.

My deepest gratitude goes to all the members of my family, for the wonderful support they all provided, especially my wife; my parents who are the reason I am here; my sisters; and my darling son.

The financial support provided by NSERC of Canada is also greatly appreciated.

I would like to thank Ms. Mary McPherson for proofreading this thesis.

Dedication

To my father,

who is always in my heart. May the blessing of God be upon him and may he rest in peace.

To my dear wife, my delightful son, and my mother.

Table of Contents

List of Figures

xiii

xvi

xviii

List of Tables

Chapter 1

Introduction

1.1 Introduction

Meeting today's energy demand is one of the most important issues in the world, so it is essential to enhance power-consumption efficiency. Since AC motors were invented, a vast range of electrical machines have been used in all aspects of modern life. Single-phase motors are used to produce mechanical power of less than about 1 kW, and three-phase motors from 1 kW to up to thousands of MW [1]. Using motor drives to control AC motors is one successful solution for improving efficiency. Thus, they are used in a wide range of power output, and in applications ranging from precise position-controlled drives in robotics to variable speed drives for industrial applications. An induction motor with an adjustable speed drive (ASD) results in a high-efficiency system and flexible control of processes and machinery, and can cover numerous types of applications. Therefore, the application of this combination has increased rapidly. A block diagram of an induction motor fed by an adjustable speed drive is shown in Figure 1-1.
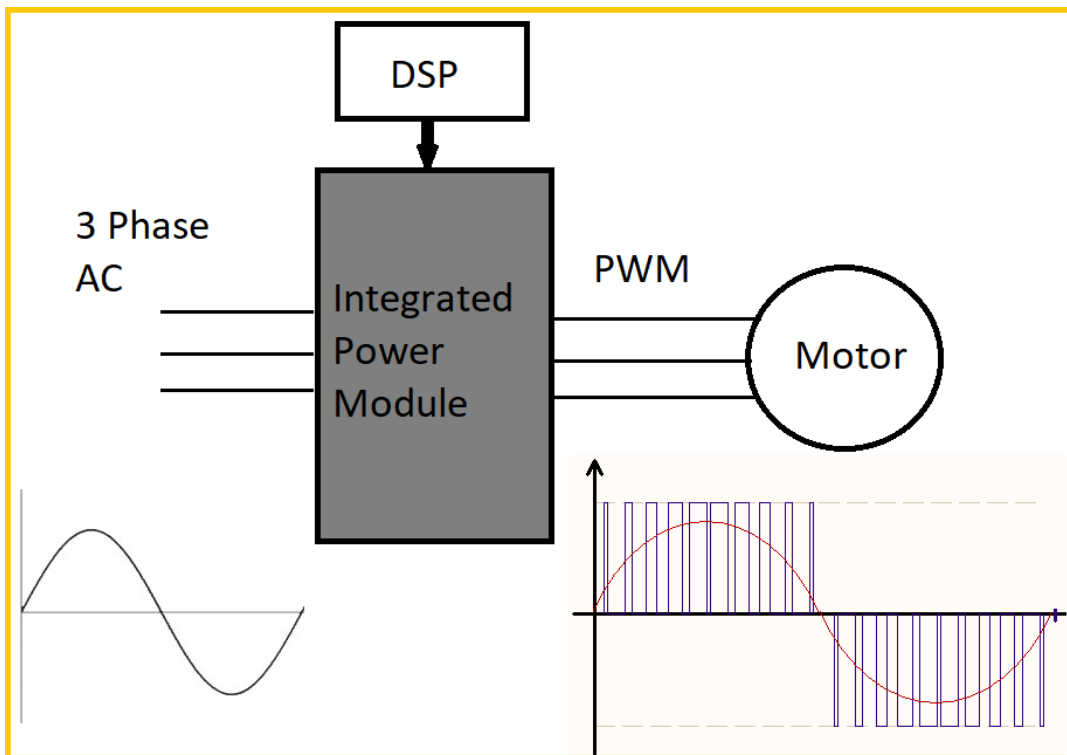
Figure 1-1: Block diagram of an induction motor fed by an adjustable speed drive.

Over the past ten years, the demand for ASDs has been growing, especially at medium voltage applied to many industries [2]. This trend has brought attention to a challenge in the insulation systems of motors, caused by the presence of repetitive pulses in the output voltage of ASDs. The immediate output of inverters is a pulsed voltage or current, and the objective of the controller is to control the fundamental component of the output voltage or current.

Conventional insulation systems work efficiently under power frequency voltage, and are expected to withstand partial discharges (PDs) and hot spots during their anticipated life. However, in recent years, early insulation failures have been reported for MV motors fed by ASDs, indicating that the insulation system is less effective under pulsed width modulation (PWM) voltage systems, as a result of their high frequency components that lead to elevated electrical and thermal stresses and thus faster ageing. PWM voltages produce extra stresses on insulation systems, leading to enhanced dielectric heating and PD, both of which degrade insulation systems. The life of polymeric electrical insulation is known to be highly influenced by temperature [3]. Moreover, the repetition frequency and the fast rise time of the PWM pulses create additional losses and dielectric heating in an insulation system, affecting its lifetime.

The fast rise time, repetition frequency, and voltage overshoot of PWM pulses are the most-important parameters influencing insulation systems [4]. The distribution of the voltage and electric field along the coil in overhang regions is changed by these pulse parameters, leading to an elevated electric field and thus hot spots in these regions. In addition, a fast rise time produces space charge, which increases the electric field, leading to temperature rise, especially at the slot exit, and producing hot spots there [4]. The higher the switching frequency, the higher the insulation stress. The number of pulses per second is increased by increasing the switching frequency, thus enhancing temperature rise. Voltage overshoots can produce an elevated electric field that can be greater than the threshold electric field and causes partial discharges. Stress grading system is among the most important aspects of the insulation systems of form wound medium voltage (MV) motor coils that has to withstand for these types of stresses from PWM voltages.

The thermal life expectancy for an insulation system operating at its continuous temperature rating is approximately 20,000 to 25,000 h under ideal environmental conditions [1]. Based on the Arrhenius equation for calculating chemical reaction time as a function of temperature, the thermal life expectancy of insulation systems is reduced by one half when the operating temperature is raised by 10 °C [1].

Thus, any elevated electric field and temperature rise lead to hot spots in insulation systems and can reduce the system's thermal life.

Multilevel (ML) drivers have output-voltage waveforms with a better harmonic spectrum, and limit the conventional insulation stress because of the lower jump voltages. However, increasing the number of levels leads to add more number of components, such as steering diodes, flying capacitors, power devices and isolated power supplies, which tends to reduce the overall reliability and efficiency of the power converter. In addition, multi-level designs have to use different circuits, different stack design and different PWM control at different converter voltages. On the other hand, an inverter with a low number of output levels would need a large and expensive LC output filter to reduce the conventional insulation stress [5–9]. Thus, the challenge is to reduce the level of drivers without using the large LC filters, to reduce the cost and weight of drivers, and to ensure high insulation system quality and life time. Such goals will be achieved by using a proposed stress grading system, as described in this thesis.

In response to these challenges, the main objective of this thesis is to optimize the builds of stress grading systems and the properties of their materials in order to minimize the effects of field enhancement, partial discharges, and consequently heat production. The following sections first explain form wound coils insulation and the stress grading systems in medium voltage (MV) motors, and then review the specifications and conduction mechanism of common stress grading materials. In addition, the effectiveness of stress grading systems under PWM voltages and methods of modelling are discussed, followed by a comprehensive literature review.

1.2 Form Wound Coil Insulation Systems

MV induction motors used in heavy-industry applications such as pumps, compressors, mixers, grinders, crushers and cranes have a rated voltage from just above 700 volts up to 13,800 volts. The windings of MV motors are made from insulated form wound coils that are preformed outside the stator and then inserted into the slots of the motor stator. Form wound coils consist of rectangular wires or strands formed into a number of turns that must be insulated from each other (turn insulation) with additional insulation (main wall insulation) applied over the coil loops. There are two types (Type I and Type II) for insulation systems of motors. The insulation on motors rated less than 700 volts are randomly wound in the slots of the stator is referred to as Type I as defined by IEC 60034-18-42 [10]. This standard also describes Type II insulation systems used in the stators of motors rated 700 V and above. This type of insulation system experiences PD during operation, and its life is limited by PD

3

and elevated temperatures. The standard addresses the requirements of insulation systems to withstand inverter pulses, which are characterized by elevated voltage, fast rise times, and high frequency.

Type II insulation systems consist of the following components: strand insulation, turn-turn insulation and main wall insulation. For motors rated higher than 6 kV in power frequency voltages and 4 kV for motors fed by ASDs, a stress grading system is also used to prevent any PDs and hot spots in the insulation systems [1]. Figure 1-2 shows the configuration of form wound coils with Type II insulation for MV motors.
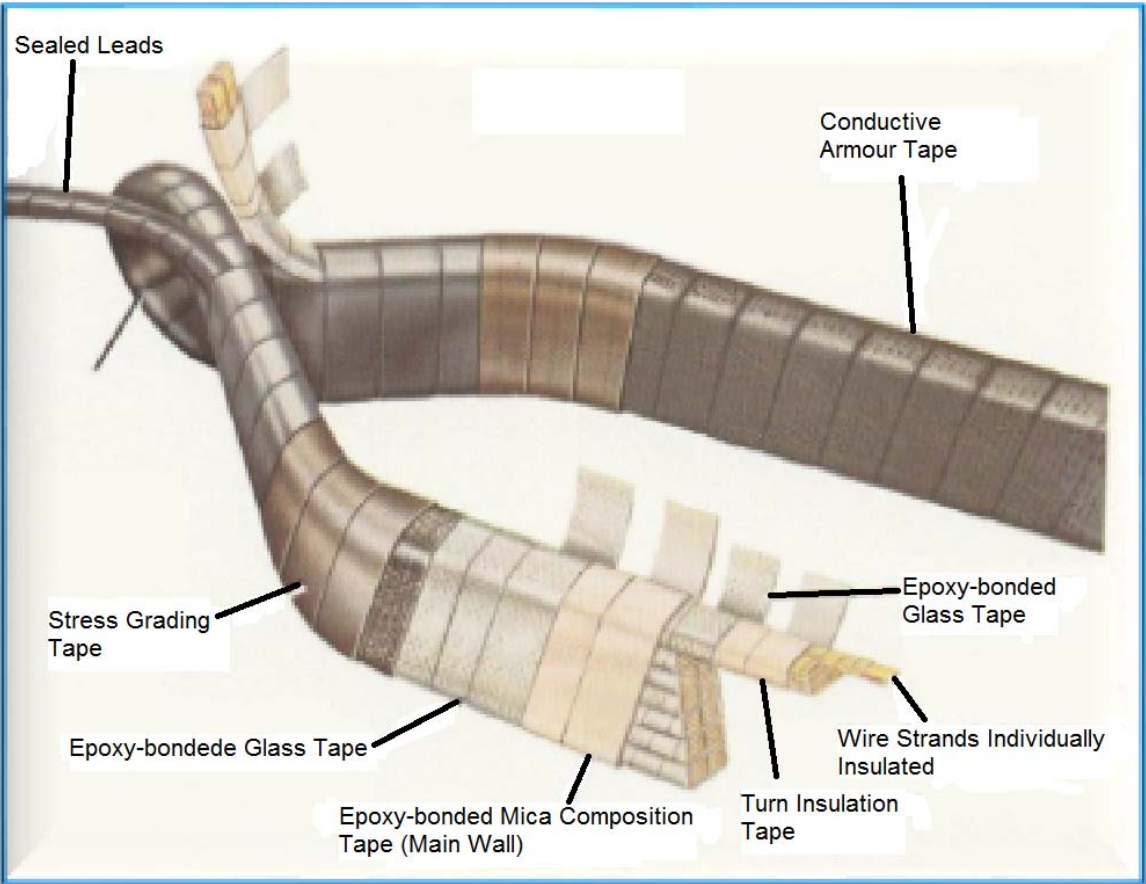
Figure 1-2: Configuration of a form wound coil with Type II insulation of MV motors.

Individually insulated strands or magnet wires are used to reduce the eddy current and skin effects in form wound coils. The strand insulation is applied through machine taping of individual strands with a thin mica flake tape. To protect against PD, turn insulation systems are made of corona-resistant enamel tapes that consist of magnet wires coated with enamel or polymer film containing additives

such as alumina or special materials with resistance to discharges [3]. This type of corona-resistant enamel is more important for motors fed by ASDs [11].

Main wall insulation is the most important part of the insulation systems that separates the copper conductors from the stator core. Main wall insulation failure usually leads to ground faults that activate ground fault relays, taking the motor offline [1]. This system is subjected to extreme electrical, thermal, and mechanical stresses during operation; therefore, reliable system designs are critical [4]. Electrical solid insulation systems are classified into five common thermal classes: Class A (105 ^{o}C); Class B (130 ^{o}C); Class F (155 ^{o}C); Class H (180 ^{o}C); and class N (200 ^{o}C) [1]. Class F insulation systems, commonly used for form wound coils, consist of small mica flakes deposited onto a glass fibre backing tape. After the tape is wrapped around the conductors, the synthetic resin is cured at an elevated temperature and pressure. Vacuum pressure impregnation (VPI), which provides void free impregnation, is done on either individual coils or the entire stator (global VPI) [12]. The global VPI process has a significant advantage, as it locks the coils in the stator slot and fills the felt blocking materials and ropes [11].

1.3 Stress Grading Systems

Stress grading systems, among the most important parts of the insulation systems of MV motor winding, are used to prevent partial discharge (PD) in the air gaps between the surfaces of coils, and also in the end winding region [12-15]. In these regions, the electric field is increased more than the critical electric field, leading to PDs. PD can deteriorate the insulation system, causing eventual motor failure. In addition, it produces ozone, which is harmful for insulation and also for the metal parts of motors. A stress grading system consists of two main parts: conductive armor tape (CAT) and stress grading tape (SGT). CAT is used to prevent slot discharges and is commonly made of carbon black embedded in a fiber-glass tape. The conductivity of CAT is one of the most important parameters affecting electric field distribution, and it can change temperature profiles and hot spot regions. It not only changes the voltage distribution in the CAT, but also affects the peak voltage on SGT [15, 16]. The electrical and thermal conductivities of the CAT and SGT control the electric field, joule heat production, and temperature profile in stress grading systems [16].

SGT prevents the occurrence of PD at the end of CAT. Its conductivity, which depends on the electric field, is increased by high electric fields and is high at the end of CAT, where the electric field is very high, and gradually decreases along the SGT [17, 18]. Therefore, it makes the electric field at

the end of the CAT more uniform. SGT is normally made of a composite that includes silicon carbide powder, which exhibits electric field dependent conductivity. The conductivity is enhanced by increasing the particle size of the powders as fewer grain-to-grain contacts are needed, and because the cross-voltage contact is increased [19, 20]. This conductivity differs significantly with various tape builds and after VPI [21, 22]. SGT conductivity can also change with time, thus increasing the stress at the end of CAT, resulting in PD [22]. Figures 1-2 and 1-3 show the stress grading system in the overhang region of a motor.
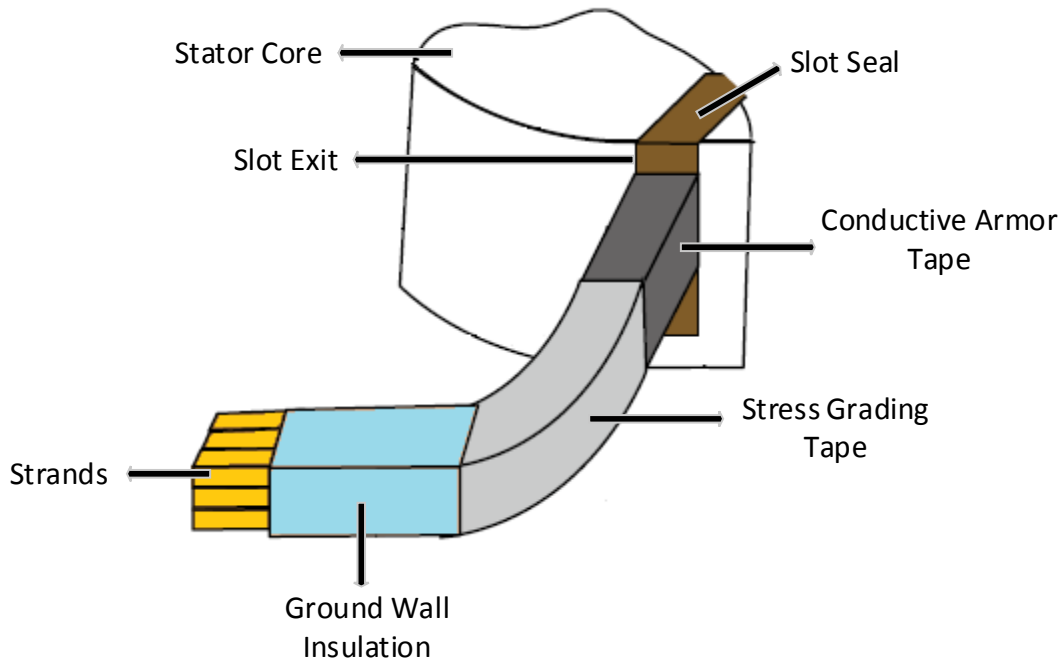
Figure 1-3: Schematic diagram of the stress grading system in the overhang section of a MV motor.

The functionality of the stress grading system of MV motor coils in the overhang region is important to the insulation's life because of the high electrical stress and the close proximity of other coils [23]. Conventional stress grading systems work efficiently under power frequency voltage but are less effective under PWM voltage systems, because the high frequency components lead to elevated electrical and thermal stresses. Fast rise times, high repetition rates and voltage overshoots of PWM pulses are the three main parameters affecting the electric field and temperature profiles of stress grading systems [24]. The high frequency components of the output voltages of ASD produce complex transients that stress motor insulation. The overshoot voltage at the edge of the pulse, due to the impedance mismatch between motor and cable, increases the risk of insulation breakdown [25]. An important problem

of MV motors is the performance of the stress grading system under these fast-pulsed voltages [26]. Temperature rise due to joule heat is a problem caused by a high electric field in the stress grading system of a conventional form-wound coil stressed by an ASD.

1.4 PWM Waveform Stresses on Stress Grading System

Most electrical energy produced in industrialized countries is utilized to feed induction motors in a wide range of applications. The capability of controlling the speed and torque of these motors is one of the most important aspects of their use, and use of ASDs helps to achieve these purposes. Nowadays, solid-state switches, in the advanced form of ASDs, are increasingly used in different industrial processes or domestic appliances. A voltage-source converter (VSC) is the most commonly used type of switch-mode converter [27-29]. When the length of the cable connecting AC terminals to the load is very long, for example in submerged pump applications, pulsed voltages act as travelling waves. Due to impedance mismatch, the reflected waves at the interface between the cable and the motor terminal create an overshoot. The result is voltages of a magnitude a few times larger than the terminal voltage, requiring motors with improved insulation strength to withstand large and steep-front voltages.

The drawback of a driver is that the high frequency components of the voltage lead to overvoltage and accelerate aging [26]. The overshoot voltage at the edge of the pulse due to the impedance mismatch between motor and cable increases the risk of insulation breakdown, and fast rise time pulses enhance this overshoot. Stress grading system effectiveness is reduced by increased frequency, and so the crucial problem of large MV motors is the performance of their stress grading systems.

A current-source converter (CSC) is another type of switch-mode converter. CSCs are mainly used in active power filters and high-power AC motor drives with a long cable connecting the converter to the motor, for example, converters driving submerged AC motors with pump loads [27-29]. The immediate output currents are pulsed and filtered by a capacitive filter bank.

Modern motor drives produce a controllable output voltage, as a sinusoidal waveform whose magnitude, phase, and frequency are controlled by PWM technique applied to the inverter switches [17, 27]. The higher the switching frequency, the higher the quality of the resulting waveforms. But, high switching frequency produces complex transients that stress motor insulation. This stress has to be reduced by determining the effects of these types of voltage on the insulation system, especially in the overhang region where there is a high electric field.

The overheating on the overhang region of motors fed by PWM drivers is caused by the high resistive losses inside the CAT and the SGT layers, and by the PD that happens due to the high electric stress on the surfaces of stress grading systems, especially in some contaminated and wet conditions [30]. The imperfect contact between the CAT and the slots after lengthy operation can make air voids, leading to local high electric fields and PD in these voids, and making the overheating serious. Resistive loss and PD are two main factors that can accelerate one another, and degrade stress grading systems.

Three types of power electronic switches with high capabilities are used in drivers: the insulated gate bipolar transistor (IGBT), the integrated gate commutated thyristor (IGCT) and the metal oxide semiconductor field effect transistor (MOSFET) [9, 31-32]. IGBTs commonly used in drivers, have advantages such as high switching frequency, low cost and mature technology [9, 33]. Different topologies exist for the motor drivers, related to the rated voltage of the motors. Two-level drivers are mostly used for low voltage motors, and more than two-level (commonly three-level drivers) are utilized for MV motors. Increasing the level of drivers reduces the jump voltage of pulsed voltages, reducing stresses on the insulation systems, but increases the cost, weight, and space.

ASDs based on PWM-VSCs and fast switches are the most popular drives for MV induction motors. In spite of their benefits, they introduce new voltage stresses to the stress grading system of form-wound coils in MV motors. New solid state switches are capable of withstanding higher voltage ratings and faster rise times. On the other hand, the fast rise time and high repetition rate of the PWM pulses have adverse effects on insulation systems, particularly stress grading systems. Although a fast rise time has little impact on the temperature rise of the SGT, especially at low switching frequency, it significantly affects the temperature rise of CAT at the slot exit and produces hot spots there [3]. In addition, the hot spots that occur in the CAT or the SGT due to an enhanced electric field result in higher temperature rise. PD, increased joule heating, and the creation of hot spots are the main reasons for degradation of the main insulation. Therefore, understanding the mechanisms whereby stress grading systems age under PWM-VSC voltages has great importance for industry. Figure 1-4 shows a typical voltage waveform for ASDs at the terminals of a driver and a motor, and also the shape of a pulse at the motor's terminal.
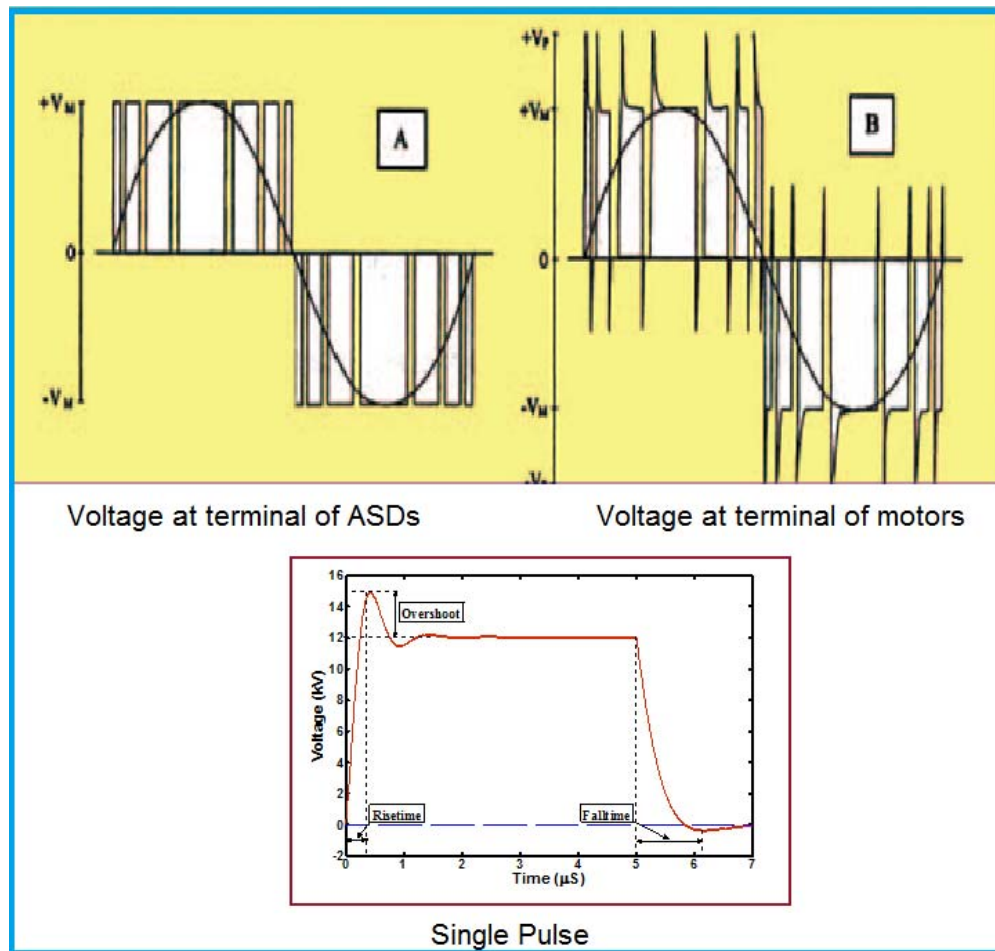
Figure 1-4: Typical voltage waveform of ASDs.

1.5 Literature Review

This section reviews the literature related to this thesis. The first part discusses the materials of stress grading systems. The next part explains the behavior of stress grading systems under power frequency voltages and pulsed voltages. Finally, the modelling and simulation of stress grading systems are explored.

1.5.1 Materials

1.5.1.1 Conductive Armor Tape

As CAT is commonly made of carbon black (CB) in a fiber glass tape, the conductivity of this composite is changed widely by the types and concentrations of the carbon black; therefore, for each

9

application, the design of the material conditions must be optimized. Zois et al. [34], investigating the behavior of CAT in composites, found that it acts as an insulator at high frequencies and at low carbon black content. Alternatively, it acts as a conductor at low frequencies and at high CB content. The study showed that at the critical weight concentration of CB, an infinite network of conducting components is produced. But, the AC conductivity of composites is almost constant in a wide range of frequencies at high CB content [34].

In percolation theory, physical contact between conductive clusters is necessary. In contrast, there is no need for physical contact in tunneling, and the charge carriers can move from one cluster to another by tunneling. Nakamura et al. [35] explained that the fluctuation induced tunneling model can be used to explain the temperature dependence of the resistivity of CB composites. Their research stated that tunneling forms even beyond the transition of insulating to non-insulating properties and interrupts the formation of the infinite clusters of the CB.

CAT conductivity differs significantly with tape builds and with vacuum pressure impregnation (VPI). It can be changed by orders of magnitude by the VPI process, as it affects surface and volume conductivities, particularly in the transverse (thickness) direction. In addition, conductivity is dependent on temperature and tape builds; the manufacturer's specified electrical conductivity, usually given at room temperature, is not accurate, particularly after VPI and at operating temperatures [15]. High temperatures and high electric fields stress CAT during operation and enhance partial discharge (PD) activity. PD and contamination can change the bond between CAT and the ground plane, thus decreasing contact conductivity [36]. The simulations in some studies consider only manufacture supplier values, which is usually specified for room temperature only, or from the literatures for CAT conductivity [37-40]. Therefore, the simulation results are inaccurate. The operating temperature point is much above room temperature, so evaluating conductivity at elevated temperatures is necessary. The effect of VPI and temperature on surface conductivity has been studied in previous works [21, 22]. In addition, [15, 16] investigated how VPI, various builds, and temperature affect both surface and volume conductivities. The authors showed that the VPI process changes the top thin layer of CAT, thus decreasing its conductivity. Under the thin low-conductivity layer of CAT, there is still a highly conductive layer, so the volume conductivity in the longitude direction that affects the voltage distribution along samples is not changed significantly. Temperature and build type also affect conductivity; hence increasing the number of layers and temperature leads to increased conductivity [15, 16].

10

High temperature speeds up the degradation of CAT, thus increasing its conductivity. Thermal ageing data shows that the conductivity of CAT can increase three fold during a forty-year lifetime [21]. Espino et al. [41] determined that the electric field distribution on CAT decreases by the increment of conductivity of CAT, but the stress on the SGT is enhanced, perhaps causing PD on the surface of the SGT.

1.5.1.2 Stress Grading Tape

The electric stress is enhanced at the end of CAT on the end winding and leads to PD in this region. Therefore, SGT is necessary to control the electric field and prevent this PD. Generally, two types of stress grading exist for applying to high voltage systems; namely capacitive and resistive.

Capacitive stress grading

There are various methods for applying stress grading. One of them is to apply a layer of high permittivity material. This layer decreases surface resistance, reducing the electric field [42]. This method is used more in cable terminations and, due to the unavailability of high permittivity materials in the class F temperature category and the thickness of this layer, it is not practically applicable for motor windings. The next method uses a stress cone, which reduces the electric field. Again, this method is common in cable terminations but, because it increases the coil dimensions, is not suitable for motor winding. Another method, which uses metal foils inside the insulation, is commonly used on bushing and is not practical for motor winding due to manufacturing difficulties [42]. Sharifi showed that the last method is effective in PWM voltage wave forms and reduces the electric field on the stress grading system, eliminating any hot spots in this region [43].

Resistive stress grading

Non-linear resistive materials are generally used in stress grading systems. The resistance of these type of materials depends on the electric field and is increased by a high electric field. These type of composites can be produced using compounds, such as insulating polymer, with a semiconductive filler. Varnishes, epoxy resins, polyester resins, and silicone rubber are among the base polymers used in stress grading composites [17]. Percolation effects as well as potential barriers at the contacts can make conduction paths in these materials [44]. The conductivity is enhanced by increasing the particle size, because fewer grain-to-grain contacts are needed, and also because the voltage across the contacts is increased. On the other hand, the permittivity has a weak dependency on the particle size, particularly at high frequency [19].

One type of filler, SiC, commonly used in a motor winding, has been utilized as a nonlinear field grading material for many years. This semiconductive material has good thermal and mechanical properties. Some manufacturers reach the appropriate resistivity range for SiC by mixturing different grades of powder to improve the electric field distribution for a given application [48]. The SiC grains employed on the insulating polymer matrix make a percolated system that produces conducting paths. A contact between grains of SiC can be modeled by two Schottky-like barriers, which have a forward and a reverse barrier in series [49]. Martensson et al. [49] modeled the contact between grains by a nonlinear resistance in parallel with a nonlinear capacitance and a linear capacitance, in which the components are considered frequency independent; however, the conductivity and permittivity of the grading materials are changed by frequency. Therefore, they suggested a network of unique contact zones with different properties to explain the frequency dependency [49]. The electrical properties of SiC composites can be widely changed by grain sizes, distribution, chemical composition and concentration [20, 50]. The larger the Sic particles, the lower the resulting material resistivity, because fewer grain-to-grain contacts are needed to obtain a conductive path and there is increased voltage across each contact [19].

Another type of material used in stress grading is ZnO-filled polyester whose conductivity is enhanced in a high electric field, so the space charge accumulation is dissipated at the end of electric tree channels, leading to a reduced local electric field. As a result, the tree growth is decreased; therefore, the lifetime of insulation materials is increased [45]. The properties of fillers and composites have the same field dependence; however, because of the interface resistance between the grain-to-grain fillers caused by the polymer, the conductivity of the composite is less than that of the filler. If the volume content of the filler is greater than the percolation limit, the properties of the composite are slightly independent of the processing conditions [46].

The nonlinear conducting characteristics of ZnO/silicone rubber composites with different shapes and diameters in their fillers was studied through experiment and simulation in [47]. The authors showed that variation of the shape and diameter of fillers affects the conduction paths as well as the overall contact resistance, necessitating adjustment of the nonlinear property of a composite. In addition, the shape of fillers can change the switching field of composites, but the nonlinear coefficients of composites remain almost the same. Therefore, the nonlinear characteristics of composites can be optimized to meet specific requirements simply by controlling the filler's basic physical properties such as shape and size.

For field-dependent resistivity materials, the filler content must be greater than the percolation threshold; therefore, the particles form a continuously connected network to make conducting paths through the composite [51]. These materials can be classified depending on whether:

- The particle–particle contacts lead to nonlinearity.

- The nonlinearity is caused by an intrinsic property of the filler particles.

Resistive and capacitive current densities are proportional to the conductivity and product of the dielectric constant and the frequency ($\varepsilon\omega$). Therefore, when $\varepsilon\omega$ is greater than σ, the system is capacitively graded, and when the conductivity is greater than $\varepsilon\omega$, the system is resistively graded [52]. The conductivity in the high electric field region is increased until the dielectric relaxation time constant becomes comparable with the time constant of the applied voltage; thus, the space charges limit the electric field [52]. Okamoto et al. [53] showed that the conductivity of a composite made with SiC is not remarkably changed by the electric field for a volume ratio below 0.15 and becomes highly nonlinear when the volume ratio is increased. However, the nonlinearity is fixed for a volume ratio greater than the percolation threshold, due to nonlinear behavior caused by the tunneling conduction between SiC grains [53].

The electrical conductivity of SGT is one of the important parameters influencing electric field distribution. Therefore, measuring the SGT conductivity after VPI and at operating conditions is important. Since excessive temperature rise in the SGT material occurs during measurements in a high electric field under DC condition, in [18] the measurement was done under pulse conditions. Increasing the electrical conductivity of the SGT decreased the space charge limited field (SCLF), resulting in uniform voltage and electric field distributions [16, 18].

1.5.2 Behavior of the stress grading system

The functionality of the stress grading system of MV motor coils in the overhang region is important to insulation life because of the high electrical stress and the close proximity of other coils. A conventional stress grading system can perform well under power frequency voltages, but its exposure to inverter drives with fast switching devices can result in rapid degradation and early failure. For form-wound motors, the coils are fabricated outside of the stator core; therefore, they must be thinner than the width of the slots. Thus, an air gap between the coil surface and the slot is inevitable. Although VPI may fill in the gap with epoxy resin, because of thermal cycling considerations, there are still air gaps between the bars and the slots. Since the permittivity of air is less than that of the main insulation, a

13

high electric field appears in the air gap. If the electric field in the air gap exceeds a threshold related to the temperature and pressure, PD will occur and eventually erode the main insulation [1]. Therefore, CAT is used to prevent PD in the slots.

SGT is used to control the stress at the end of the CAT, by changing the surface impedance of the main insulation. Figure 1-5 shows the effect of SGT on the surface voltage and the electric field at power frequency voltage. It is clear that, with SGT, the electric field at the end of CAT is reduced significantly, preventing PD in this region. A nonlinear resistive SGT has the following features [17]:

- The conductivity of SGT is enhanced where the electric field is high.

- The electric field during any over-voltages is limited.

- The material has reproducible characteristics.
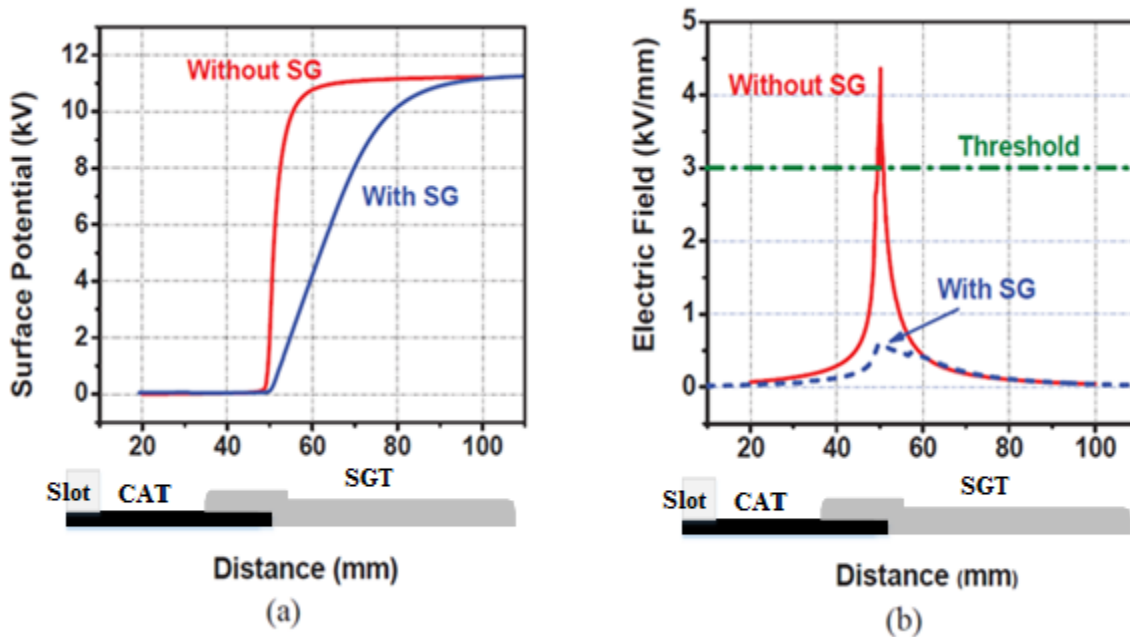
Figure 1-5: Effect of SGT at power frequency voltage on (a) surface voltage, and (b) electric field profile along the end winding [3]. The threshold shown in (b) is at atmospheric pressure and 20 °C.

The threshold and maximum acceptable electric field, the maximum voltage at the end of the SGT, and available length and thickness of tapes are usually the important parameters for designing and optimizing an effective stress grading system. Minimizing power loss in the stress grading system can also be the main objective function for any optimization activity [54, 55]. Other possible objective

14

functions include the maximum electric field, which usually occurs at the beginning of coatings and must be kept below the breakdown strength of the air, and the voltage difference between the end of the stress grading system and the surface of the main insulation [56, 57]. If this difference is large, it can produce discharges at the end of the stress grading system. On the other hand, an effective stress grading system for power frequency may not work properly in PWM voltage conditions. A fast rise time and pulse repetition rate can change the electric field profile, leading to hot spots and PD in insulation systems. Therefore, the performance of stress grading systems has to be investigated under PWM voltages.

In [38], measuring the voltage distribution along the stress grading system under various types of voltages showed that the DC component of the voltage has no effect on the thermal and electrical distribution of the stress grading system. However, the electrical conductivity of stress grading system materials and their configuration do affect it. The effect of CAT conductivity on the electric field and on heat density in CAT and SGT have been investigated by Espino et al. [41, 58]. Authors determined that both the electric field and heat density are reduced when the ASD voltage levels are increased. It is clear that such an increase decreases heat density, but as the number of voltage level rises the size and cost of the inverter also increases [58]. Increased CAT conductivity decreases the electric field and heat density on the CAT, but in turn, enhances the stress of the electric field on the SGT, which may cause PD in this region [41]. Although the authors suggested increasing the conductivity of the SGT to decrease its electric field; doing so increases heat density. At the leading edge of a pulse, the maximum stress is in the CAT, right at the slot exit; during the rest of the pulse, it moves to the SGT [59]. Increasing the CAT conductivity transfers the stress during the rise time to the SGT, but increases heat density in the SGT, which must be considered in the SGT design.

When [23, 60] investigated how the thickness of stress grading system affects its average heat production, authors determined that increasing the CAT thickness by increasing the number of layers, reduces the electric field and heat production in this region. Although the electric field in the SGT region increases slightly with this increment, the heat production in the SGT region reduces. In addition, it boosted the electrical and thermal performances of the stress grading system, but this approach has limitations due to narrow slots. On the other hand, the electric field in the SGT region reduces with the increased SGT thickness. But, the electric field in CAT does not change. Although increasing the SGT thickness leads to better electrical performances during rise time, the average heat production in the SGT and CAT regions increases slightly.

15

The effect of the CAT-SGT overlap on the power dissipation factor, investigated by simulation for four topologies in [61], showed that the total power dissipated in the SGT changes minimally when the CAT-SGT interface topology changes. The concentration of the current in this interface can result in excessive temperature rise in this region. By theoretical analysis, the authors found that the power dissipation weakly depends on the CAT-SGT interface area, and mainly depends on the current. Also, a new surface potential measuring system was developed to measure the voltage distribution under PWM voltage by using a Pockels sensor [40] that can be used for evaluating simulation results.

An investigation in [62] showed that the nonlinearity of SGT conductivity is also altered by temperature and humidity. The nonlinearity is also changed by the size and the intrinsic property of the filler particles [51]. Authors in [63] investigate how the nonlinearity level of the SGT conductivity affects the electric field and temperature profile of a stress grading system under pulse voltage. Increasing the level of the nonlinearity of the SGT conductivity was shown to expand the high electric-field region of SGT; therefore, the SGT is efficiently used, significantly reducing the peak of the electric field in this region. However, the thermal performance is unacceptable as the maximum temperature rise is increased. On the other hand, the thermal performance under a low level of nonlinear SGT conductivity is acceptable, but the peak of the electric field is very high in the SGT, which might lead to PD inception in this region, depending on the operating temperature and field conditions.

Varistor-type materials can be used as stress grading and can keep the electric field very low, even with fast rise time pulses [50]. On the other hand, a high electric field can occur on the CAT and produce PD. Increasing the CAT conductivity increases eddy current loss in the stator lamination, so Espino et al. [50, 59] suggested that only the conductivity of the area just beyond the slot exit should be increased. Waveform parameters, such as fundamental frequency, rise time, switching frequency and the number of voltage levels can change the heat density in a stress grading system. Lower rise time leads to higher heat density. Whenever the rise time decreases, the capacitive impedance decreases, so the current passing through the SGT is increased [58]. The most important parameter is the switching frequency. For high speed applications that need a high fundamental frequency, the corresponding switching frequency is also high; thus resulting in high heat density in stress grading systems.

The width of pulses affects electrical loss in the SGT, and the thermal stress on the SGT differs depending on whether an impulse train is applied or a square pulse train with the same peaks and rise times. On the other hand, the thermal stress on CAT depends on the rise time of pulses, and the hot spots on the CAT at the slot exit are greatly affected by the rise time [14, 24]. Sharifi et al. [24] showed

that the worst thermal stress condition for the CAT happens under the fastest rise time, and for the SGT, under the lowest rise time at the maximum frequency. Poor electrical contact between the CAT and the stator slots may increase the stress, especially at the slot exit [13]. Tucci and Vitelli, using a numerical study, showed that stress grading system performance is more affected by the electrical properties of materials along the longitudinal direction than the radial direction [15, 64]. Optimizing CAT conductivity is one of the key factors in insulation systems for converter-fed motors, and according to the acceptable electric field and temperature rise for stress grading systems, a suitable conductivity has to be selected [39]. Umemoto et al. [39] suggested an evaluation method, based on simulation results, for selecting appropriate CAT conductivity.

Boggs et al. [14] showed that CAT has a critical frequency that is related to conductivity. If the frequency of an applied voltage is below this critical value, the voltage on the CAT is very low compared to the applied voltage, and the voltage distribution along the SGT is not affected by the CAT. On the other hand, if the frequency of an applied voltage is greater than the critical frequency, the CAT cannot discharge the capacitive current efficiently, thus increasing the voltage along the CAT and reducing the electric field on the SGT. The research determined that the power dissipation in the CAT happens during the rise time and is increased by reducing that time. However, the power dissipation in the SGT is negligible and is independent of the rise time, because it happens after the transition in the SGT.

Ageing, temperature and VPI can change the conductivity of stress grading systems [15, 21-22]. As such, the surface conductivity of the SGT can be changed during the life time, thus the stress is enhanced, particularly at the end of the CAT and produces PD [22]. Wheeler et al. [34] showed that the nonlinear electrical conductivity of the SGT changes under different temperature conditions. An ageing process involving temperatures up to 155°C was developed and tested on three market-available SGTs. The surface electrical resistivity of these samples, measured at certain temperatures, was found to drop with increasing temperature. One of the tapes almost lost its nonlinear property at 155°C. Returning to room temperature, the resistivity of two tapes became much higher than the original value.

Nakamura et al. [37] showed that the maximum stress at the interface of the CAT and the SGT is higher under PWM voltages than rectangular ones. Since the space charges of opposite polarity are accumulated at the interface of CAT and SGT, and due to the fundamental frequency of PWM voltages, the highest electric field happens during the first pulse after polarity reversal [37]. Experimental results showed that the light emission from PD also becomes intensive after the polarity is reversed in PWM

voltages [37]. However, the DC component of an applied voltage has little influence on the electric field distribution or on the thermal profile, and only charges the main insulation [38, 65].

The problem of hot spots in the SGT, including how the temperature increases with the frequency of the applied voltage, has been evaluated. The negative effect of PWM voltage in the SGT at the overhang region of large motors was explored in [26]. SGT was shown to be ineffective in limiting the electric field below the PD onset, suggesting a need for intense research in this area. The high gradient voltage in stress grading material is located in the CAT/SGT interface for low rise time rectangular voltage; whereas, this phenomenon happens in the CAT near the end of the stator core when fast rise time voltage (e.g., 300 ns) is applied [38].

1.5.3 Modelling and simulation of SG systems

In recent decades, the development of computer processors has provided an appropriate way for electromagnetic computation to determine the interactions of electromagnetic fields with complicated physical objects. Equivalent circuit method, finite difference (FD) and finite element method (FEM) are commonly used for modelling stress grading systems. FD and FEM are two numerical computational techniques widely used for solving partial differential equations (PDE) such as the Maxwell's equations. These methods use differential equations and require the meshing of the entire domain in which the electromagnetic fields are solved. The validation of such methods has been difficult, but a good approximation to the effectiveness of parameters can be achieved with the correct use of these simulation models. Verifying the reliability of the numerical simulations under PWM voltage is useful. However, measuring voltages or field distribution under this voltage is difficult. Only a few studies have attempted to measure the transient voltage distribution on stress grading material under pulse voltage by Pockels sensor [37, 38, 65].

If the frequency of an applied voltage is low enough to make the period of an applied voltage greater than the relaxation time of the materials, the materials act as a resistor. Since the relaxation time of CAT is very low (estimated to be less than 1 nanosecond), CAT can be modeled by a distributed resistor even in the rising part of the pulsed voltages [38]. Kumada et al. [37] estimated that the relaxation time of the SGT changes from 10 ms to 100 μs under electric fields of 0.1 kV/mm to 0.5 kV/mm, respectively. Figure 1-6 shows the equivalent circuit used to simulate the stress grading system [34]. Each section of the CAT was modeled by a resistance with the corresponding capacitance of the main insulation under the CAT. On the other hand, the SGT was modeled by a field dependent resistor in parallel with a capacitance of the SGT. CAT conductivity is much higher than SGT conductivity; thus

the SGT parts act as stronger low pass filters than the CAT parts [38]. The capacitance of the CAT and the SGT can be ignored when a low frequency voltage is applied [65]. When the frequency of an applied voltage is greater than the cut-off frequency of the CAT, the highest electric field happens in the CAT at the slot exit. If the applied frequency is between the cut-off frequency of the CAT and the SGT, the highest field occurs on the SGT at the end of the CAT [65]. The model used in [65] may have an acceptable result for design, but there are many limitations in applying this method to a study of a stress grading system with other insulation components for fast rise-time transient studies. In addition, this model has no capability to model temperature-dependent materials for electrical and thermal analysis at the same time.
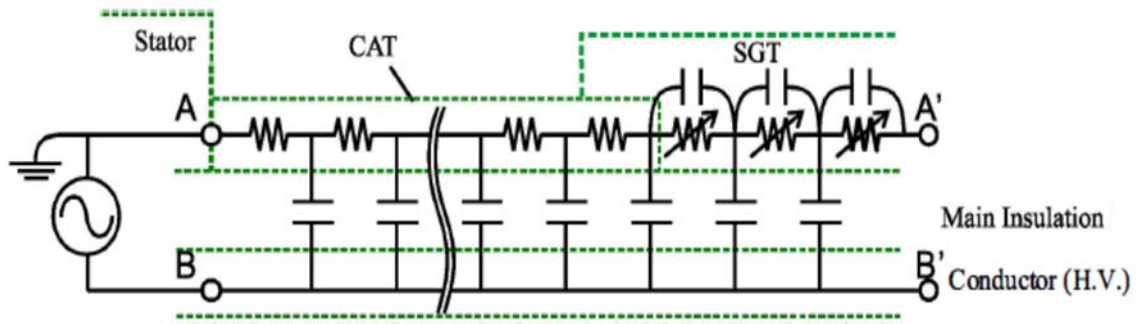
Figure 1-6: Equivalent circuit diagram of the stress grading system in overhang region [38].

In the FEM method, electric fields can be described by truncated versions of the Maxwell's equations applied to relatively low frequencies, electro-quasi-static (EQS), compared to radio and microwave frequency. The stress grading system in motors can be considered as an EQS problem because the physical size of the system is considerably smaller than the wavelength [66]. This multi-dielectric system with different insulation characteristics and semiconductive nonlinear material makes a complex system that needs a powerful tool for modelling and analyzing. For simplicity of modelling, it is assumed that the stress grading system is homogeneous and isotropic. Thus, there are no comprehensive simulation models to represent all of the material characteristics and to analyze their response to different operational conditions such as repetitive fast pulse voltages and high temperature [67].

Zheng and Boggs [68] discussed the problems of using the finite element method to compute field parameters for a transient nonlinear field. The authors developed a one-dimensional FEM software for their case studies. Espino [17] performed 2D-transient FEM simulations for stress grading systems,

either conventional for normal power frequency or sectionalized for PWM voltages. In addition, by adding a heat transfer module, the author studied the temperature variation in different areas, but only under AC sinusoidal steady state condition with linear materials. Sharifi [4] simulated a 2D-transient FEM model for anisotropic AC conductivity of SGT, and also evaluated a capacitive stress grading system using this method. The author noted that running a transient coupled electro-thermal FEM simulation for repetitive fast pulses is impractical because the computation becomes complex and laborious. Therefore, for modelling and computer simulation, a stationary analysis based on two sinusoidal voltages of different frequencies was proposed as an alternative to a transient analysis for pulse voltages. In [16], a coupled electro-thermal FEM simulation was used to evaluate the temperature profiles. The simulation was run for three cycles, and the average heat source of the domains during these cycles was then calculated using another time transient ordinary derivative equation (ODE) interface. This average was used for a stationary heat transfer study in order to obtain the temperature profiles at steady state.

Transient FEM analysis with highly nonlinear elements is associated with convergence problems. Thus, adoption methods are always necessary to overcome this problem. On the other hand, the accuracy of the results depends strongly on the initial conditions. Therefore, more work is needed to find a technique for setting accurate initial values for field dependent elements. In addition, the combination of EQS and heat transfer models with nonlinear materials creates a complex model.

Measuring the electrical properties of stress grading systems is a key to accurately modelling such systems. As discussed, the conductivity differs significantly with various tape builds, and with VPI and temperature. Therefore, measuring these parameters under the same conditions of normal operation is crucial. Also measurement methods must be accurate; for example, Umemoto et al. [39] showed that the larger the gap between two electrodes, the more accurate the measurement. Measurements also show that CAT conductivity is anisotropic, and it is essential to use the correct conductivity in simulations [13, 15, 64].

Since the electric field in the SGT is increased greatly during operating condition, the conductivity of the SGT has to be measured under a high electric field [18]. Boggs at al. [69] determined a method for measuring the conductivity of the SGT in high electric fields. Since the temperature of the SGT is extremely increased, the SGT properties cannot be measured under DC above more than 0.5 kV/mm; therefore, pulsed voltage was used to measure the properties at higher fields.

1.6 Aim of the Present Work

A review of the literature on stress grading systems has identified that the electrical and thermal conductivities of materials used in these systems can be significantly changed by VPI, temperature and tape builds. In addition, fast rise time PWM voltages can affect the conduction mechanism and dielectric losses. Also, the heat generated in a stress grading system can cause localized hot spots. Therefore, it is important to understand the mechanisms of conduction and heat dissipation under repetitive fast rise time pulses.

A comprehensive numerical simulation for electro-thermal analysis needs the electrical and thermal conductivities of the materials under actual operating conditions as input. Thus, in this research, the thermal and electrical conductivities of stress grading materials under real operating conditions were measured. In addition, the SGT conductivity has to be measured in a high electric field, so pulsed voltage was used for measuring this conductivity under high electric field conditions.

The effects of the pulse parameters (rise time, magnitude, and frequency) on hot spots, PD, and temperature profile can be assessed using a high voltage PWM generator. Some of the samples that represent the actual form-wound coil used in the overhang region of MV motors are used to study the fundamentals of rise time and switching frequency on PD and hot spots. These samples were prepared by the General Electric Company in Canada. The relationship between each parameter and hot spots have been extracted. In addition, the effect of stress grading conductivity and builds on heat distribution was evaluated.

From the results of the parametric studies, the dominant factors that contribute to hot spot occurrence, as well as their effectiveness under PWM-VSC voltages, can be identified. Simulation studies of stress grading systems using FEM analysis contributed to the understanding of ageing process. The combined outcomes will enable designers to effectively use available insulations and suggest an optimum conductivity for materials and types of builds, thus ensuring long insulation lifetimes.

In the context of the above discussion, this research has examined the influence of pulsed voltages on the stress grading system in the overhang region of a MV motor. The purpose of this study has been to examine the heat produced by PWM in the CAT and the SGT and to examine ways of distributing the production of heat so as to minimize hot spots. Hot spots cause materials to degrade according to the Arrhenius law; hence machines need to be de-rated to prevent this, thereby reducing efficiency. The following summarizes the goals of this research:

- Understanding of the stress grading system performances theoretically and experimentally under repetitive fast rise time pulses.

- Developing an accurate simulation model to account the effects of material properties under operation condition.

- Verifying the model with experimental measurements.

- Investigating the effects of material parameters and builds of the stress grading systems on their thermal and electrical performances.

- Optimizing these parameters to obtain the desired performances (minimizes hot spot temperature and/or lower heat production, but without exceeding the corona inception on the surface of the stress grading systems).

  o Determining the working range and optimum conditions.

  o Modifying the stress grading system under PWM voltages.

Evaluating the effect of such high-frequency pulses on insulation systems has required thorough study, including of all the procedures stressing insulation under pulsed voltages. First, the electrical parameters of the stress grading materials were measured to develop an accurate simulation model of the stress grading system, appropriate for this purpose. In parallel with the modelling, measurements were performed to gather data on the practical voltage and temperature profile in the overhang region. The next stage of the research was to perform a simulation, inclusive of dielectric properties of the material as functions of the electric field and temperature. Then, a laboratory experimental study was carried out on the motor winding samples to compare the practical behaviour of the stress grading system to the simulation results. Once the simulation showed good agreement with the laboratory measurements, the numerical simulation was used to determine ways to reduce temperature rise and/or eliminate hot spots.

The rest of the thesis structured as follows:

- Chapter 2 outlines the materials, test setups and methods utilized in this research.

- Chapter 3 presents the results of experimental studies, simulation model verifications and design modification impacts.

- Chapter 4 discusses the results obtained in this research and recommends new materials and builds.

- Chapter 5 summarizes this research, provides conclusions and highlights the research contributions. The thesis ends with possible direction for future work.

Chapter 2

Samples, Experimental Setup, and Methods

This chapter describes the experimental setups, procedures, materials, and design-modification methods used in this research, then introduces the program used for simulation study of the stress grading systems. The first section describes the design and preparation of the test samples as well as the reasons for the specific features of each sample. The next section explains the measurement procedure for evaluating the samples and for modifying the simulation model. Finally, it discusses the finite element method (FEM) based computational method, under repetitive pulses that is used here to model the electric and thermal characteristic of the stress grading system.

2.1 Sample Preparation

For both surface and volume conductivity measurements, the CAT and SGT were applied to two separate sample aluminum bars having a cross section of 50.8 mm x 12.7 mm. For the CAT conductivity measurement, first, one half-lapped layer of CAT was wrapped around the total length designated for tape-application. Then one additional half-lapped layer was wrapped around the half of this total length (Figure 2-1 a), followed by the application of two slot-simulator plates on the half-length of each taped area, which was followed by vacuum pressure impregnation (VPI) using epoxy resin. Ultimately, each build had two regions, one not exposed directly to resin, to simulate CAT inside the slot, and another completely immersed in resin, to simulate CAT outside the slot. Similar samples were used to examine conductivity in the longitudinal direction, or along the length of the samples. For these samples, main wall insulation (or ground wall insulation) was applied to the aluminum bar, followed by the steps described above (Figure 2-1 b). The same procedure was followed for the SGT except that a 2/3 lapped layer was used for SGT. Figure 2-2 shows an illustration of the samples.
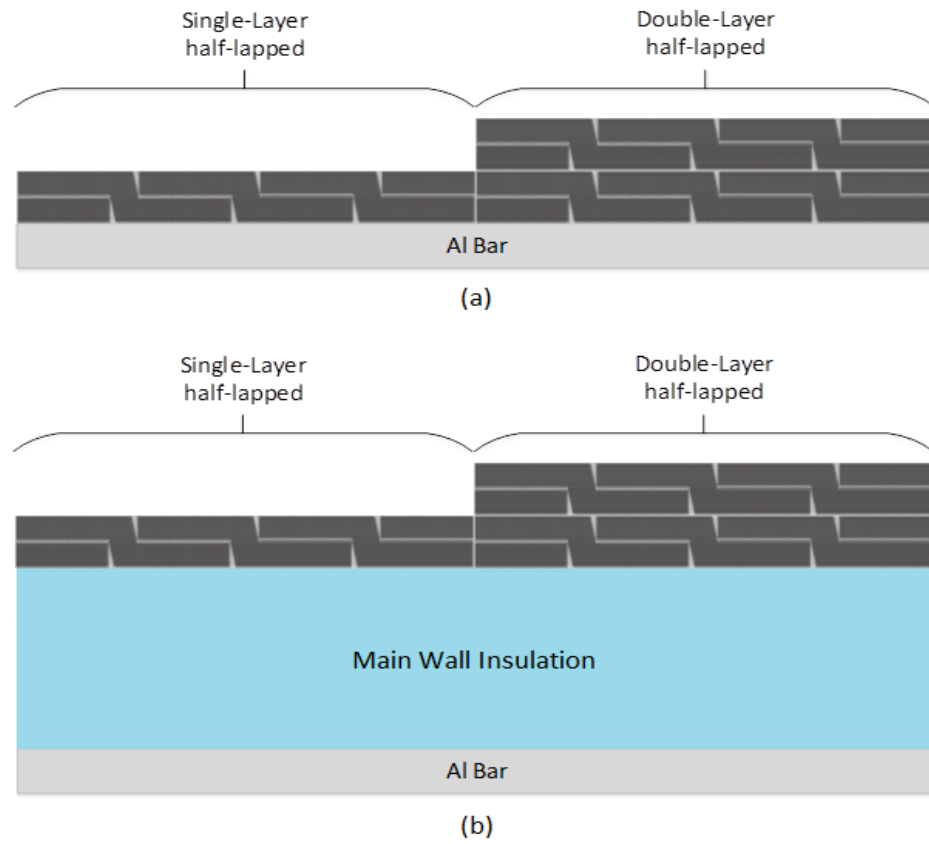
Figure 2-1: Illustration of half-lapped single-layer and double-layer constructions (a) for surface, volume thickness and (b) for volume longitudinal conductivities.

Figure 2-2: Photograph of samples prepared for conductivity measurements (courtesy of General Electric Power Conversion of Canada, Peterborough, Ontario).

Additional samples were prepared to measure the temperature and voltage distribution along the overhang region under PWM voltages. For each sample bar, first the main wall insulation tape was applied to the bar. Then CAT was applied on the main wall insulation. Next, SGT was applied, making sure that the SGT application overlapped the CAT by 20 mm. The number and length of each layer are identical to those of actual 13.8 kV motor coils. Once the bars were insulated, slot simulator plates were applied to each bar. In the end, the prepared bars were subjected to VPI process. Figure 2-3 shows the completed samples received from General Electric Power Conversion of Canada.

Figure 2-3: Photograph of completed samples (courtesy of General Electric Power Conversion of Canada, Peterborough, Ontario).

2.2 Measurement Procedure

2.2.1 Electrical Conductivity Measurements

Suppliers commonly provide the surface resistivity or conductivity of their tapes to customers. This parameter is a material property as received but not after processing, and is the common practice in industry. These values can change by orders of magnitude after VPI, thereby making simulation results inaccurate. In addition, normal operating temperature is well above room temperature so using the conductivity at the operating temperature is necessary for accurate analysis. Therefore, FEM modelling requires a precise measure of the volume conductivity. According to ASTM D257-14 [70], conductivity can be measured using two or three electrodes. Figure 2-4 (a) shows a circuit diagram of volume

conductivity measurement in the transverse direction; the middle silver paint electrode, the aluminum bar, and two-sided silver electrodes are connected to the positive voltage, the incoming probe of the ammeter, and the ground, respectively. Figure 2-4 (b) shows a circuit diagram of surface conductivity measurement, and the middle silver paint electrode, the aluminum bar and two-sided silver electrodes are connected to the positive voltage, the ground, and the incoming probe of the ammeter, respectively.

For measuring the conductivity in the longitude direction, two narrow cuts 30 mm apart were made through the tapes down to the main wall insulation. The cuts were filled with silver paint and then used for measuring conductivity in the longitude direction (Figure 2-4 (c)). More details on the sample preparation are shown in Figure 2-5.
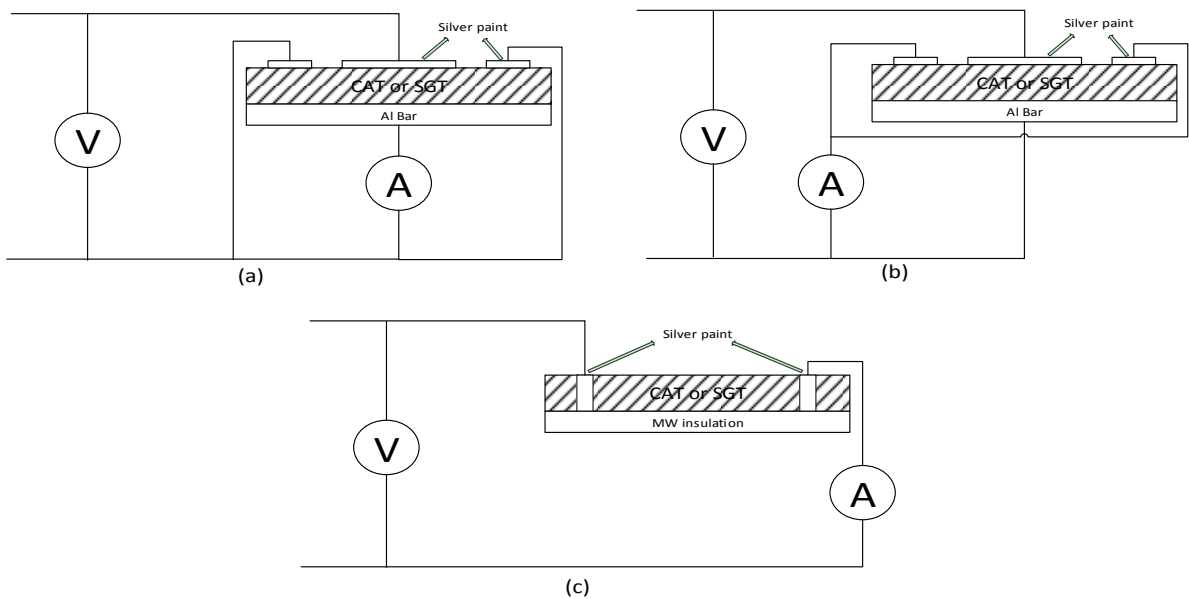
Figure 2-4: Circuit diagram of conductivity measurement, (a) for volume conductivity in the transverse direction, (b) for surface conductivity, (c) for volume conductivity in the longitude direction, the gap between electrodes is selected according to ASTM D257-14.

27
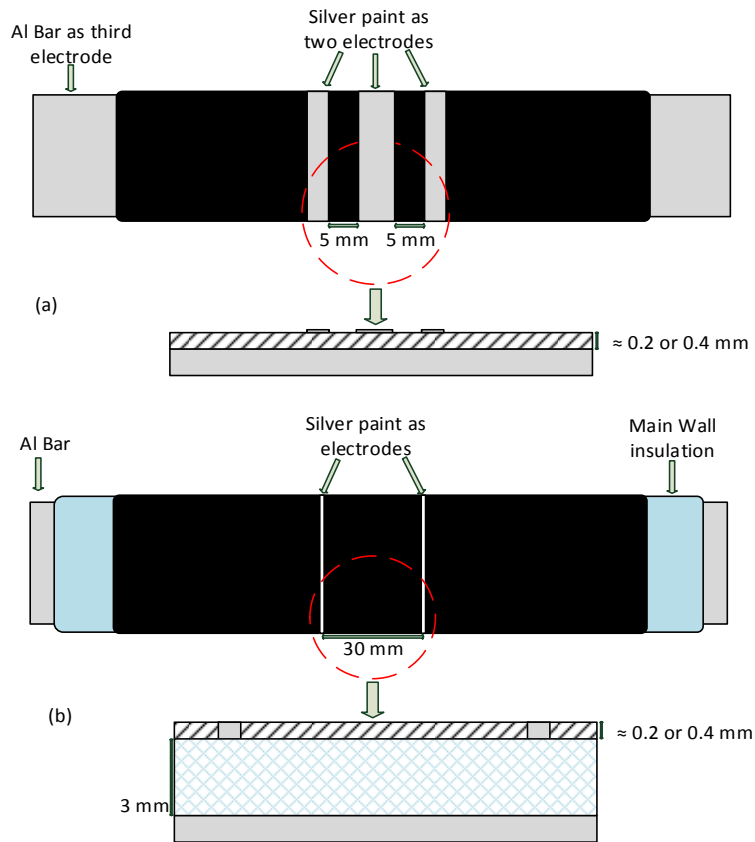
Figure 2-5: Schematic diagrams of surface and volume conductivities in (a) transverse direction and (b) longitudinal direction.

To measure the conductivity of the CAT, a variable voltage DC source and a highly sensitive ammeter (Electrometer Keithly 6514 with a minimum ampere range of 20 pA and 10-4 pA resolution) were used. In contrast, the conductivity of SGT has to be measured in a high electrical field, but it is not possible to measure conductivity by a DC voltage above 0.6 kV/mm due to excessive heating during the measurement. To reach higher fields, the measurement must be carried out under pulse conditions. Therefore, a pulse voltage was used to apply a high electric field to the SGT. Figure 2-6 shows a diagram of the measurement circuit. The shunt resistor was selected to provide a measureable voltage at the oscilloscope without excessive voltage drop across the resistor.
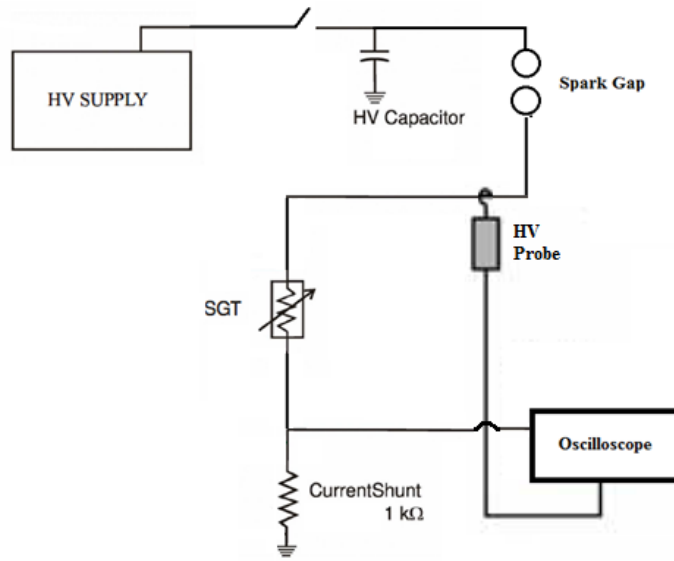
Figure 2-6: Experimental configuration employed to measure SGT sample conductivity.

The circuit shown in Figure 2-7 was used to measure conductivity above the room temperature. Two sets of CTs were used in reverse for circulating current through the sample to elevate its temperature. The surface temperature was monitored using an IR camera.
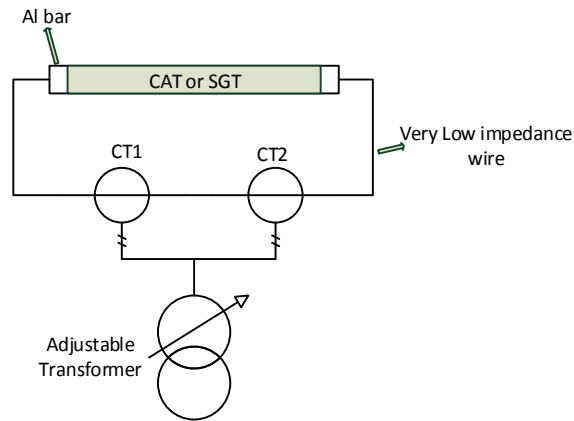
Figure 2-7: Circuit for measurement in high temperature.

2.2.2 Thermal Conductivity Measurements

The thermal conductivity of materials was measured in accordance with ISO 22007-2:2015 [71]. The method entails the use of a hot disk transient plane source (TPS) instrument. Two samples of each material were used. Directional thermal properties were measured using the TPS anisotropic test

module. TPS sensor #5465 (3.189 mm radius) with a Kapton® insulation, a test time of 10 seconds and output of power to the TPS sensor of 0.03 Watts were determined to be the optimal measurement parameters. The input volumetric specific heat was 1.46 MJ/m^{3}K. Multiple directional thermal property tests were performed to confirm the reproducibility of measurements. The averaged thermal conductivity was used in the simulation. For this measurement, samples were cut from the prepared coils to consider the effect of VPI. The instrument is shown in Figure 2-8.
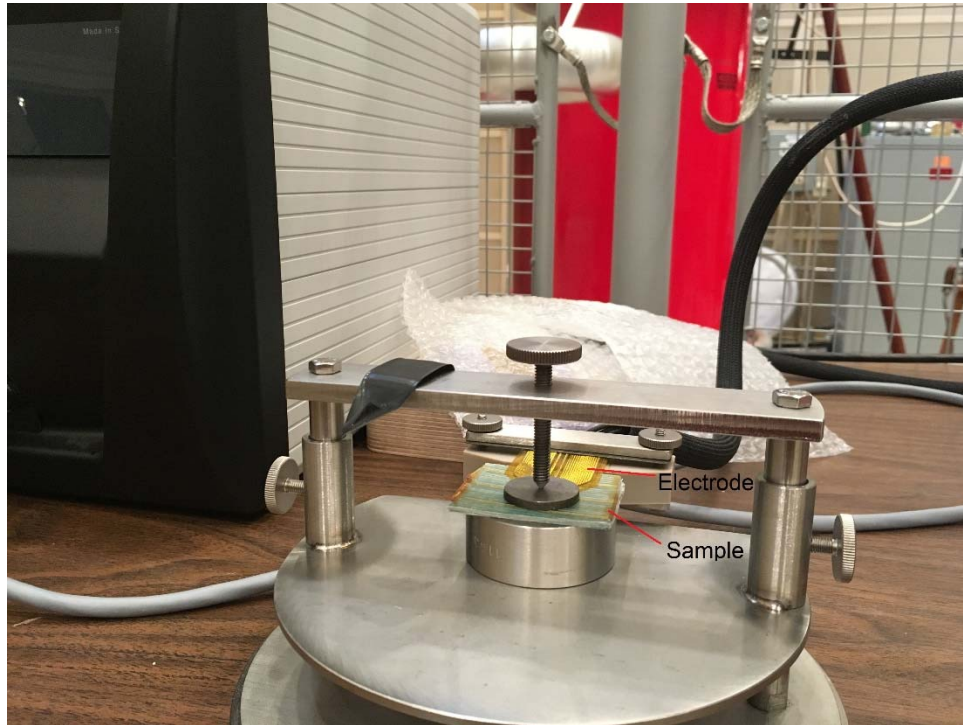
Figure 2-8: The hot disk transient plane source (TPS) instrument used in thermal conductivity measurements.

2.2.3 Relative Permittivity Measurement

The Agilent E4980A [72] and special software were used for relative permittivity measurement in a wide range of frequencies (1 kHz to 100 kHz). This parameter was measured under a low electric field; however, for a high electric field and high frequencies, these measurements are usually difficult. On the other hand, the relative permittivity of semi-conductive materials (CAT) is too large and exceeds the rating of this setup. The samples used for this measurement were the same as the samples used for thermal conductivity measurement. Figure 2-9 shows the setup used for this measurement.

Figure 2-9: The setup used for relative permittivity measurement.

2.2.4 Electrostatic Voltmeter for Voltage Distribution Measurements

The best way to evaluate stress grading effectiveness is to measure the surface voltage or electric field distribution along the overhang region. For instance, measurement of the surface voltage by electrostatic voltmeter is reliable and accurate. This research uses an advanced electrostatic voltmeter (TREK 341A) to measure the voltage distribution. For this equipment, the maximum voltage can be 20 kV DC; the speed response is better than 200μs for a 1 kV step change, and the accuracy is better than 0.1 % at full scale. The operating principle of this voltmeter is based on the electric field nullifying technique, and a vibrating Kelvin sensor must be placed 3 mm ± 1 mm from the surface [73]. Figure 2-10 illustrates the circuit used for voltage distribution measurements with the electrostatic voltmeter.
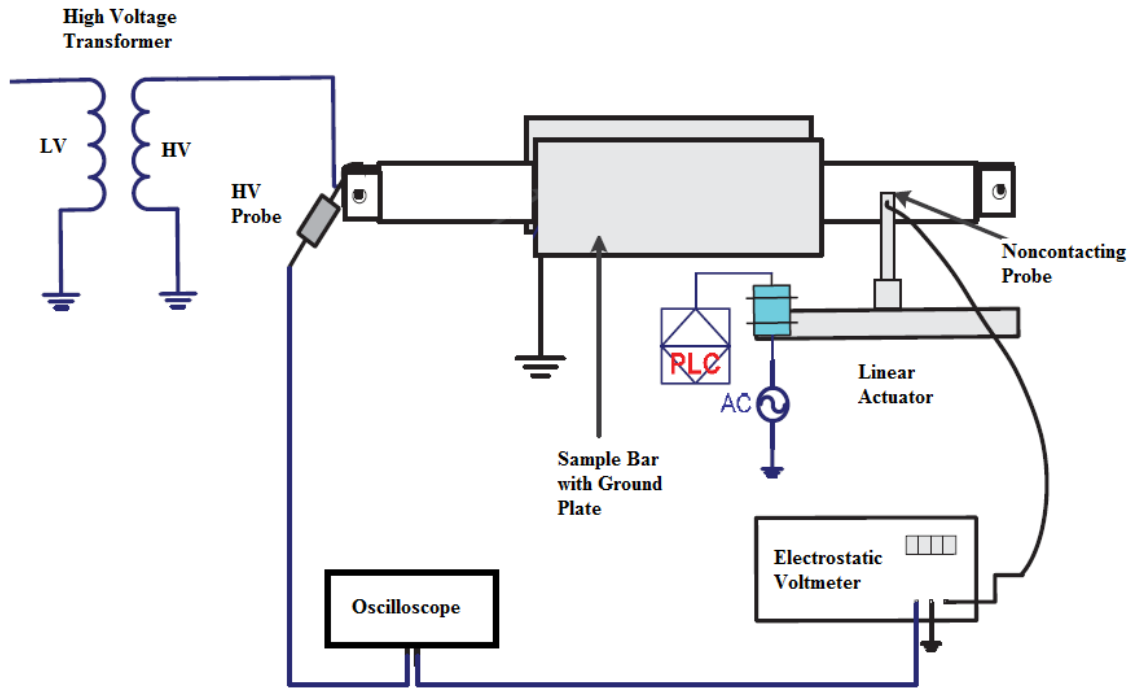
Figure 2-10: Schematic diagram of circuit employed for voltage distribution measurement using an electrostatic voltmeter at power frequency AC.

2.2.5 Temperature Measurement using the Infrared Camera

The thermal performance of the stress grading systems was evaluated using an advanced infrared camera and a thermo-vision acquisition software. The infrared camera is a FLIR T650sc having an infrared detector with a spectral range between 7.5 -13 μm. The temperature distribution is displayed in a 640×480 pixel array image. The accuracy is ±1 °C in the range of 5 to 120 °C [74]. The acquisition software, ResearcherIR, allows for post processing of the temperature distribution. The emissivity calibration was done using the temperature measured with a thermocouple as a reference.

To test the stress grading system under normal operating conditions, the temperature of the conductor must be elevated to the operating temperature; therefore, circulating current was used to raise the conductor's temperature. To reach a sufficient temperature, two sets of CTs were used for circulating current through the sample. The circuit was isolated from the high voltage pulse generator used to energize the sample. Figure 2-11 shows the experimental setup used for measuring the surface temperature profile.
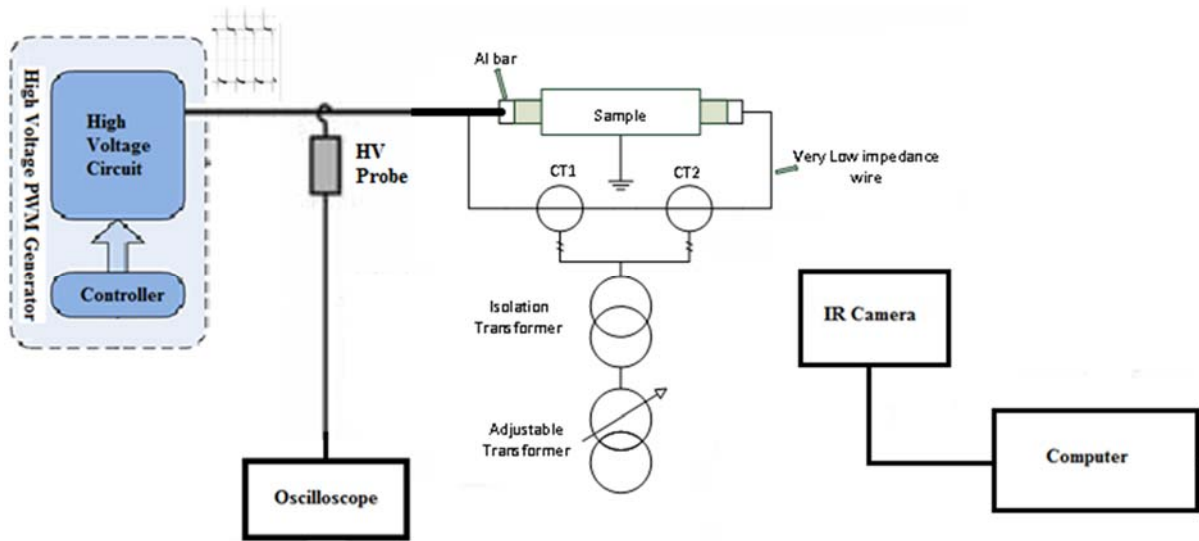
Figure 2-11: Experimental setup for the measurement of the surface temperature profile.

2.2.6 PD Measurement

PD plays a significant role in the aging of insulation under PWM voltages. Hence, the detection of PD is of great importance in assessing high-voltage insulation systems. This test is not recommended in IEC TS 60034-18-42 [10] for the evaluation of stress grading systems during the pulse aging test, but it was used in this research to analyze the PD trend when the CAT length is changed in the presence of pressure fingers. PD measurements were done at power frequency and under pulsed voltages. At power frequency, the PD setup consists of a 0-150 kV/20 kVA AC dielectric test set (Hipotronics 7150-20AMAX-G) with a PD level < 2 pC and a PD Detector (Hipotronics, DDX 9101). This setup, with a low-noise background in the laboratory (less than 2 pC) meets all IEC and ASTM standard requirements [75, 76]. The main components of the test system are a test transformer, regulator, calibration capacitor, control unit, and coupling capacitor. The DDX 9101 PD detector is one of the new generation of digital wide-band partial discharge detectors, with special software for data analysis once the unit is connected to a computer.

The PD inception voltage (PDIV) and extinction voltage (PDEV) are two important parameters used for insulation systems. They are related to a specific low threshold value of a PD magnitude. Voltage is increased from 0.2 Un to 1.2 Un in steps of 0.2 Un, where Un is the phase-to-ground voltage of the rated voltage of the rotating machine. At each voltage step, the average of the PD measured during one minute with a sample rate of four measurements per second and is considered the PD at that level.

Conventional PD measurement under AC waveform can be easily done by monitoring current and applying a simple filter to reject power frequency and its harmonics. A different approach is needed when PWM waveforms are used, due to the large capacitive current in the insulation generated by the application of fast rise time voltage. This current is much greater than that of PD pulses, making it quite difficult to detect PD. Using an antenna is the most popular method for detecting PD under pulsed waveforms where the capacitive current of the sample can be ignored. Selecting an appropriate frequency range makes it possible to disregard the effect of the supply pulses. This method has been used in [77-80]. A high-frequency current transformer (HFCT) [81, 82] can also be used to measure the current waveform. Post-processing software is used to disregard the supply current, retaining only the PD pulses. However, this technique may fail to detect PD at fast rise times due to similar frequency components in the supply and PD currents.

The PD test setup under pulsed voltage is shown in Figure 2-12. A monopole antenna was used for a non-contact PD measurement, and a high-pass filter was used to attenuate interference from the pulsed voltage. The pulsed voltage level for the 13.8 kV coil was taken as 11.3 kV peak and at 2.5 kHz switching frequency. This applied voltage waveform and PD were displayed on a 400 MHz, 5 G s/sec digital oscilloscope. The output from the antenna is voltage which can only be used for comparison.
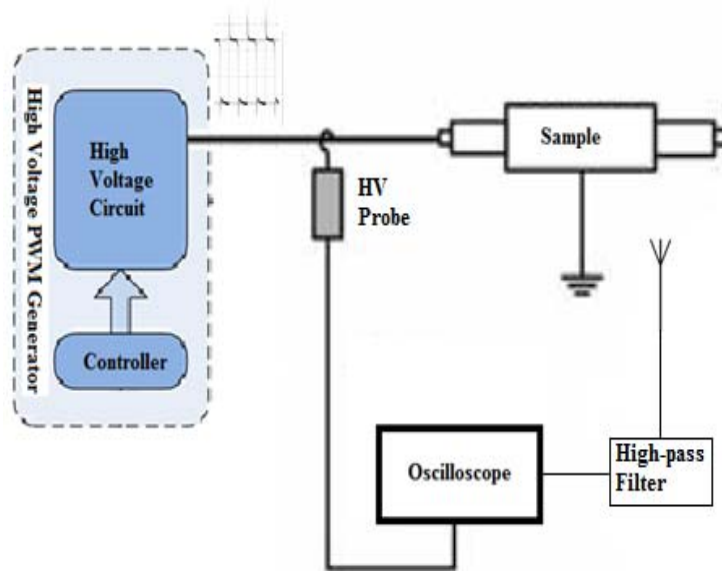
Figure 2-12: Pulsed PD measurement setup with antenna and high pass filter.

2.3 High Voltage Square Wave Generators

This section introduces the design and implementation of the high voltage square wave generators used throughout the research to assess the thermal and electrical performances of stress grading systems.

2.3.1 Bipolar/Unipolar Square Wave Generator

The present high-voltage pulsed generator uses a Marx generator configuration in which the capacitors are charged in parallel and are discharged in series [83]. This unipolar generator produces only unipolar voltage, and is therefore of limited applicability. In addition, the fall time is considerably slower than the rise time, which might affect results. Hence, a modified high-voltage generator that can address these requirements was designed and implemented.

The schematic of the high-voltage square wave unipolar/bipolar generator is illustrated in Figure 2-13. The generator uses QIS4506001-powered IGBTs to generate square pulses of up to 4.5 kV peak-peak. The circuit provides the option to switch between bipolar and unipolar configurations, using a high-voltage vacuum switch. The pulse characteristics do not alter when the output is switched between unipolar and bipolar, as similar topology is used for both modes.
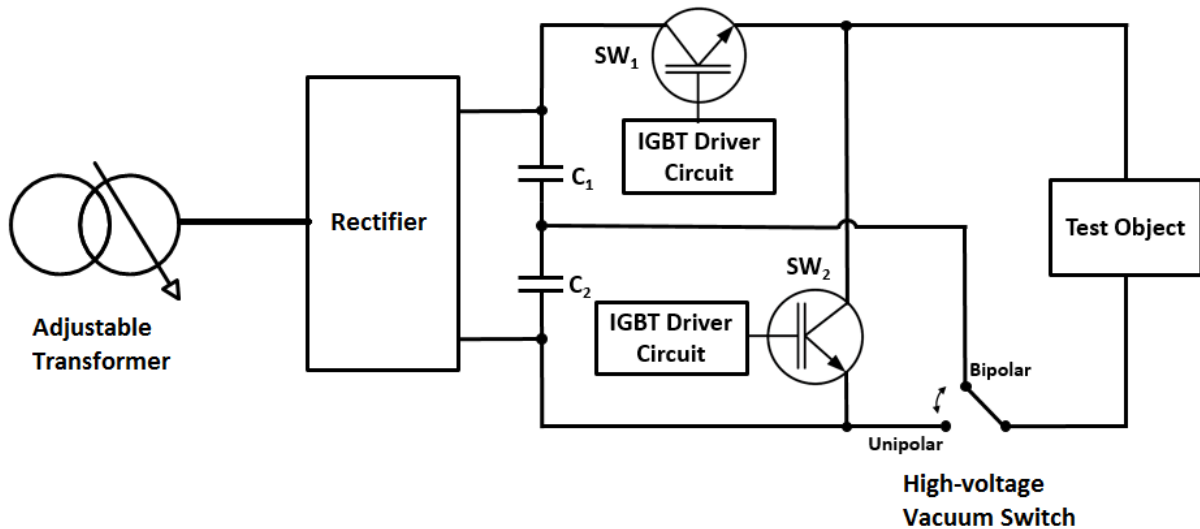
Figure 2-13: Schematic of unipolar/bipolar square wave generator.

In the unipolar mode, the capacitors are in series and connected to a test object via SW1 when SW2 is open; therefore, a voltage equal to the DC charge voltage is applied to the test object. After a short delay, SW1 is turned OFF, and the load is short circuited by SW2, leading to a fast fall time independent of the load. In both modes, each capacitor is charged to half of the input DC voltage. In bipolar mode,

35

during the positive half-cycle, SW1 applies a $+V_{DC}/2$ on the load when SW2 is open. Then SW2 charges the load to $-V_{DC}/2$ in the negative half-cycle when SW1 is open. A typical output voltage and the generator are shown in Figures 2-14 and 2-15, respectively.
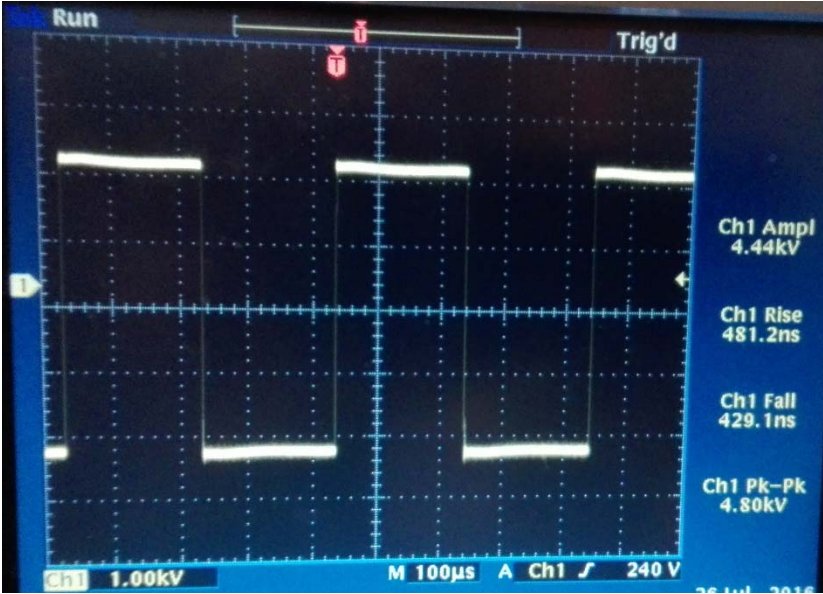
Figure 2-14: Typical output voltage of unipolar/bipolar generator.
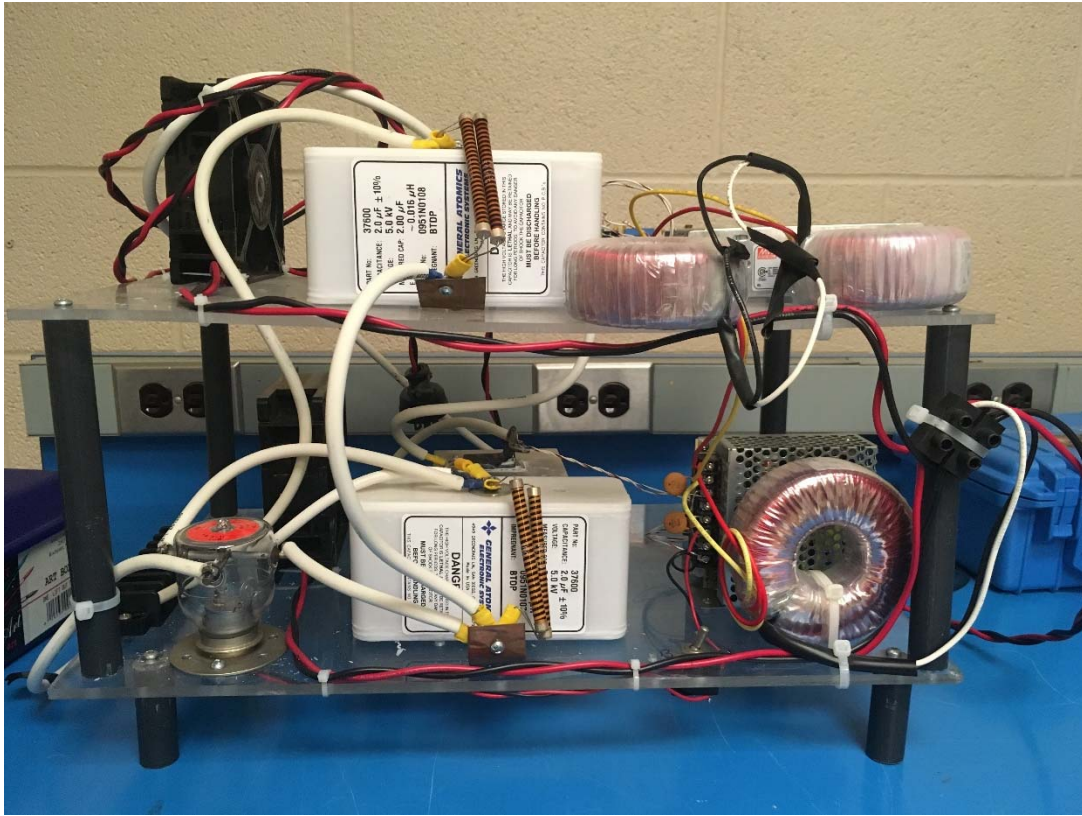
Figure 2-15: High-voltage unipolar/bipolar square wave generator.

2.3.2 Full-Bridge square/PWM generator

A full-bridge inverter is composed of two converter legs, each having two switches. The output terminals are formed by the middle of the converter legs and there is no need for the center-tapped dc voltage source arrangement that was necessary in the previous generator for bipolar mode, unless a neutral point is required. This generator can impose square pulses of up to 9 kV peak-peak. The two switches in each leg receive complementary switching signals to avoid short circuiting of the dc voltage source. Furthermore, due to the finite time that it takes for a switch to turn ON and turn OFF, a short delay time has been implemented between the turn-on signal of the incoming switch and the turn-off signal of the outgoing switch, preventing overlap of the ON periods of the two switches in the same leg. Figure 2-16 shows this generator schematically.
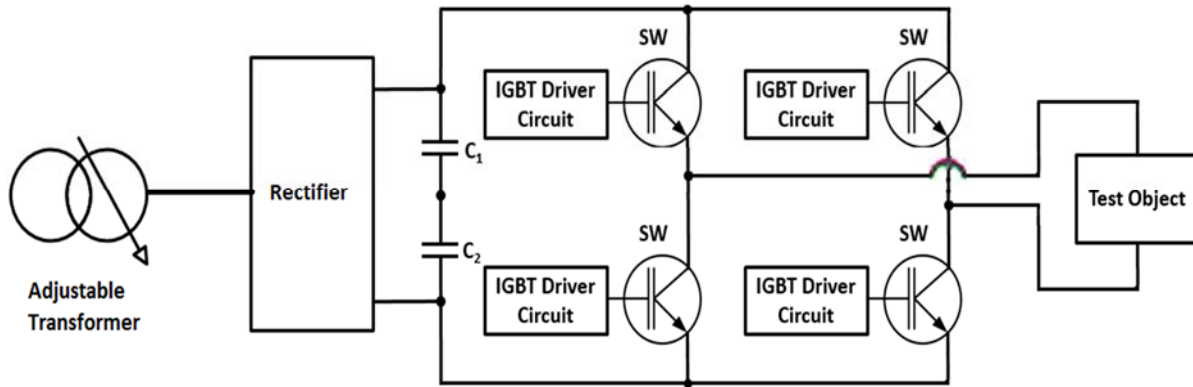
Figure 2-16: Schematic of full-bridge square/PWM generator.

In PWM voltage switching, diagonal switches are treated as a pair and are turned on and off together. A sinusoidal control signal with the same frequency and phase shift angle as in the fundamental component of the desired output voltage is compared with a triangular carrier signal, and the intersection points of the two signals define the beginning of the ON and OFF periods of the switches. Additional information are mentioned in Appendix B. Figures 2-17 and 2-18 show a typical output voltage and the generator, respectively.
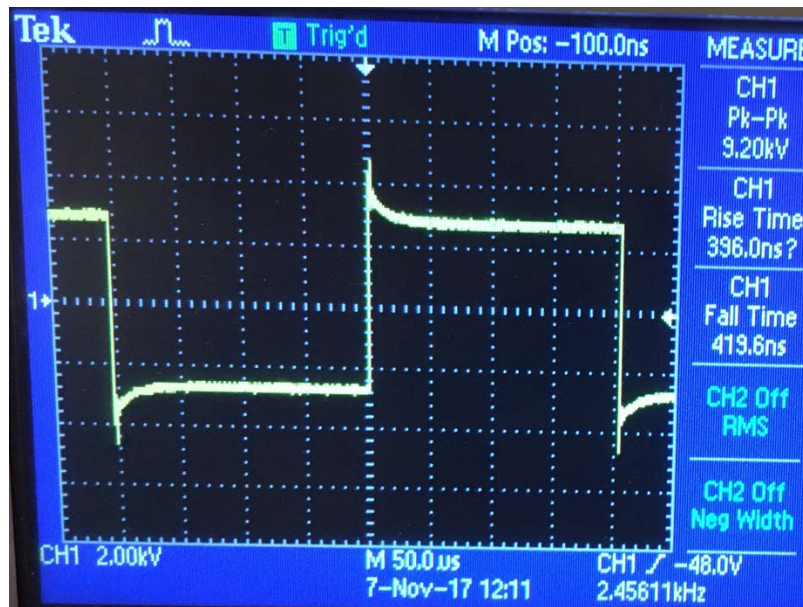
Figure 2-17: Typical output voltage of full-bridge square/PWM generator.

Figure 2-18: High-voltage full-bridge square/PWM generator.

2.4 Numerical Simulations

In the present work, COMSOL$^®$ Multiphysics version 5.3a is used to compute the electric field, voltage, charge accumulation and temperature along the stress grading system in the overhang region. For this purpose, two main application modes, electric quasi-static and heat transfer, are used. In electric quasi-static mode, the coupling between the electric and magnetic fields is neglected. In mathematical terms, where B is the magnetic field, it implies that:

$$\nabla \times E = -\frac{\partial B}{\partial t} = 0 \tag{2.1}$$

meaning that the electric field can be expressed only in terms of the electric voltage, $E = -\nabla V$. Based on Gauss' law $\nabla . D = \rho$, and the constitutive relation $D = \varepsilon_0 E + P = \varepsilon_0 \varepsilon_r E = \varepsilon E$, the program solves (2.2) and (2.3) for the stationary and transient time analyses, respectively:

$$J = \sigma E + J_e \tag{2.2}$$

39

$$J = \sigma E + \frac{\partial D}{\partial t} + J_e \tag{2.3}$$

where J_e is the external current density. In these equations, the conductivity (σ) and relative permittivity (ε_r) can be a linear or nonlinear function of dependent parameters as well as isotropic or fully anisotropic. For heat transfer, the program solves the equations below for the stationary and transient time analyses, respectively:

$$\rho C_p \nabla T + \nabla(-k\nabla T) = Q \tag{2.4}$$

$$\rho C_p \frac{\partial T}{\partial t} + \rho C_p \Delta T + \nabla(-k\nabla T) = Q \tag{2.5}$$

where ρ, C_p, k and Q are mass density, constant pressure specific heat, thermal conductivity and heat transfer rate, respectively.

A coupled electro-thermal FEM simulation using transient time analyses study was used to calculate the temperature profile along the sample. The temperature rise associated with one cycle of pulsed voltage is very small. However, a prolonged transient coupled electro-thermal FEM simulation, for example for one-hour, is impractical because the computation time becomes very long. Running transient time simulation, which uses formulas (2.3) and (2.5), for one, two, three, four and five cycles showed that the average heat source after three cycles was about the same as for four and five cycles. Thus, a three-cycle simulation was selected for this study. Then the average heat source of domains during these cycles was calculated by another time transient ODE interface. This average was used as an incoming heat source in a stationary study of heat transfer to obtain the temperature profile at steady state. Figure 2-19 depicts the geometry of the stress grading system under the 2D axisymmetric module. For the simulation studies, the actual dimensions of a 13.8 kV bar sample were used along with its measured electrical and thermal conductivities.
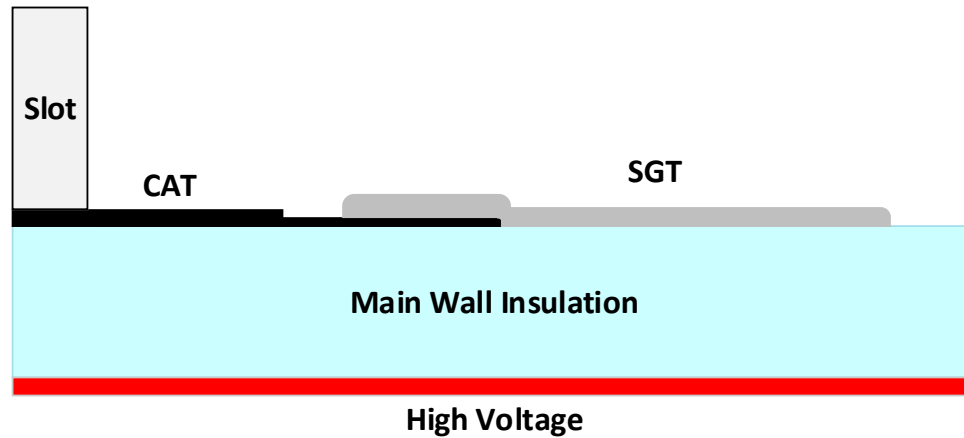
Figure 2-19: Structure of the stress grading system studies using the 2D axisymmetric module in COMSOL® Multiphysics version 5.3a.

For accurate simulation results, the applied pulsed voltage, shown in Figure 2-20, was digitized and used as the input voltage for the simulation. The simulations and measurements were done under a unipolar impulse voltage with a 0.3 µs rise time, 2.5 kHz frequency, 50% duty cycle and an 11.3 kV peak. As previously discussed, different voltage levels exist for ASDs related to the rated voltage of the motors. Development in power electronic switches may lead to use three-level drivers for all MV motors soon. Therefore, in this research, the worst-case scenario, using three-level drivers, was investigated. The thermal simulation considered the aluminum conductor and iron plate (core simulator) as well. In all outer boundaries, the convection heat flux to the ambient was considered. The measurement was done in a laboratory with no forced air circulation; therefore, the convection heat transfer coefficient in the simulation was considered to be 20 [84].
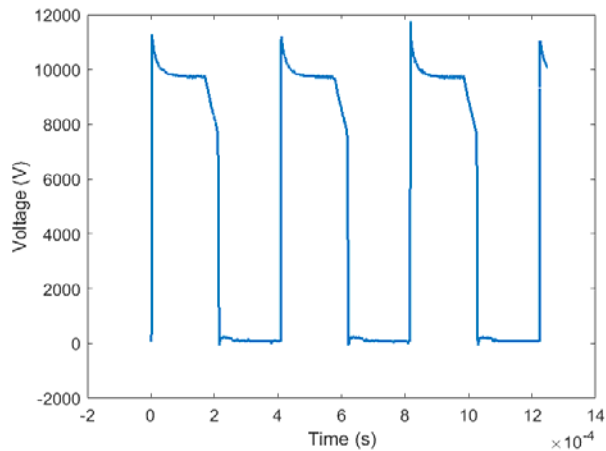
Figure 2-20: A digitized voltage waveform used in simulation studies based on the applied voltage used in experimental studies.

Actual motor coils are rectangular and not axisymmetric. In addition, there is no connection between the CAT and the slot of a stator on the top of the coils. 3D simulations can consider these practical conditions more precisely than 2D ones and provide details and indicate the effect of discontinuity between the CAT and stator connection on the top of the coils. This discontinuity increases the electric field on the CAT at that point. Therefore, for precise assessment, the stress grading system was also modeled in a 3D configuration, with evaluation its electrical and thermal performances. Figure 2-21 shows the 3D configuration used in COMSOL.
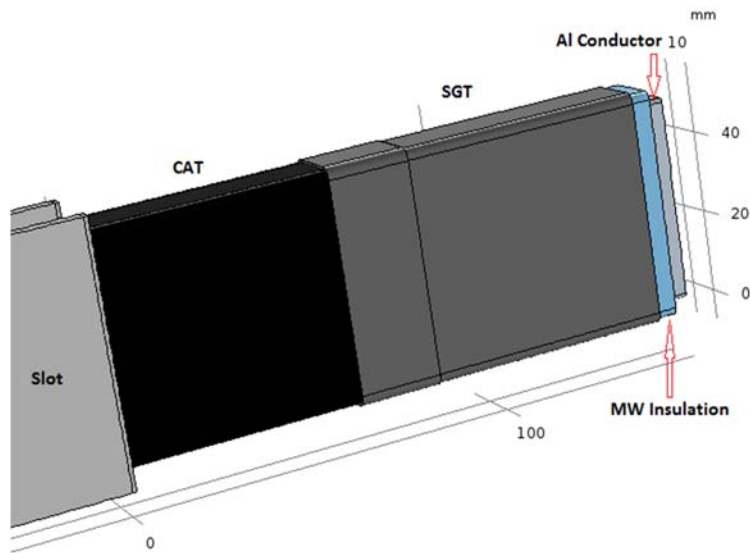
Figure 2-21: Structure of the stress grading system studies using the 3D module in COMSOL.

Chapter 3

Results

3.1 Introduction

This chapter presents experimental and simulation results and the measurements carried out to enable precise modelling of the systems, including the electrical and thermal conductivities done under operating conditions, and the dielectric properties measurement of stress grading materials. To validate the simulation results, the temperature profile along the stress grading system was measured and simulated under pulsed voltage at room temperature and at elevated room and conductor temperatures. In addition, the voltage distribution along the stress grading system under power frequency and high frequency voltages were measured and simulated to compare the results. The chapter also details 2D and 3D coupled electro-thermal FEM simulations and provides the simulation results for a proposed stress grading system. A comprehensive study was performed to check the effect of each parameter of the stress grading system, such as the electrical and thermal conductivities, thickness and length of layers on the temperature and electrical characteristics of this system under pulsed voltages.

3.2 Electrical Conductivity Measurements

The conductivity of the stress grading materials is one of the most important parameters in the modelling. The V-I measurement setup (section 2.2.1) was used to measure the volume and the surface conductivity of the CAT and the SGT after VPI at different temperatures. For each conductivity, several sets of electrodes were used, and the average of these measurements was used.

3.2.1 CAT Surface Electrical Conductivity

Figure 3-1 illustrates the surface conductivity of single-layer and double-layer CAT at 30, 50, 80 and 100ºC outside the slot. It is clear that the surface electrical conductivity is not related to the type of build, as the CAT surface does not change with an increase in the number of layers. As such, the surface electrical conductivity is slightly enhanced when more layers are present due to the effect of VPI, which causes deeper resin penetration in a single-layer CAT.
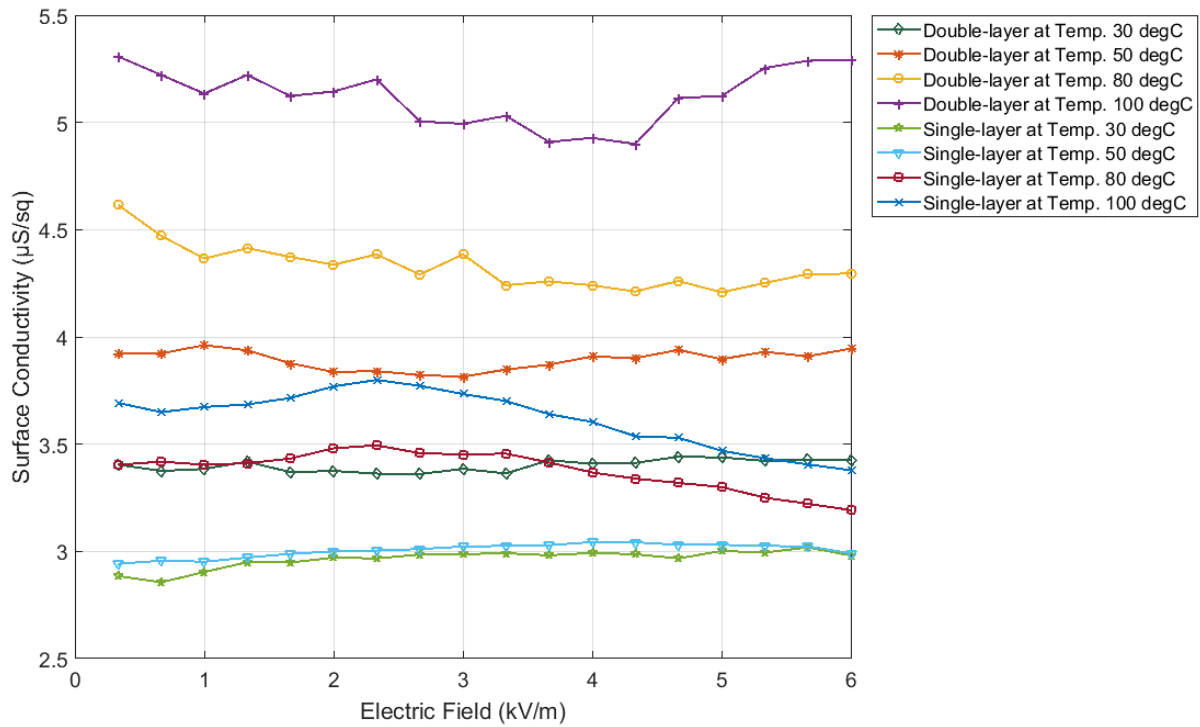
Figure 3-1: CAT surface electrical conductivity of two tape builds outside the slot as a function of electric field at various temperatures.

Figure 3-2 shows the surface electrical conductivity of single-layer and double-layer CAT at 30, 50, 80 and 100°C inside the slot. A comparison of these two figures (Figures 3-1 and 3-2) shows that the VPI process significantly changes the surface electrical conductivity, which is more than one order of magnitude greater inside the slot than outside the slot. Increasing the temperature also enhances the CAT electrical conductivity.
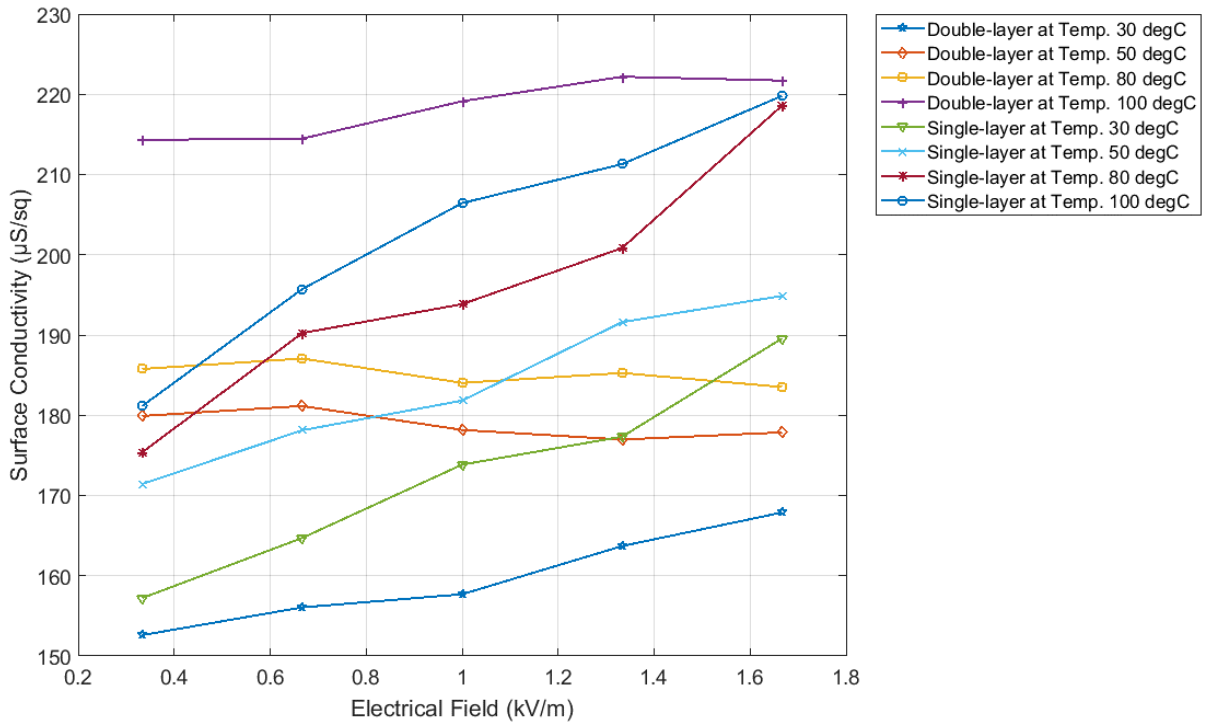
Figure 3-2: CAT surface electrical conductivity of two tape builds inside the slot as a function of electric field at various temperatures.

3.2.2 CAT Volume Electrical Conductivity in the Transverse Direction

Figure 3-3 and Figure 3-4 illustrate the significant differences in the volume electrical conductivity between single-layer and double-layer CAT outside the slot, respectively. The effect of build type on volume electrical conductivity is remarkable, especially outside the slot. The penetration of resin into the single-layer CAT is greater than that into the double-layer; therefore, it makes a significant difference in the electrical conductivity outside the slot. In addition, resin makes the CAT electrical conductivity slightly dependent on the electric field; otherwise the CAT electrical conductivity is independent of the electric field.
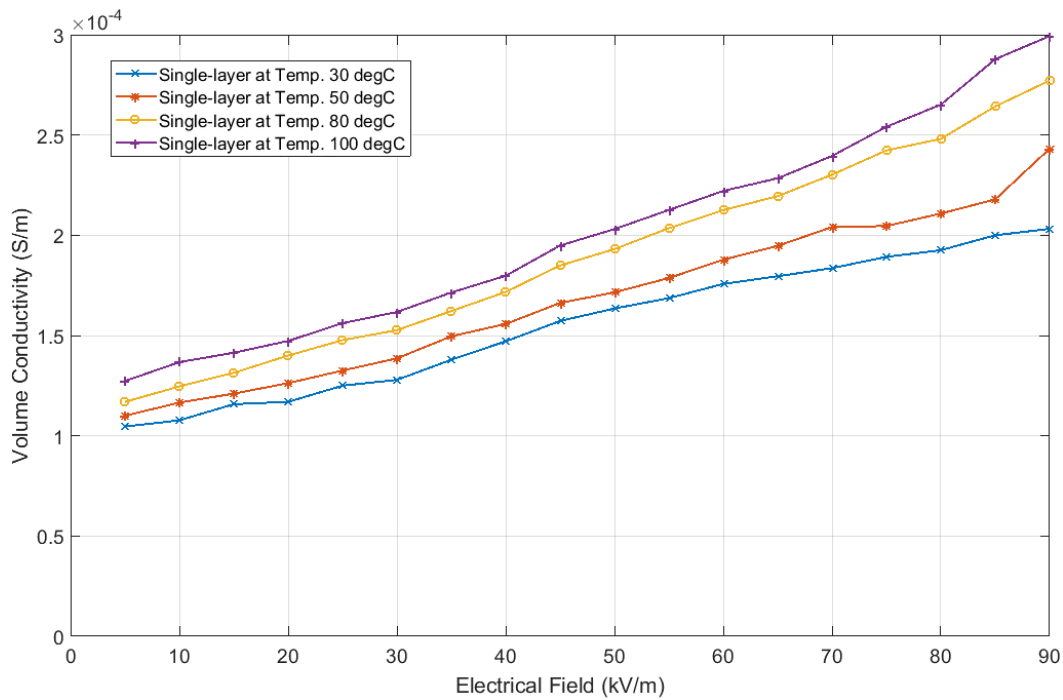
Figure 3-3: CAT volume electrical conductivity in the transverse direction of single-layer outside the slot as a function of electric field at various temperatures.
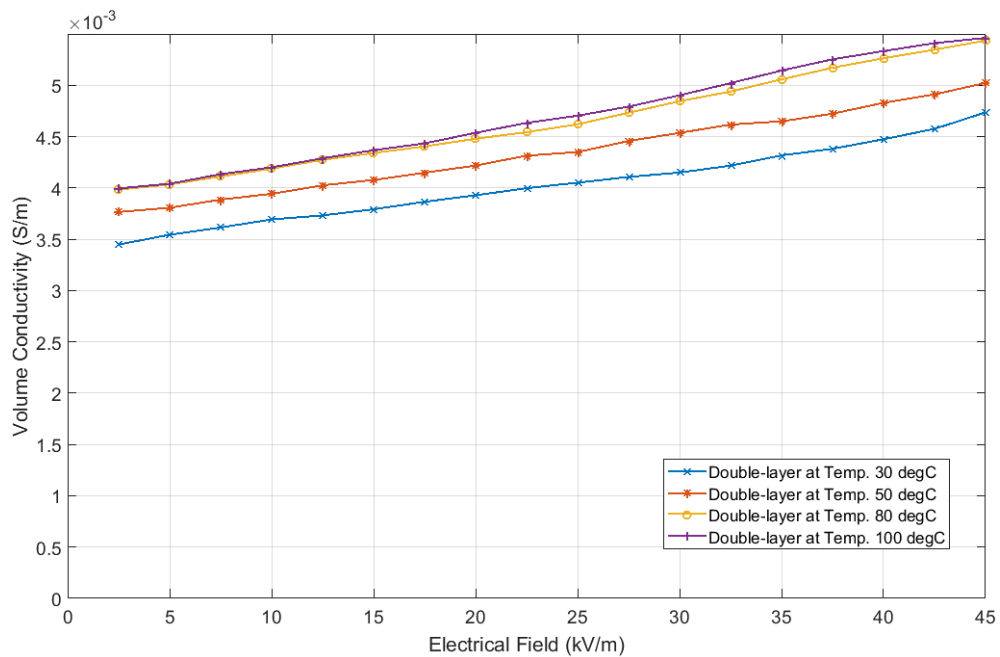
Figure 3-4: CAT volume electrical conductivity in the transverse direction of double-layer outside the slot as a function of electric field at various temperatures.

46

Figure 3-5 shows the volume electrical conductivity in the transverse direction of single-layer and double-layer CAT inside the slot. The volume electrical conductivity of single-layer CAT outside the slot changes from 0.0001 to 0.0002 S/m, but inside the slot is around 0.15 S/m. Therefore, the effect of VPI on the volume electrical conductivity in the transverse cannot be ignored, especially in a single-layer CAT.
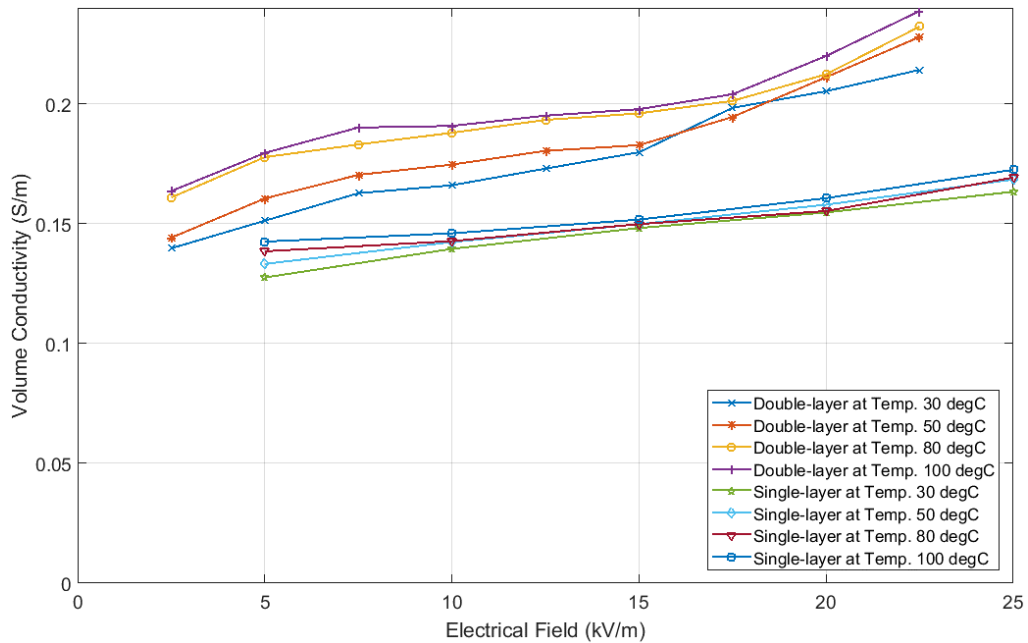
Figure 3-5: CAT volume electrical conductivity in the transverse direction of double-layer inside the slot as a function of electric field at various temperatures.

3.2.3 CAT Volume Electrical Conductivity in the Longitudinal Direction

Figure 3-6 illustrates the longitudinal volume electrical conductivity, which is the most important factor for voltage distribution, of single-layer and double-layer CAT at selected temperatures. Although the conductivity is constant as a function of electric field as expected, increasing the number of layers and temperature increases the conductivity. The effect of VPI on the electrical conductivity can be seen in Figure 3-7. Clearly, the VPI process decreases the electrical conductivity of the layer as the penetration of resin between layers reduces the number of points of contact between layers. On the other hand, this conductivity is not changed as much as surface and transverse conductivities. According to the amount of resin penetration, the VPI process changes the top thin layer of CAT, thereby decreasing the surface conductivity and volume conductivity in the transverse direction of CAT. On the other hand, under the

thin low conductivity layer of CAT, there is still a high conductivity layer of CAT that keeps the volume conductivity in the longitude direction almost constant.
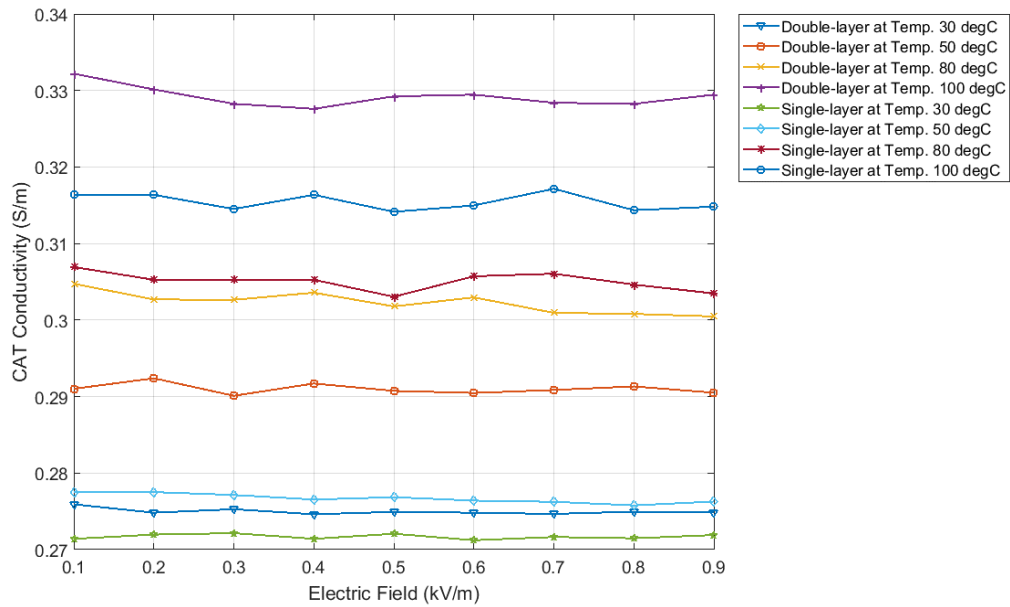
Figure 3-6: Electrical conductivity of single-layer and double-layer CAT as a function of electric field and temperature outside the slot.
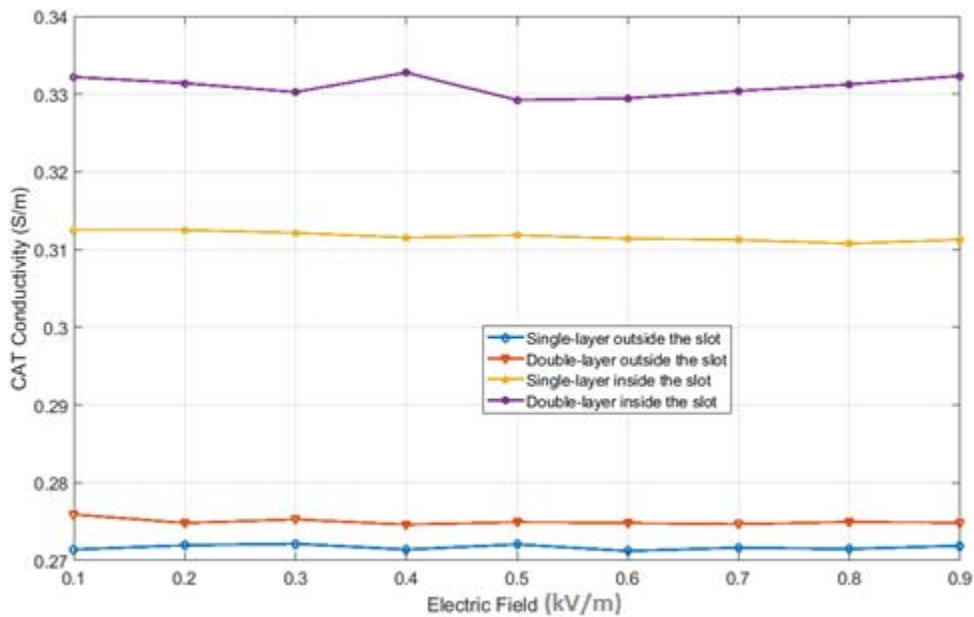
Figure 3-7: CAT volume Electrical conductivity in the longitudinal direction as a function of electric field and VPI process (inside and outside the slot) at 30°C.

3.2.4 SGT Electrical Conductivity

3.2.4.1 SiC Based SG

As previously discussed, the conductivity of the SGT cannot be measured in a high electrical field by DC voltage above 0.6 kV/mm due to excessive temperature rise in the SGT material. Therefore, the measurement was carried out under pulse conditions. Figures 3-8 and 3-9 illustrate a sample of voltage-current measurement and the conductivity as a function of the electric field, respectively. The sampling rate of the oscilloscope is 0.4 µs, and as these two figures show, the data has a lot of high frequency noise. MATLAB® software was used to filter the data for a smoother plot, and to allow the fitted function of the conductivity to be found. Figure 3-9 also shows the filtered data. Finally, the exponential fit function of MATLAB was used to find the exponential formula of the conductivity as a function of the electric field.
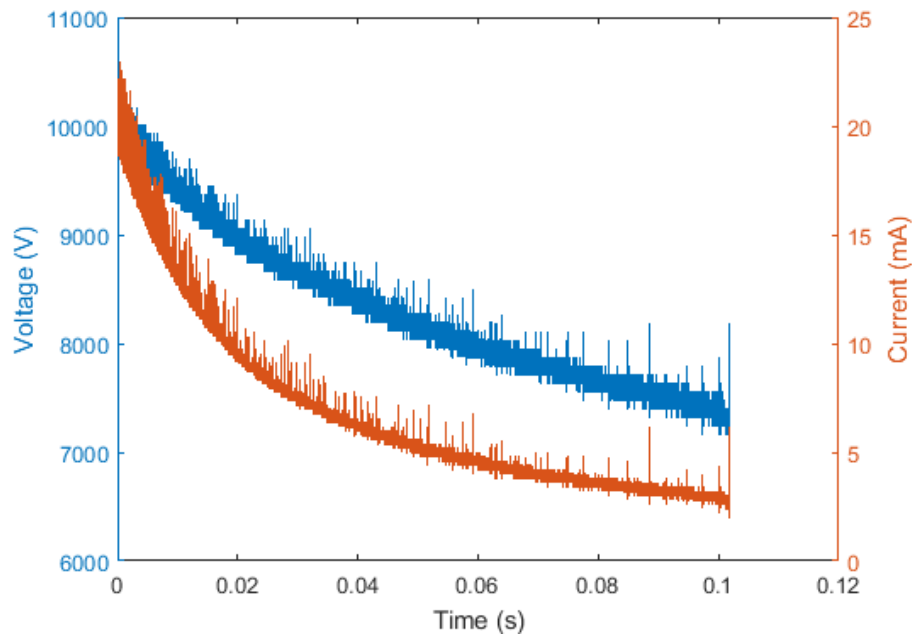
Figure 3-8: Voltage across and current thorough SGT sample as a function of time.
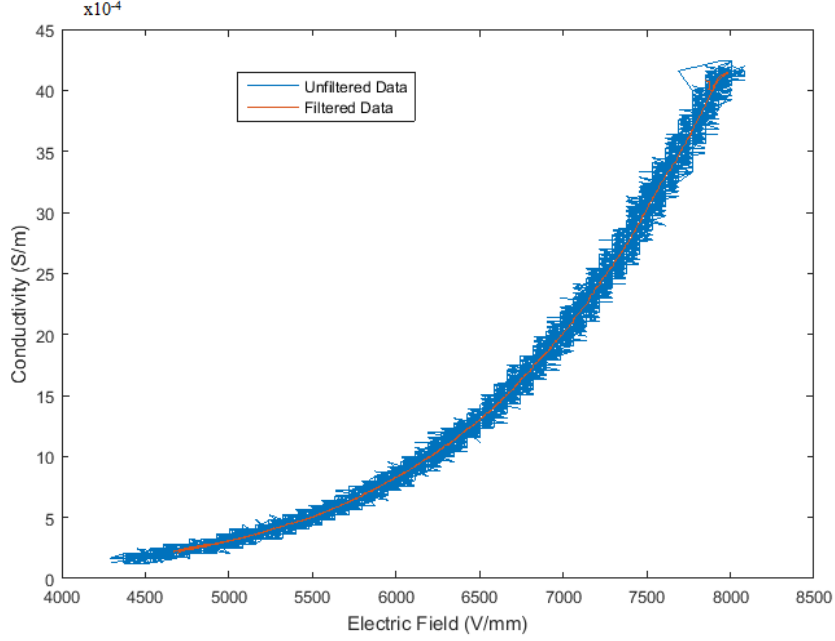
Figure 3-9: The electrical conductivity as a function of the electric field for unfiltered and filtered data.

Figure 3-10 shows the conductivity of single-layer SGT as a function of the electric field at different temperatures. The electrical conductivity is considered to be an exponential function. Thus,

$$\sigma = \sigma_0 \times exp^{k \times E} \tag{3.1}$$

Therefore, the coefficients σ_0 and k can be obtained as a function of temperature. Thus, the electrical conductivity of the single-layer SGT can be written as:

$$\sigma = (-4 \times 10^{-8} \times T + 5 \times 10^{-6}) \times exp^{(2 \times 10^{-5} \times T + 0.0061) \times E} \quad (S/m) \tag{3.2}$$

where T is temperature in degrees Celsius and E is the electric field in kV/m.
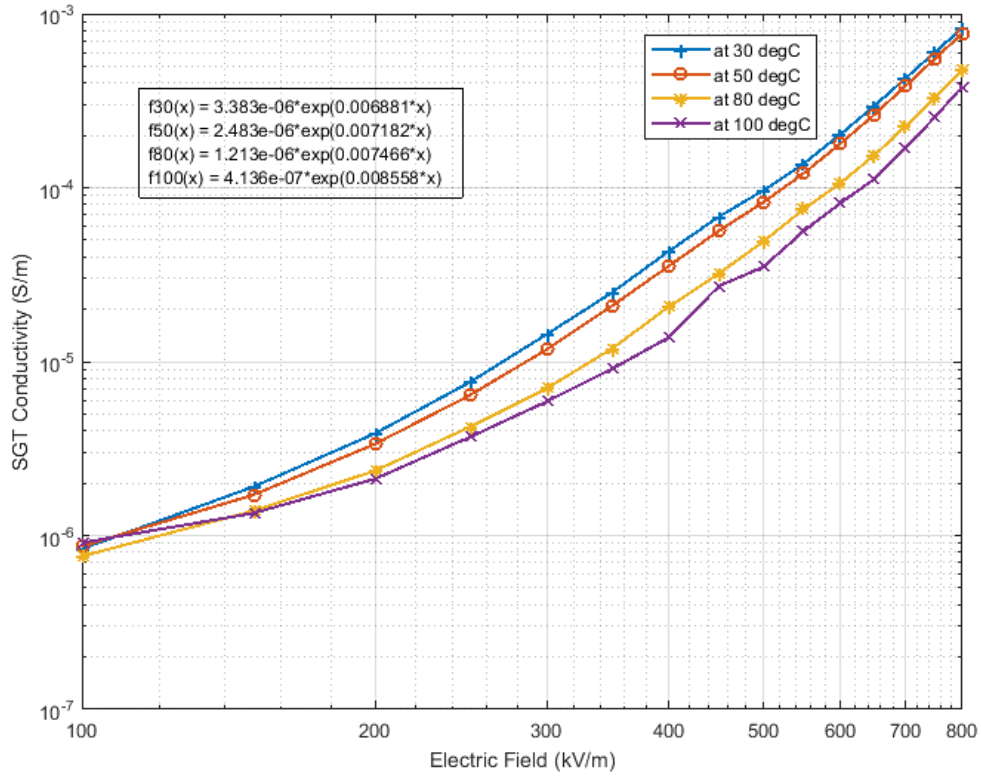
Figure 3-10: The SGT electrical conductivity as a function of the electric field for single-layer.

Figure 3-11 shows the conductivity of the double-layer SGT as a function of the electric field at various temperatures. By considering the exponential formula for the conductivity, the coefficients σ_0 and k can be obtained as a function of the temperature. So the expression of electrical conductivity of the double-layer SGT can be written as:

$$\sigma = (-9 \times 10^{-8} \times T + 1 \times 10^{-5}) \times exp^{(1 \times 10^{-5} \times T + 0.0057) \times E} \quad (S/m) \tag{3.3}$$

where T is temperature in degrees Celsius and E is the electric field in V/mm.
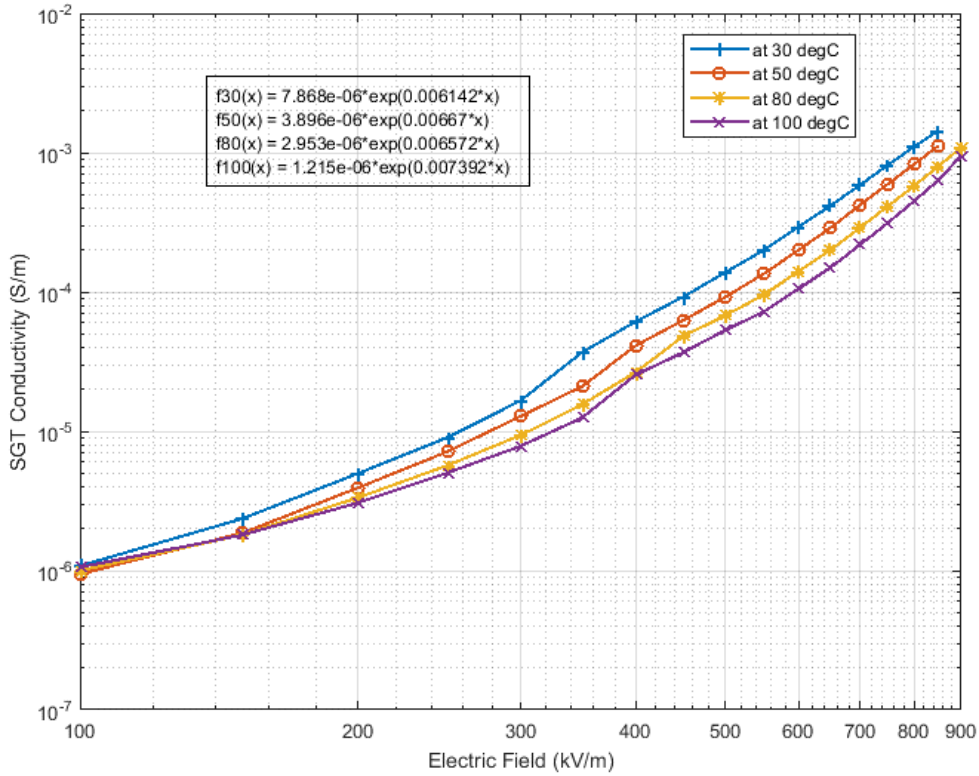
Figure 3-11: The SGT electrical conductivity as a function of the electric field for double-layer.

3.2.4.2 Micro-Varistor Based SG

The conductivity of micro-varistor-based materials was also measured, using cable termination samples made of micro-varistor materials. The same measuring procedures described earlier was carried out for all samples. Figure 3-12 shows the measured voltage and current for one sample with considerable high frequency noise. MATLAB's filter function was used to reduce the noise, and its fit function was used to find the exponential function for conductivity as a function of electric field. Figure 3-13 shows the conductivity as a function of the electric field for unfiltered and filtered data. The conductivity formula of the micro-varistor based stress grading can be written as:

$$\sigma = 6.933 \times 10^{-9} \times exp^{8.403 \times 10^{-6} \times E} \quad (S/m)$$

$$(3.4)$$

where E is the electric field in V/m.
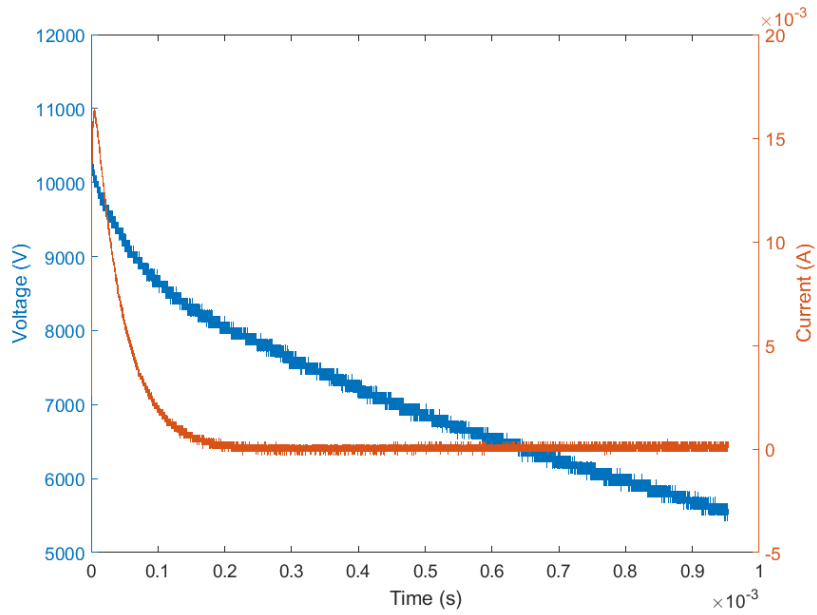
Figure 3-12: Voltage across and current thorough micro-varistor based sample as a function of time.
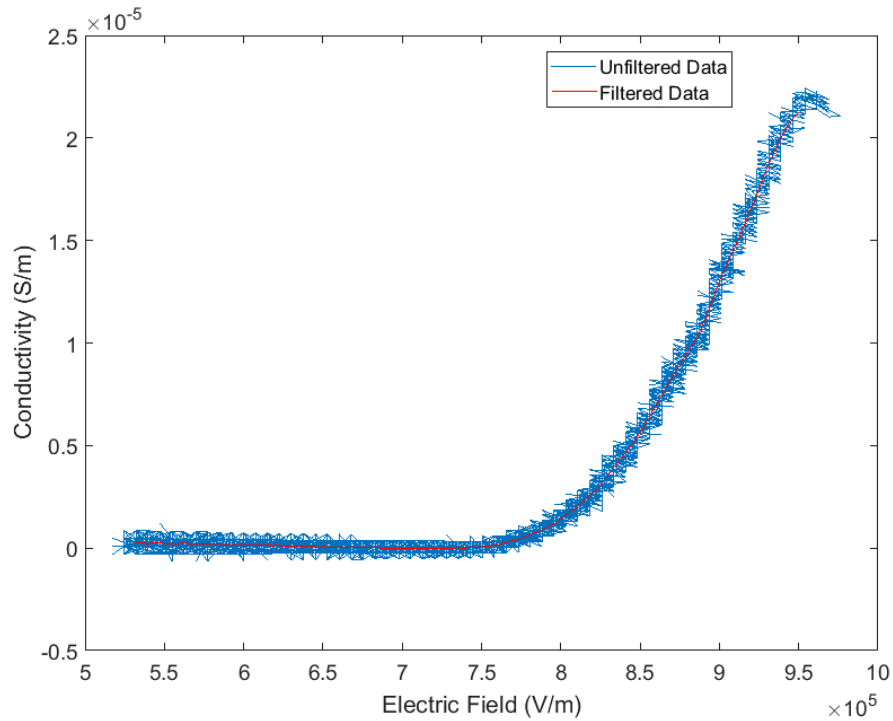
Figure 3-13: The electrical conductivity of micro-varistor based stress grading as a function of the electric field for unfiltered and filtered data.

53

3.3 Thermal Conductivity Measurements

The thermal conductivities of the CAT, SGT and main wall insulation were measured in accordance with ISO 22007-2:2015 [71]. The method has been described previously and the average of two samples was used in the simulation. The measurements were performed at room temperature. Additionally, the thermal conductivities of insulation, conductive layer and stress grading layer of cable termination were measured. Table 3-1 shows the thermal conductivities measured and used in the simulation studies.

Table 3-1: Thermal conductivity of materials at room temperature.

Material	Thermal Conductivity (W/m.K)
Main Wall Insulation	0.52
Conductive Armor Tape	0.46
Stress Grading Tape	0.39
Cable Insulation	0.82
Semi-Conductive Layer	0.8
Stress Grading Layer	0.2

3.4 Relative Permittivity Measurements

The relative permittivities of SGT and main wall insulation measurements, performed according to section 2.2.3, show that these values are almost fixed in the frequency range between 1 kHz to 10 kHz. Table 3-2 shows this value for all materials used in the simulations.

Table 3-2: Relative permittivity of materials at room temperature.

Material	Relative Permittivity
Main Wall Insulation	2
Conductive Armor Tape	100
Stress Grading Tape	15

The dielectric constant of main wall insulation is between 3 and 3.5 under 50/60 Hz. However, the measurements on our samples ware done under high frequency because the switching frequency is 2.5

kHz with 300 ns rise time, which has very high frequency components. The dielectric constant value used in our simulation work is the measured value for the bar-samples used in the experimental work and the value ranged between 2 and 2.5; thus 2 was selected.

3.5 Surface Voltage Distribution Measurement and Simulation

A non-contact electrostatic voltmeter was used for surface voltage measurement. The surface voltage under power frequency was measured by sliding the electrostatic probe in the longitudinal direction of the stress grading region in 1 mm steps. The voltmeter can measure ± 20 kV at DC, so the range of the measuring voltage is decreased in power frequency voltage condition. Therefore, 9.6 kV peak-to-peak voltage at power frequency was applied to the sample, and the peak-to-peak voltage was measured every 1 mm along the sample.

The geometry of the stress grading system used in the FEM modelling is illustrated in Figure 3-14. The actual dimensions of a 13.8 kV bar sample were used along with the corresponding measured conductivity of stress grading materials. Figure 3-15 shows the measured and simulated surface voltage distributions. The hump in the voltage profile of the simulation and measurement is a result of charge accumulation in the SGT region; that is the low conductivity of the SGT means that accumulated charge has a time constant longer than the period of the applied voltage. Therefore, as the charge does not completely dissipate, the voltage during the next cycle becomes additive.
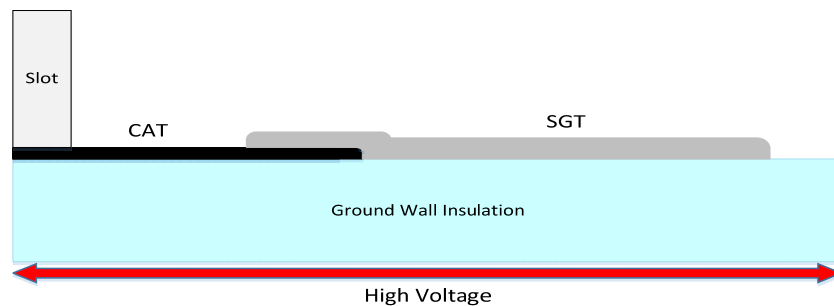
Figure 3-14: Structure of the stress grading system used in this study using COMSOL®.
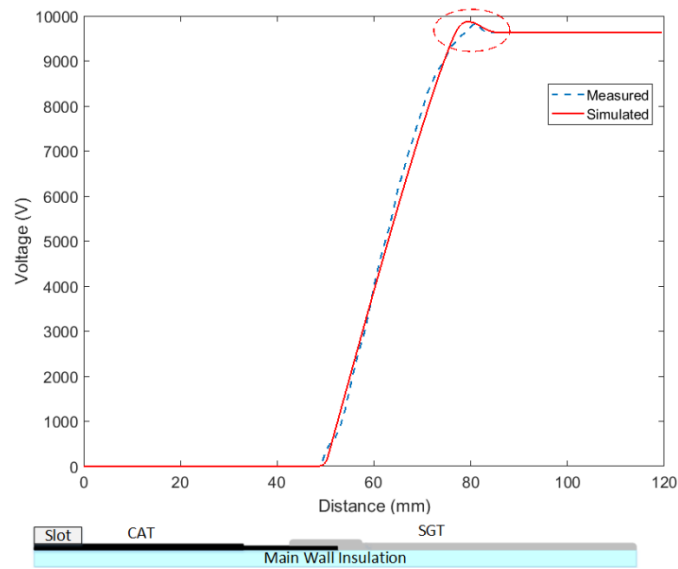
Figure 3-15: Measured and Simulated voltage distribution along sample with 9.6 kV peak-to-peak @ 60 Hz.

3.6 Surface Temperature Measurements

Evaluating the electrical performance of stress grading systems under repetitive steep front pulses is not possible using the electrostatic voltmeter. On the other hand, it is possible to measure the surface temperature which is another important criterion for evaluating the thermal performance of stress grading systems under different operating conditions. Thus, the surface temperatures in the stress grading region of the samples were measured.

3.6.1 Surface Temperature Measurements under High Frequency Sinusoidal Voltage

A high frequency sinusoidal voltage was applied to the sample for more than two hours to stabilize the temperature profile. Figure 3-16 shows the circuit used to generate this voltage. The selected frequencies were 1 and 2 kHz. The tests were done at room temperature. The limitation of the high frequency transformer necessitated a peak voltage of 4.3 kV. Accordingly, this voltage was also selected for the simulation study.
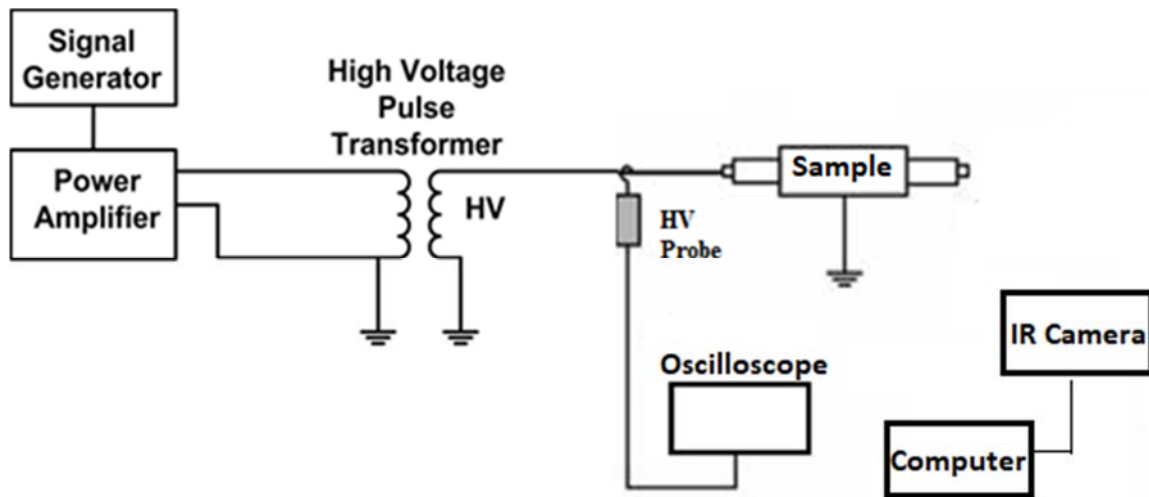
Figure 3-16: Circuit used to generate the high frequency sinusoidal voltage.

Figure 3-17 (a) and (b) show the temperatures of the sample at 1 kHz and 2 kHz, respectively. The measured and simulation temperature profiles along the stress grading system at 1 kHz and 2 kHz sinusoidal voltage are illustrated in Figures 3-18 and 3-19, respectively.
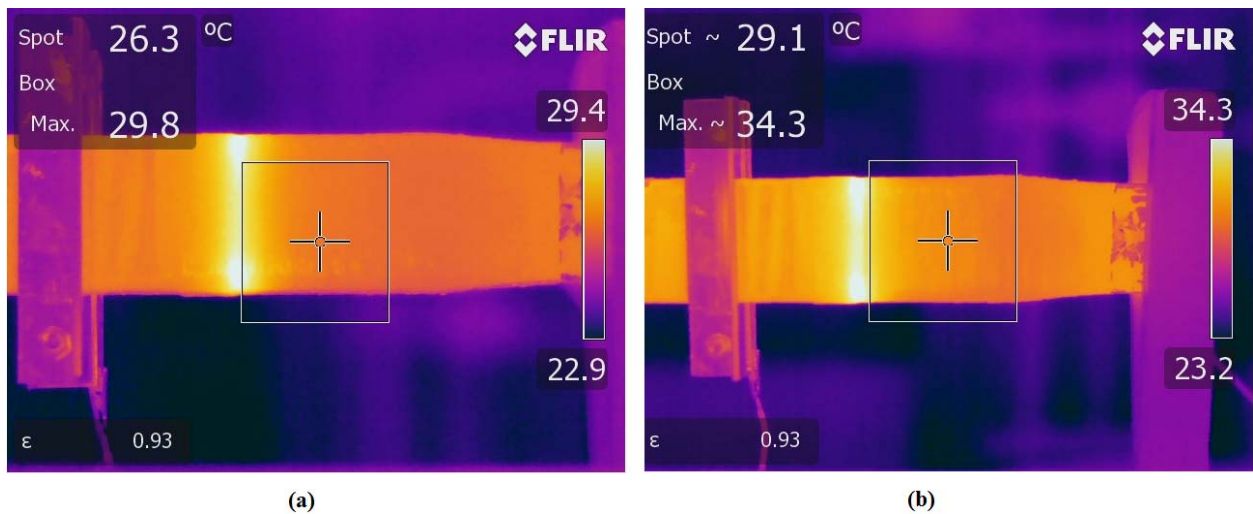
Figure 3-17: Temperature profile along the stress grading system, (a) at 1 kHz and (b) at 2 kHz.
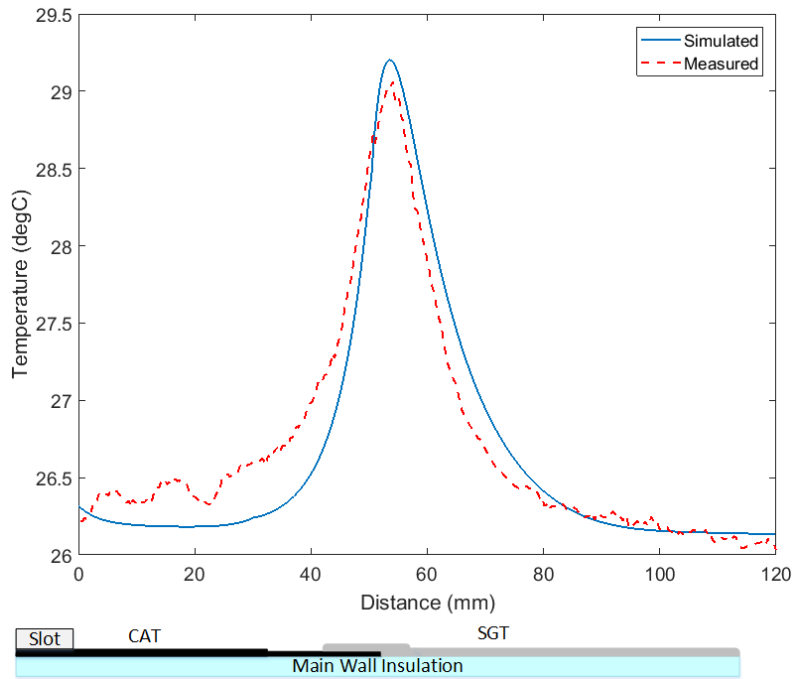
Figure 3-18: The measured and simulation temperature profiles along the stress grading system at 1 kHz and 4.3 kV.
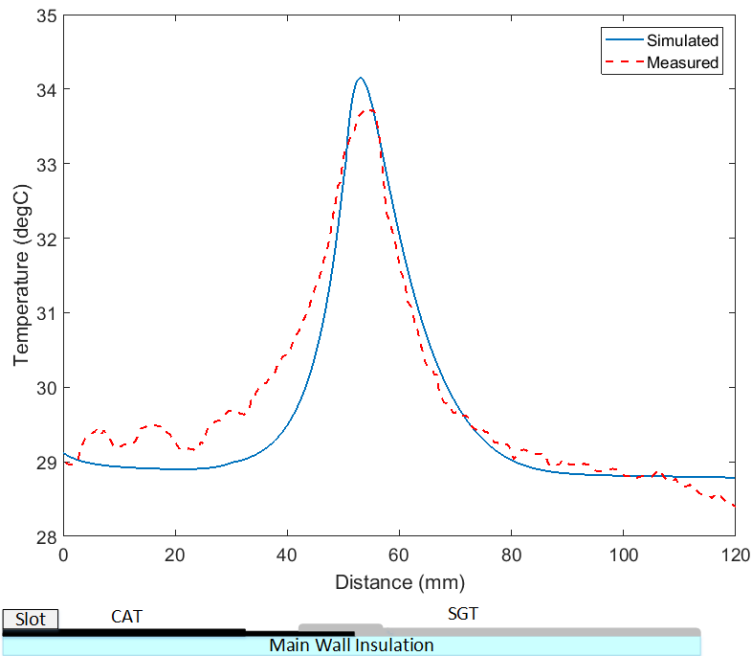
Figure 3-19: The measured and simulation temperature profiles along the stress grading system at 2 kHz and 4.3 kV.

3.6.2 Surface Temperature Measurements under Pulsed Voltage

The temperature profile along the stress grading system was measured and simulated under a pulsed voltage. To stabilize the temperature profile, a 2.5 kHz, 11.3 kV peak pulsed voltage was applied to the bar for two hours at room temperature. The measured surface temperatures of the stress grading system on the samples can be seen in Figure 3-20.
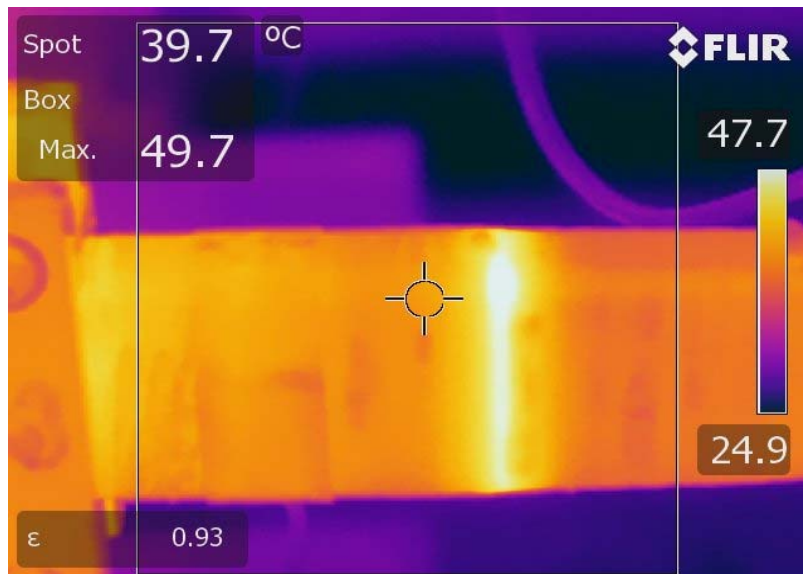
Figure 3-20: Measured temperature profile along the stress grading system under pulsed voltage.

As discussed, for accurate simulation results, the actual applied pulsed voltage was implemented as the input voltage for the simulation. For thermal simulation, the copper conductor and steel plate (the core simulator) were considered. The thermal capacities for the CAT, SGT and main wall insulation were considered to be 800, 800 and 500, respectively [24]. The simulated profile of the temperature on the surface of the stress grading system is presented in Figure 3-21. For comparison, the measured and simulated profiles of the temperature along the stress grading system under the pulsed voltage are indicated in Figure 3-22, which shows good agreement between the simulated and measured results.
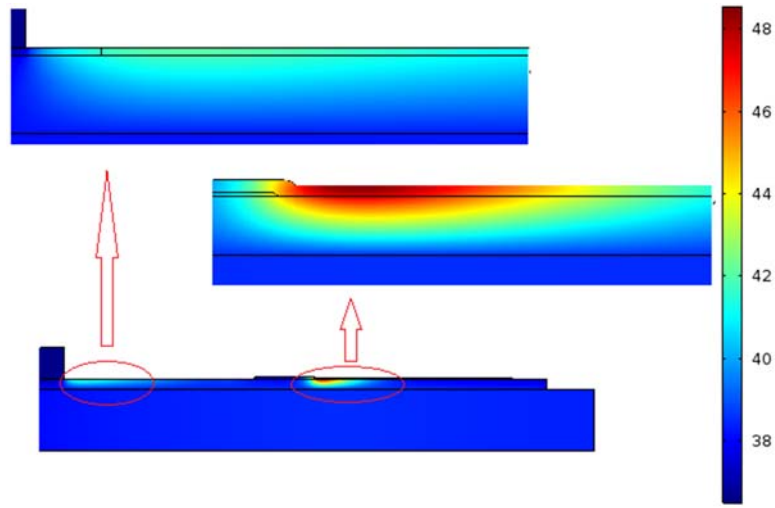
Figure 3-21: Simulated temperature profile along the stress grading system under pulsed voltage in 2D axisymmetric.
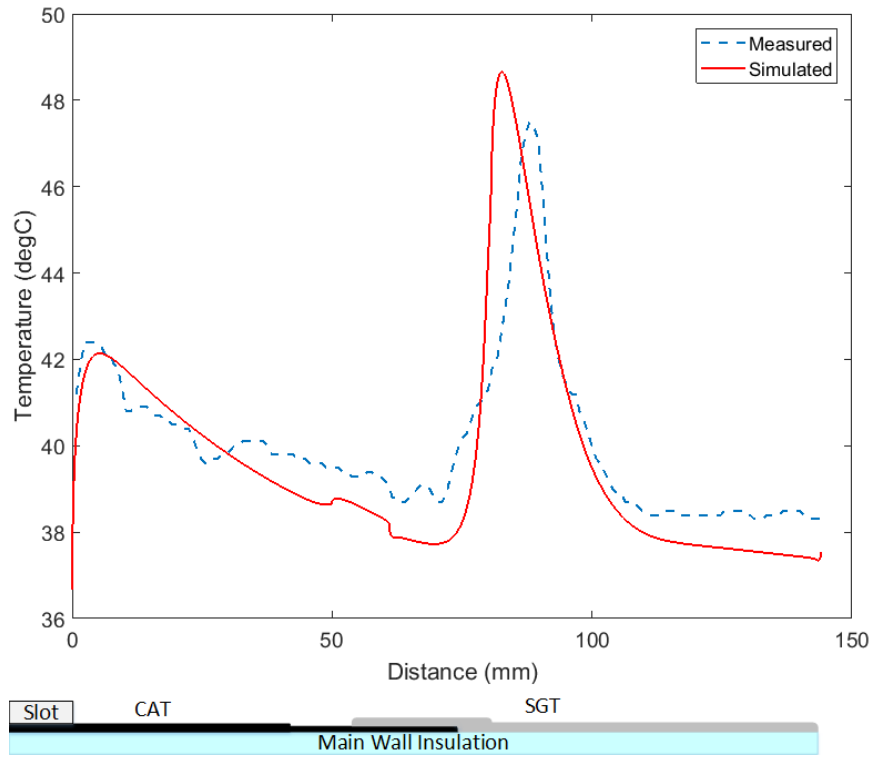
Figure 3-22: The measured and simulated temperature profiles along the surface of the stress grading system under pulsed voltage.

Measurement and simulation studies were also conducted at a high temperature (Figure 3-23). To increase the temperature, current was circulated through the aluminum bar using two current transformers in the reverse connection. Once the temperature stabilized, the same pulsed voltage was applied to the sample while the current was still circulating through the bar. The simulation and measurement results show a similarity. The rise in the SGT temperature under the elevated temperature was approximately 8 °C, which is less than that at room temperature (around 24 °C). This could be due to the increased heat convection to the air at a high temperature, which reduces temperature rise. But it still has a harmful effect on the life of the insulation system. Additionally, room temperature was increased to 35 °C, and the previous step was run. Figure 3-24 illustrates the measured and simulated temperature with circulating current and at an elevated room temperature of 35 °C.
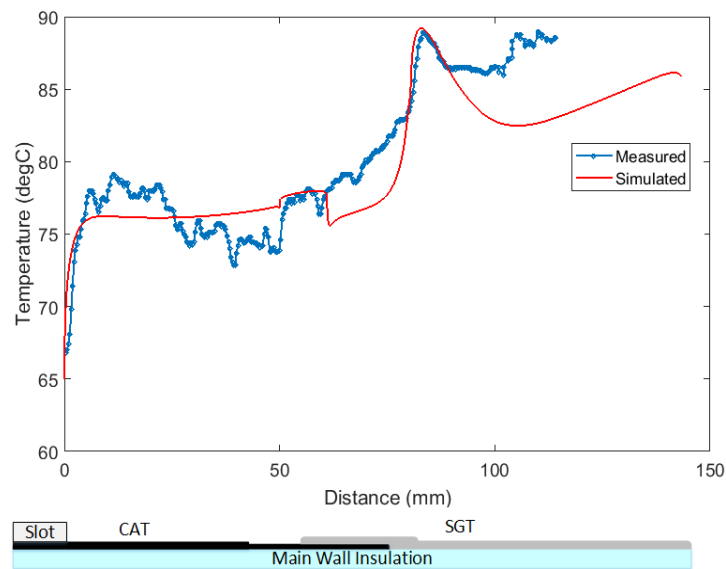
Figure 3-23: The measured and simulated temperature profiles along the surface of the stress grading system under pulsed voltage at high temperature.
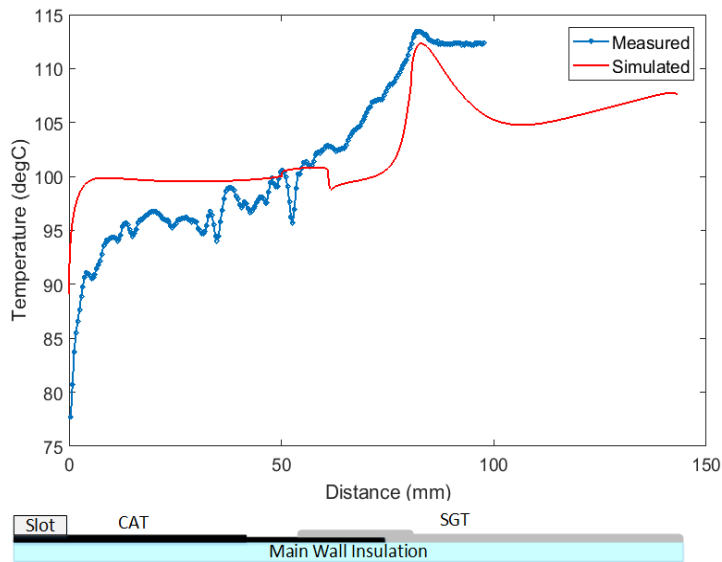
Figure 3-24: The measured and simulated temperature profiles of the stress grading system with circulating current and at elevated room temperature.

The stress grading system was also modeled in a 3D configuration to evaluate its electrical and thermal performances. Figure 3-25 shows the 3D structure of the stress grading system used in COMSOL. To verify this numerical simulation, all dimensions and material properties were considered to be the same as in an actual coil. The system was simulated and measured under a unipolar pulsed voltage with a 0.3 μs rise time and an 11.3 kV peak. The measured and simulated temperature profiles, shown in Figure 3-26, verify the simulation results.
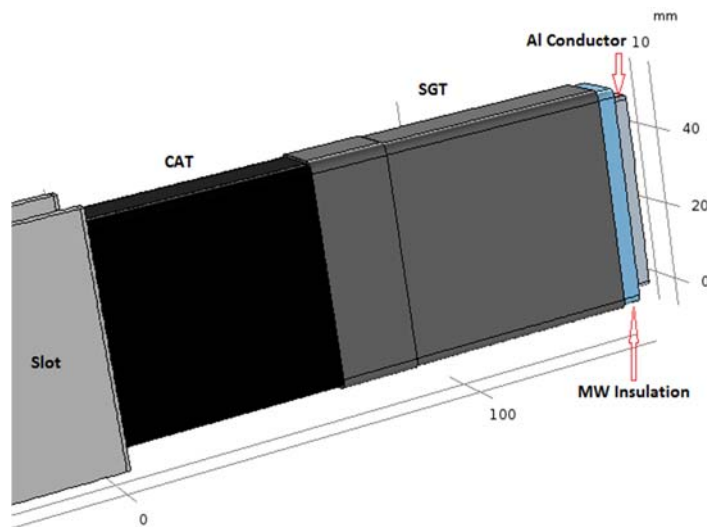
Figure 3-25: 3D structure of the stress grading system used in this study using COMSOL.

62

(a)
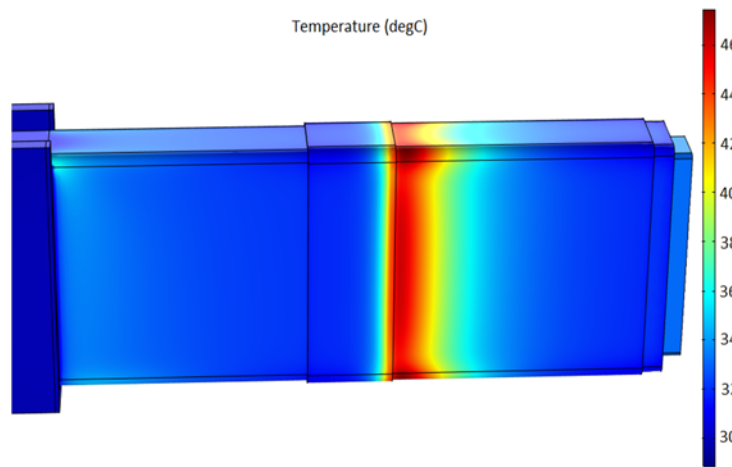
(b)

Figure 3-26: (a) Measured and (b) simulated temperature profiles along the stress grading system under pulsed voltage.

3.7 Stress Grading System Characteristics

This section describes the investigation into the effect of stress grading system parameters on the electrical and thermal characteristics of this system. The purpose is to reduce the temperature rise in the system when the maximum electric field is below an acceptable value. Figure 3-27 shows the chart that illustrates parameters studied in this thesis. Additionally, the effect of adding floating foils on the surface of the SGT is investigated and results are shown in Appendix A. For simulation studies, the measured electrical and thermal conductivities of the stress grading materials after VPI were implemented. Table 3-3 shows the parameters used in the simulations.
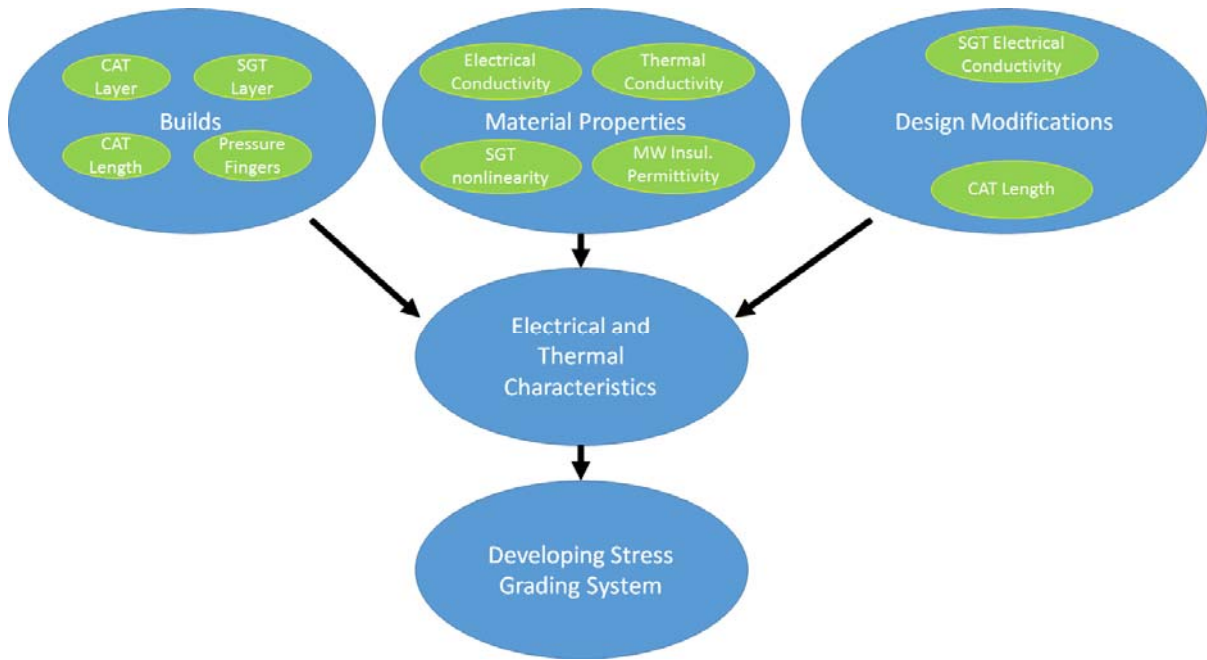
Figure 3-27: Chart of parameters studied in this thesis.

Table 3-3: Properties of materials used in the simulations.

Material	Thermal Conductivity (W/m.K)	Electrical Conductivity (S/m)	Relative Permittivity	Heat Capacity (J/kg.K)
Main wall insulation	0.52	2×10^{-15}	2	500
CAT	0.46	0.32	100	800
SGT	0.39	3.38×10^{-6} $\exp(6.88 \times 10^{-6} \, xE)$	15	800
Aluminum	238	3.77×10^{7}		900
Steel	76.2	1.1×10^{7}		440

3.7.1 Effect of the CAT Conductivity

Three different CAT conductivity values were selected for investigation with respect to their effects on the electrical and thermal characteristics of the stress grading system: 0.1, 0.3, and 1.0 S/m. The distributions of the voltage and electric field along the surface of the overhang region at the end of the pulsed voltage rise time are shown in Figures 3-28 and 3-29, respectively.
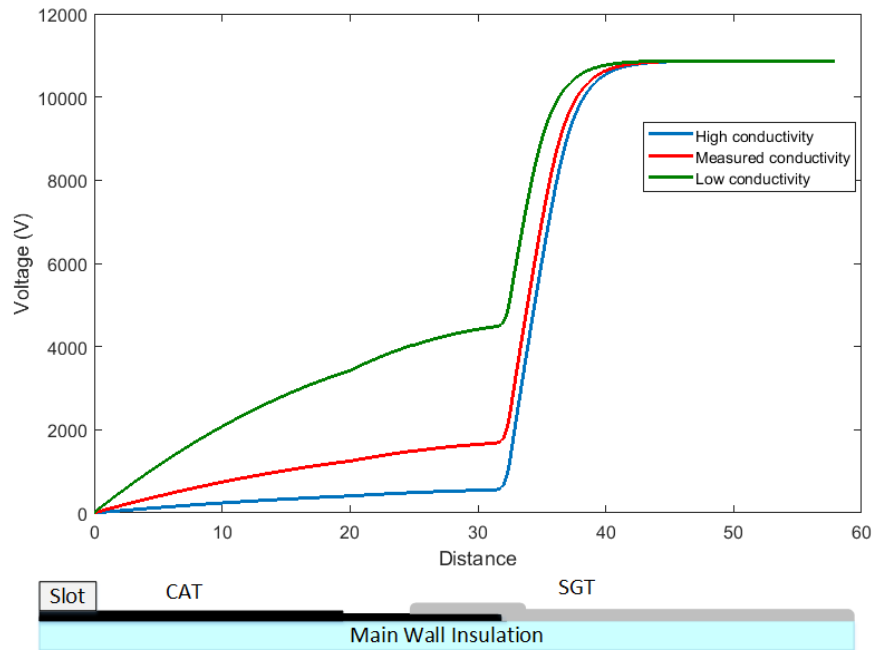
Figure 3-28: Voltage distribution along the surface of the stress grading system for three CAT conductivity conditions at the end of the pulsed voltage rise time.
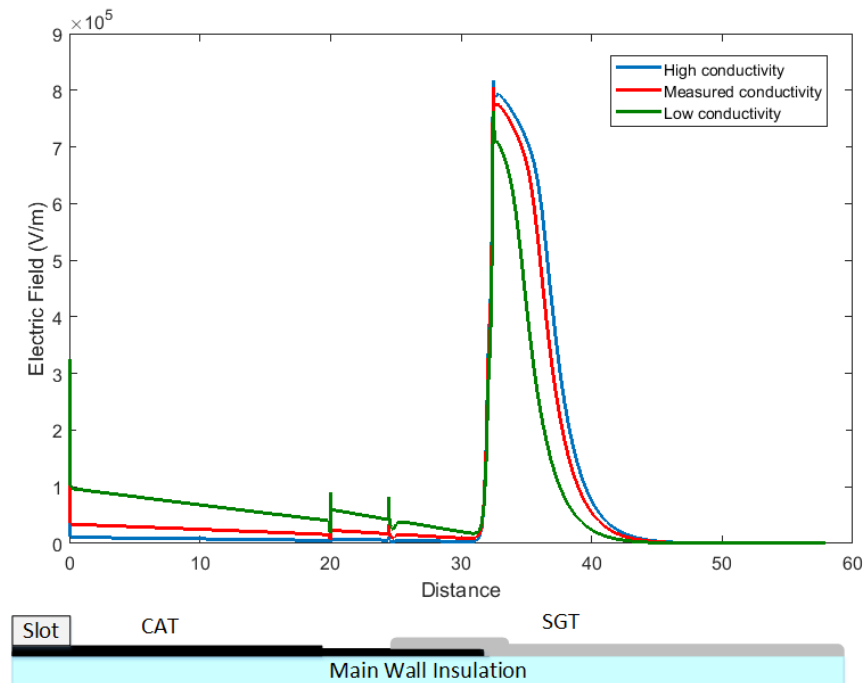
Figure 3-29: Electric field distribution along the surface of the stress grading system for three CAT conductivity conditions at the end of the pulsed voltage rise time.

Figure 3-30 provides the profiles of the temperatures along the stress grading system for the three selected CAT electrical conductivity conditions. It is clear that the temperature of the stress grading system becomes elevated with decreases in the CAT electrical conductivity. An additional observation is that the movement of the peak of the temperature profile, from the SGT region to the CAT region, which occurs with reduced CAT electrical conductivity, leads to deterioration of the CAT at the slot exit.
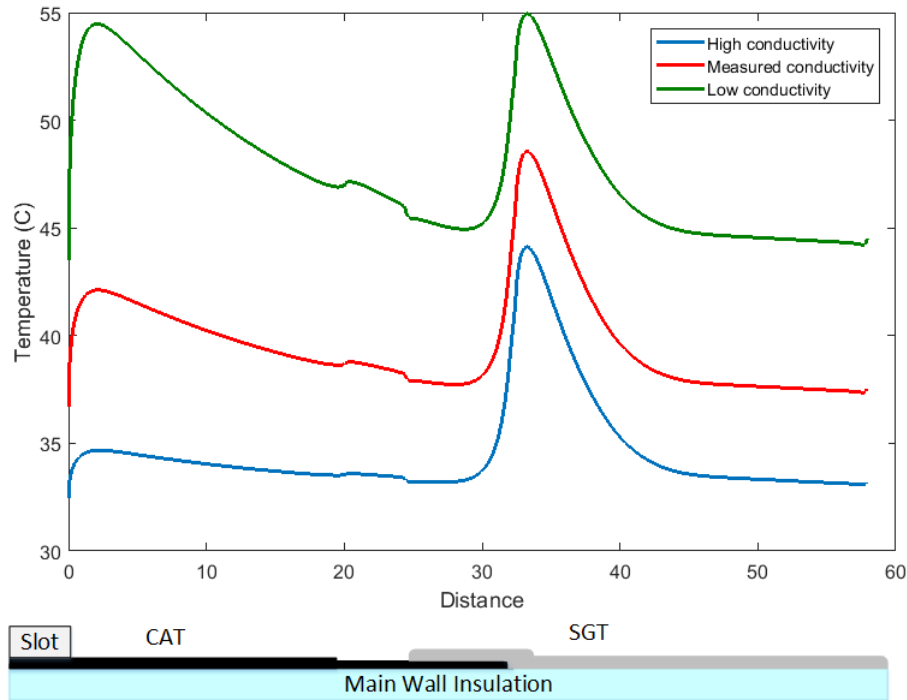
Figure 3-30: Temperature profile along the surface of the stress grading system for three CAT conductivity conditions.

Results show that increasing the CAT electrical conductivity has numerous benefits, but because CAT is also used inside the slots, and raising this conductivity can short circuit the core laminated sheets and increase eddy losses. Enhancing the electrical conductivity can also increase the electric field at the SGT region to a level greater than the threshold so that PDs can occur in this region.

Figure 3-31 indicates the average heat production during one cycle of the pulsed voltage for the three CAT electrical conductivity conditions. Heat production in the CAT is clearly reduced when the CAT electrical conductivity is increased. At the lowest CAT electrical conductivity levels, the peak

value for heat production is doubled. This peak is slightly larger in high CAT electrical conductivity conditions at the SGT due to the enhanced electric field in this region, as shown in Figure 3-29.
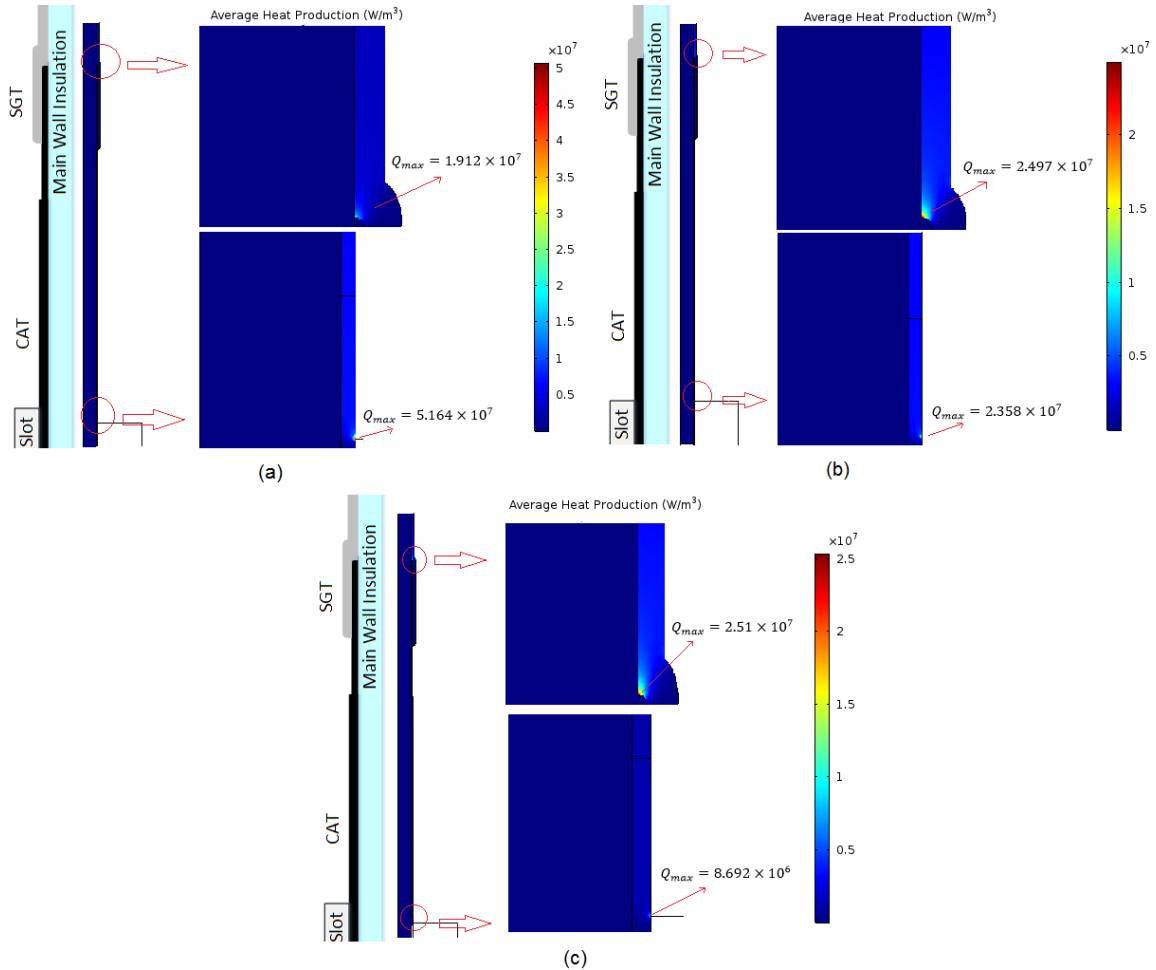
Figure 3-31: The average heat production during one cycle of the pulsed voltage for (a) low CAT conductivity, (b) measured CAT conductivity, and (c) high CAT conductivity.

3.7.2 Effect of the Initial Conductivity of SGT

The effect of SGT's initial conductivity was investigated based on the selection of three types of conductivity: the lowest at one order less than the measured level, the measured conductivity value, and the highest at one order greater than the measured one. Figures 3-32 and 3-33 respectively show the voltage and electric field distributions on the surface of the stress grading system at the end of the rise time. Results reveal that the electric field in the SGT region at the end of the CAT can be reduced by increasing

the SGT conductivity. SGT conductivity was also found to have a slight effect on the electric field in the CAT region.
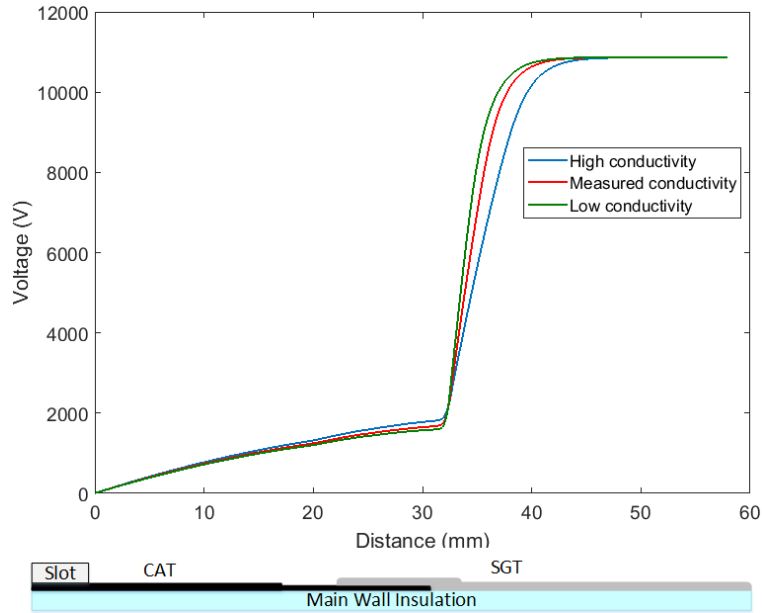
Figure 3-32: Voltage distribution along the surface of the stress grading system for three initial conductivity of SGT at the end of pulsed voltage rise time.
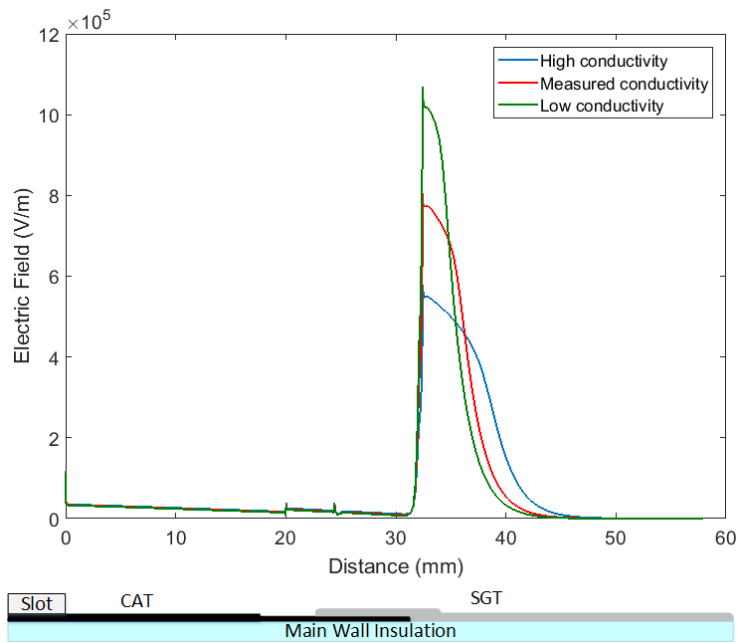
Figure 3-33: Electric field distribution along the surface of the stress grading system for three initial conductivities of SGT at the end of pulsed voltage rise time.

68

In addition, the increased conductivity leads to a good distribution in the SGT region. The field is determined by a condition in which the dielectric time constant of the grading material is equal to the applied radial frequency, $\omega = \varepsilon/\sigma(E_{Lim})$, where E_{Lim} is the space charge limited field (SCLF), which takes the form of a region with a relatively constant field [9]. If the conductivity is considered as a function of the electric field $\sigma(E) = \sigma_o exp^{k|E|}$, the limited field is equal to [14]:

$$E_{Lim} = \frac{1}{k} ln \left(\frac{\varepsilon\omega}{\sigma_o} \right)$$

(3.5)

It is thus shown that increasing the conductivity decreases SCLF.

For the three selected SGT conductivities, Figure 3-34 gives the profile of the temperature on the surface of the stress grading system. Although increase in the SGT electrical conductivity cause decrease in the electric field in the SGT region, the temperature of the stress grading system is elevated by this increase. The amount of joule heating is related to the production of the electrical conductivity and the square of the electric field given in:

$$Q \propto \sigma E^2$$

(3.6)
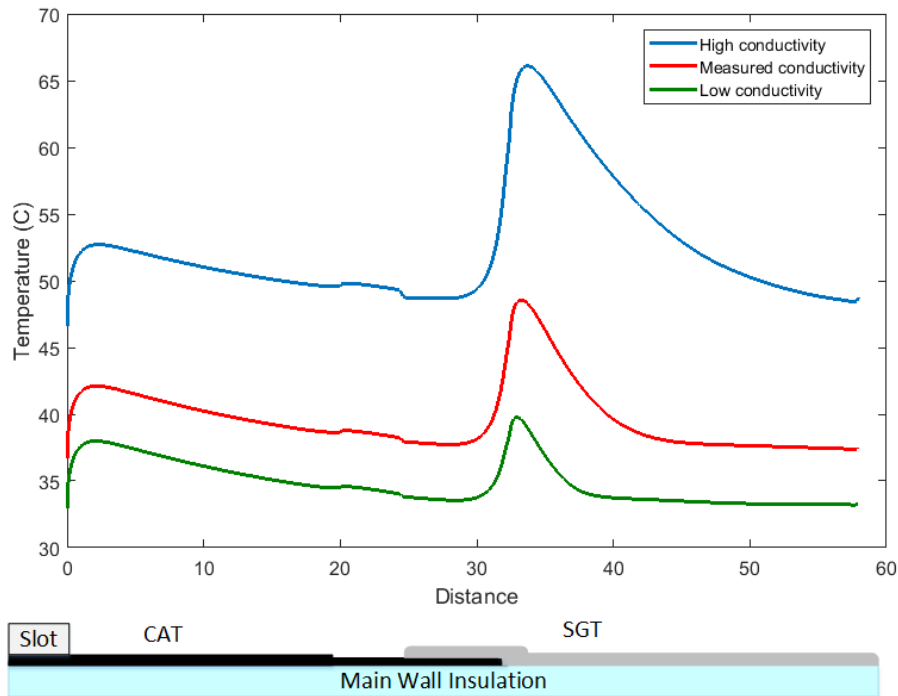
Figure 3-34: Temperature profile along the surface of the stress grading system for three initial conductivity of SGT.

69

As Figure 3-33 shows, an increase in the SGT electrical conductivity by one order of magnitude leads to a reduction in the electric field from 0.8 to 0.6 kV/mm. The decrease in the square of the electric field is therefore approximately halved, but the conductivity becomes ten times greater. Additionally, the area of the SGT that has an electric field is also expanded by increase in the conductivity. This expansion can be clearly seen in Figure 3-33, which shows, for the three SGT electrical conductivity values, the electrical field distribution along the surface of the stress grading system. For the highest level of SGT electrical conductivity, the area of the SGT that has a high electric field is expanded.

Figure 3-35 shows the average heat production during one cycle of the pulsed voltage. As discussed before, although the electric field is reduced by incremental increases in SGT electrical conductivity, heat production in the SGT increases. Additionally, SGT electrical conductivity slightly changes the heat production in the CAT region.
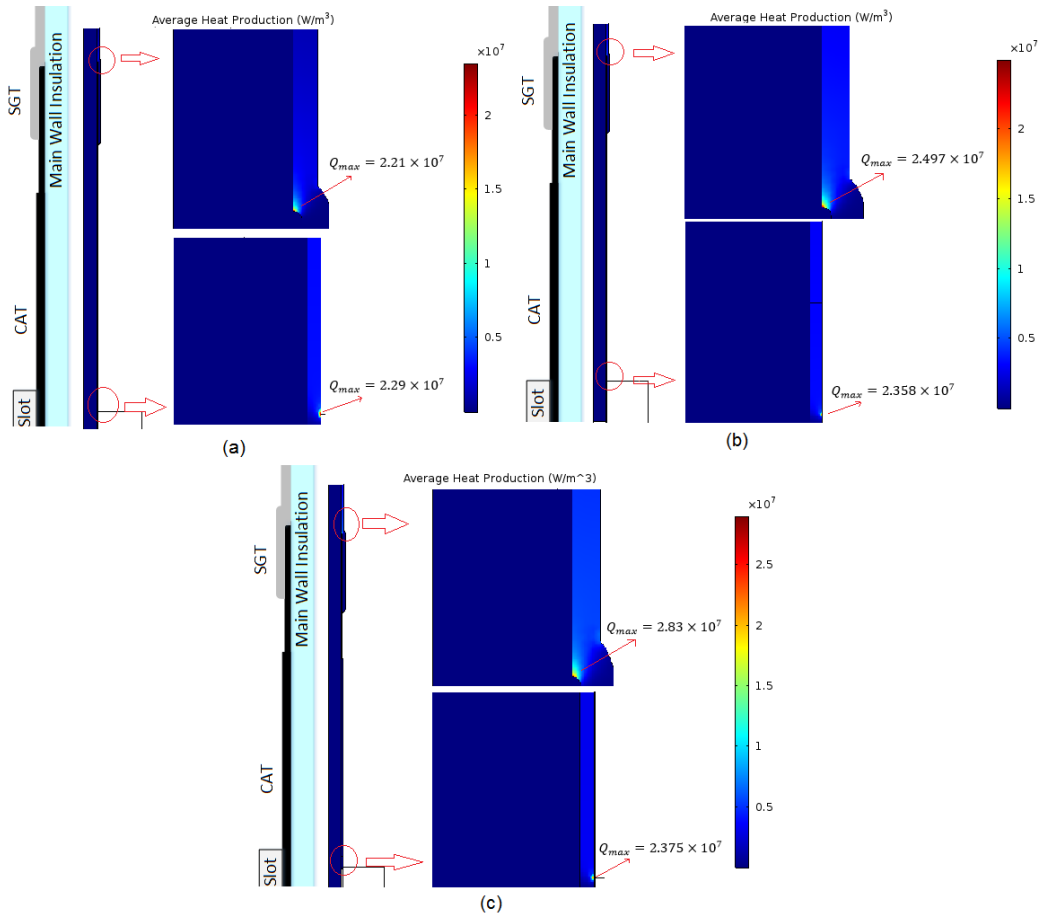
Figure 3-35: The average heat production during one cycle of the pulsed voltage for (a) low initial conductivity, (b) measured initial conductivity, and (c) high initial conductivity of SGT.

3.7.3 Effect of the nonlinearity of SGT conductivity

The nonlinearity of the SGT was altered to examine the effect of this parameter on the electric field and temperature profiles of the stress grading system. Figure 3-36 shows variations in the conductivity as a function of the electric field for three types of the SGT conductivity used in this study. The conductivity can be described as a function of the electrical field E and the level of nonlinearity α,

$$\sigma = 3.38 \times 10^{-6} \times e^{\propto E}$$

(3.6)
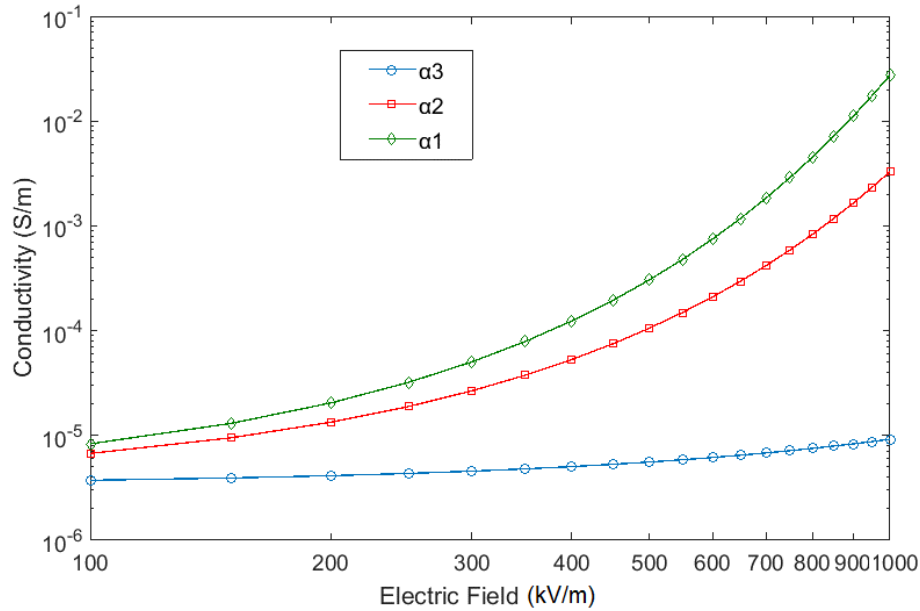
**Figure 3-36:** Variation in the conductivity as a function of the electric field for three types of the SGT conductivity used in simulation.

Simulations have been carried out to assess the effect of the three different levels of α, changing from 1×10^{-6} to 9×10^{-6}, Table 3-4. The electric field distribution at the end of the pulsed voltage rise time along the stress grading system, shown in Figure 3-37, is increased dramatically by reducing the level of nonlinearity. The maximum electric field on the surface of the SGT is nearly 3 kV/mm for the lowest level of nonlinearity which may result in partial discharge (PD) in this region. On the other hand, the electric field is reduced when the level of nonlinearity rises. In addition, the electric field distribution expands over a larger region at the highest level of nonlinearity. The electric field in the CAT region is slightly increased by increasing the level of nonlinearity, thereby increasing heat production and temperature rise in the CAT region. When the level of nonlinearity increases, the SGT current increases.

71

Therefore, the CAT current that connects the SGT to the ground also increases, enhancing the electric field in CAT.

Table 3-4: SGT conductivities used in simulation.

Nonlinearity (m/V)	Electrical Conductivity (S/m)
α_1	$3.38 \times 10^{-6} \exp(9 \times 10^{-6} \, xE)$
α_2	$3.38 \times 10^{-6} \exp(6.88 \times 10^{-6} \, xE)$
α_3	$3.38 \times 10^{-6} \exp(1 \times 10^{-6} \, xE)$

Figure 3-37: The electric field distribution along the stress grading system at the end of rise time for three different SGT nonlinearity.

Figure 3-38 shows the electric field distribution along the stress grading system at 15 µs (in the DC portion of the pulsed voltage). Results are obtained similar to those just given, in that the electric field is reduced and expanded when the level of nonlinearity increases. The electric field distribution along the stress grading system under the highest level of nonlinearity is rectangular in shape, showing that the SGT is more efficiently used in this condition than under the other two SGT conductivities.

Figure 3-38: The electric field distribution along the stress grading system at 15 µs (in the DC part of the pulsed voltage) for three different SGT nonlinearity.

The temperature profile along the stress grading system is illustrated in Figure 3-39. The temperature rise is increased when the level of nonlinearity is increased. Also, the temperature in the CAT region increases with a rise in the level of nonlinearity, due to the increased electric field in CAT region (See Figure 3-37).
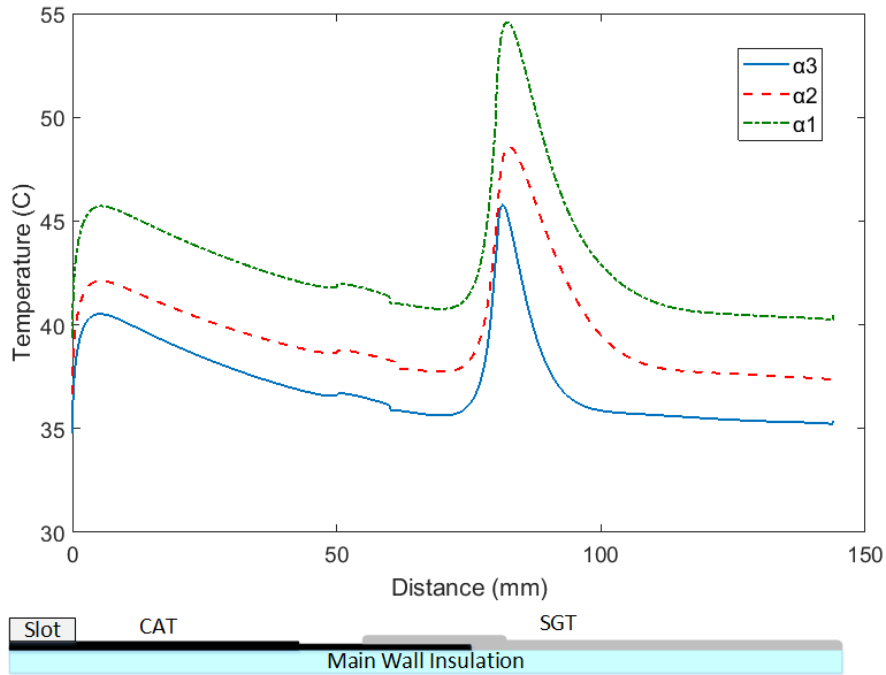
Figure 3-39: The temperature profile along the stress grading system for three different SGT nonlinearities.

The heat production is proportional to the product of the conductivity and the square of the electric field. Dramatically increasing the SGT conductivity under a high level of nonlinearity leads to increased heat production and temperature rise in the SGT region. The product of the conductivity and the square of the electric field, at the maximum electric fields for the three SGT conductivities, is calculated in Table 3-5. The results show that heat production in the SGT is increased by increasing the level of nonlinearity of the SGT conductivity. In addition, the SGT region that has a high electric field expands under the highest level of the nonlinearity; therefore, the amount of heat production increases under this condition.

Table 3-5: Product of conductivity and square of electric field in the region of maximum electric field.

	E_{max} (V/m)	σ (S/m)	σE_{max}^2
α_1	6.4×10^5	1.08×10^{-3}	44.2×10^7
α_2	7.8×10^5	0.72×10^{-3}	43.8×10^7
α_3	2.8×10^6	0.55×10^{-4}	43.1×10^7

The temperature reduces with a reduction in the level of SGT nonlinearity. For the lowest level of nonlinearity, there is a small region in the SGT with a very high electric field (see Figures 3-37 and 3-38). Therefore, the amount of heat produced drops. Figure 3-40 shows the temperature in 2D for the three SGT conductivities studied.
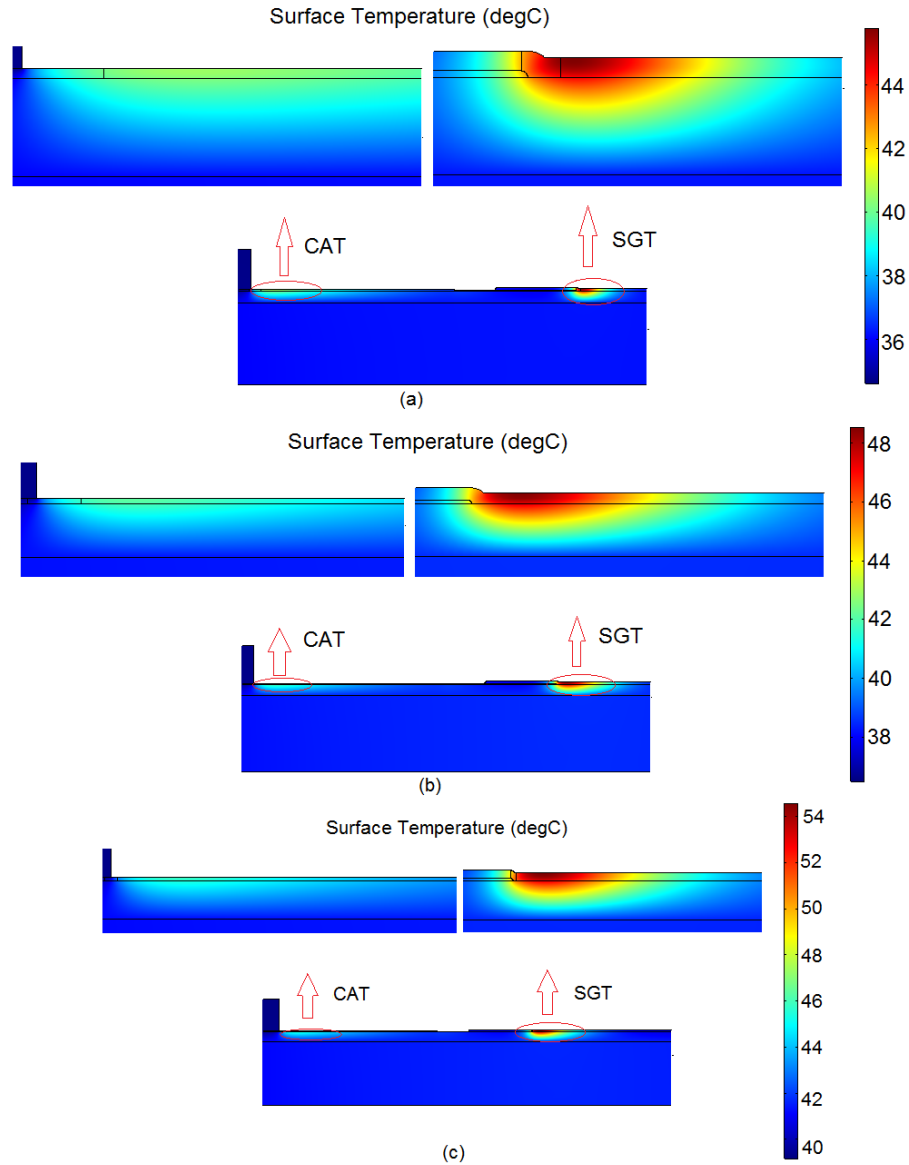
Figure 3-40: The temperature profile in 2D for (a) α_3, (b) α_2, (c) α_1 level of the nonlinearity of the SGT conductivity.

3.7.4 Effect of Thermal Conductivity on Temperature Profile

To check the sensitivity of stress-grading-system temperature profiles to the thermal conductivity of materials, the thermal conductivity of each material of interest was changed between ±20 %, while other materials' thermal conductivity were fixed. Three types of material were involved: main wall insulation, CAT and SGT.

3.7.4.1 Main wall insulation

Figure 3-41 shows the effect of the thermal conductivity of main wall insulation on the temperature profile. This thermal conductivity can change the temperature profile. Increasing the thermal conductivity of main wall insulation decreases the temperature of the stress grading system as a result of better conduction heat transfer between the stress grading system and the conductor.
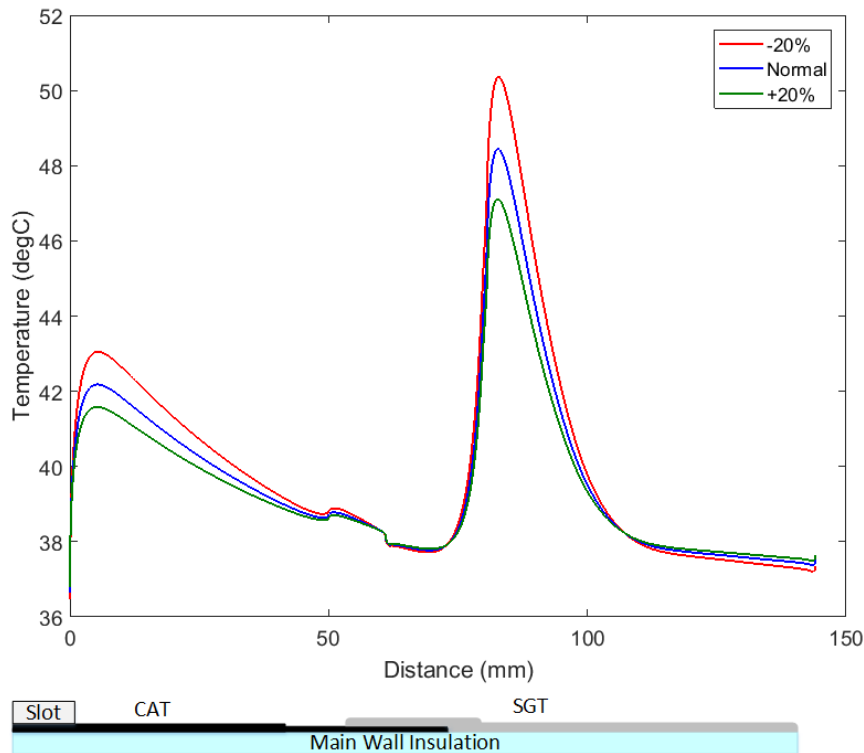
Figure 3-41: The effect of the thermal conductivity of the main wall insulation on the temperature profile.

3.7.4.2 CAT

Figure 3-42 shows the effect of the thermal conductivity of CAT on the temperature profile. This thermal conductivity has less effect on the temperature profile. Increasing the thermal conductivity of the CAT slightly reduces the temperature in the CAT region, but the temperature in the SGT region is almost fixed.
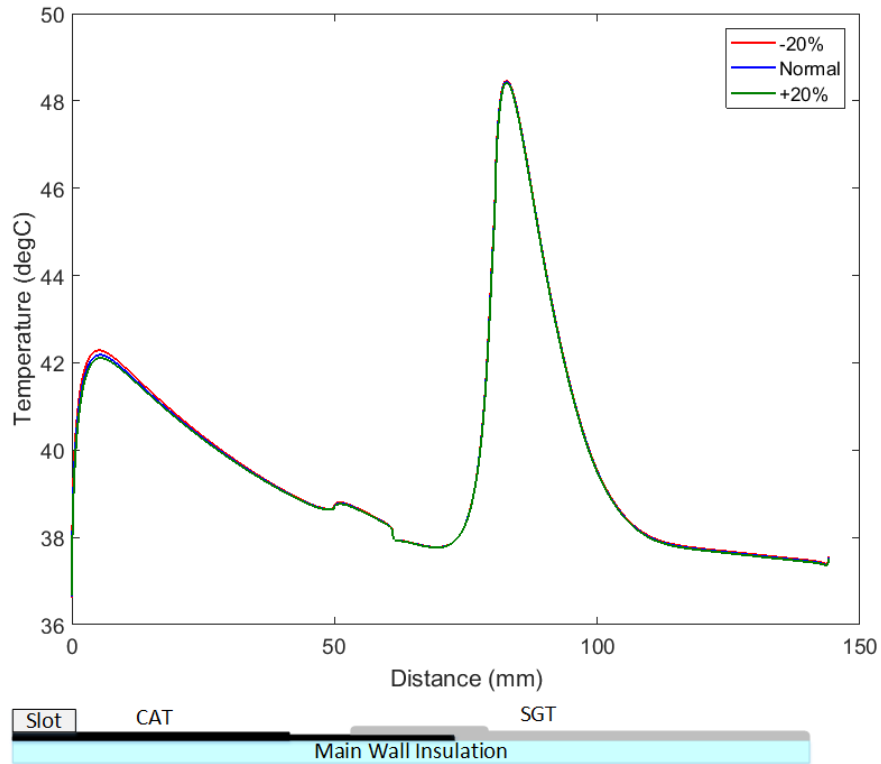
Figure 3-42: The effect of the thermal conductivity of the CAT on the temperature profile.

3.7.4.3 SGT

Figure 3-43 illustrates the effect of the thermal conductivity of the SGT on the temperature profile. This thermal conductivity, like the thermal conductivity of CAT, has a limited effect on just its region.
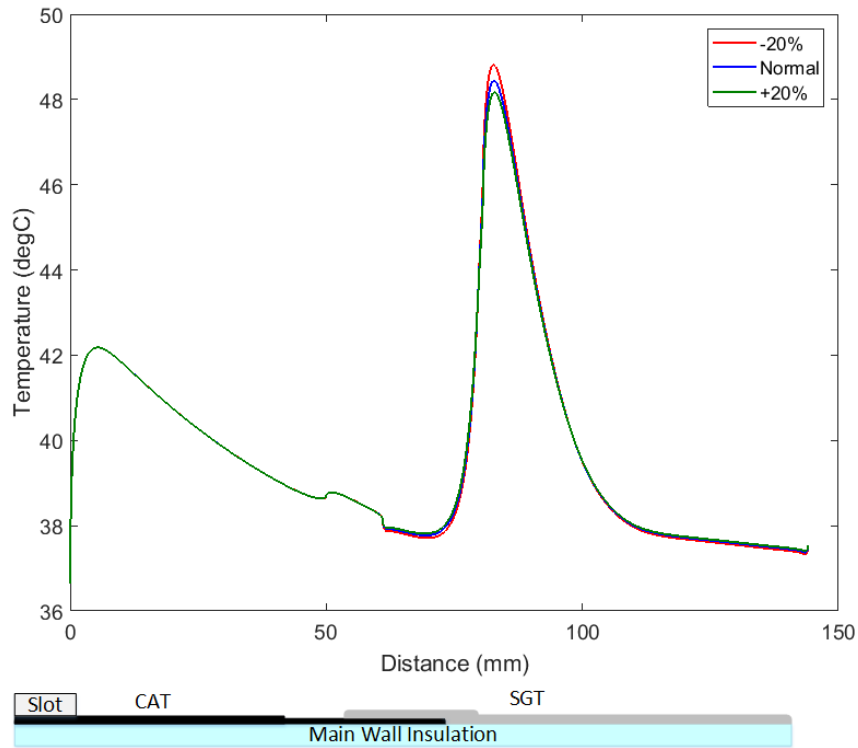
Figure 3-43: The effect of the thermal conductivity of the SGT on the temperature profile.

3.7.5 Effect of Relative Permittivity of Mail Wall Insulation

The simulations were run for three relative permittivity of main wall insulation (2, 2.5 and 3). Figure 3-44 shows the electric field distribution at the end of the pulsed rise time. The electric field in CAT and SGT increases by increasing the relative permittivity. It increases just 3.7% in SGT region and around 50% in CAT region by increasing the relative permittivity from 2 to 3.
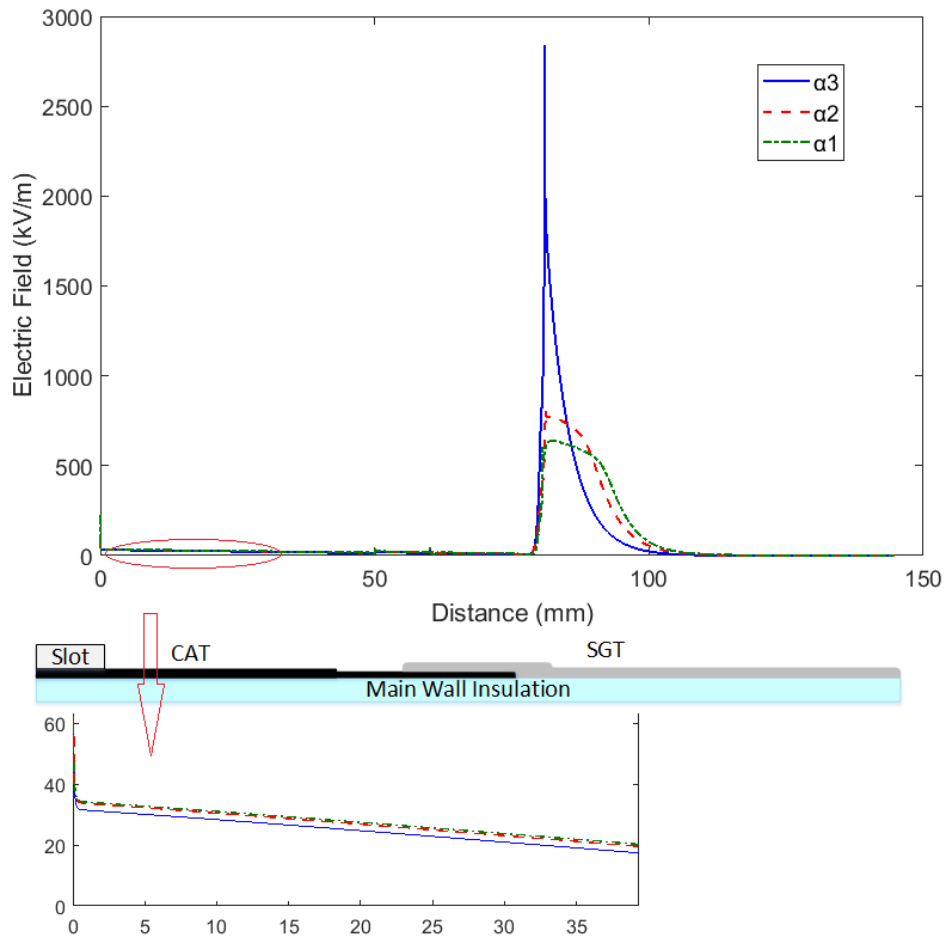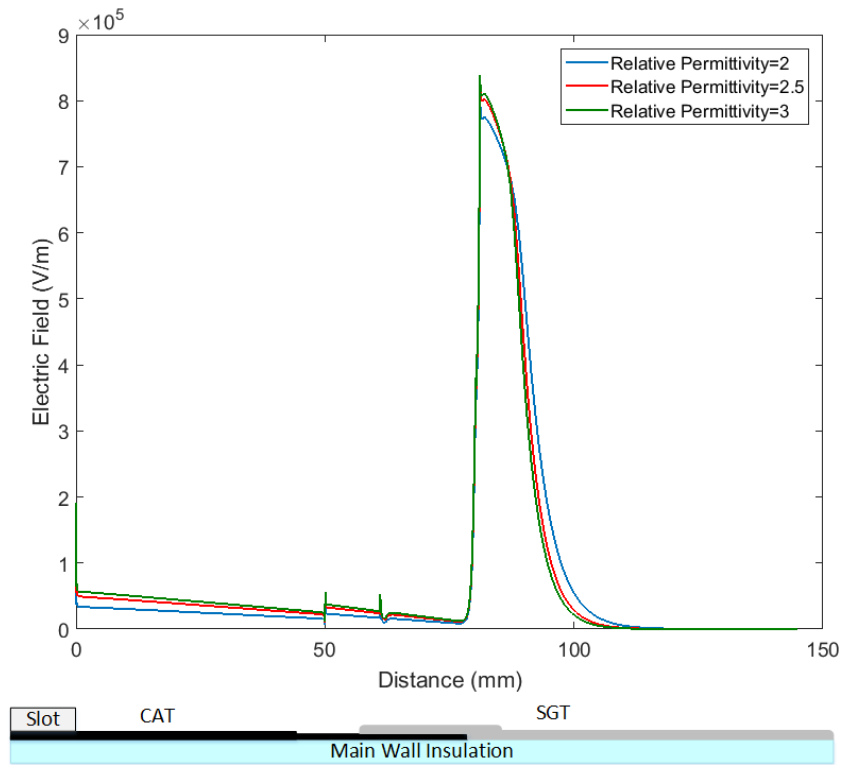
Figure 3-44: The electric field distribution along the stress grading system at the end of rise time for three different relative permittivity of MW insulation.

Figure 3-45 shows the electric field distribution at the DC portion of pulsed voltage. The maximum electric field increases approximately 14 % in SGT by changing the relative permittivity from 2 to 3. The temperature profile is shown in Figure 3-46. The temperature also increases by increasing the relative permittivity. The maximum temperature increases almost 3 degree by changing the relative permittivity from 2 to 3.
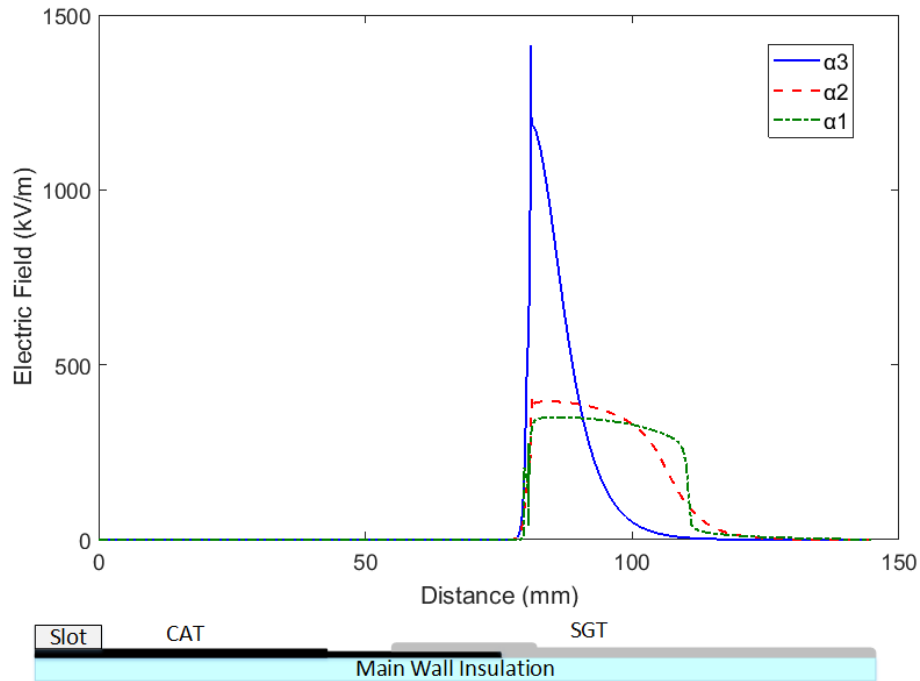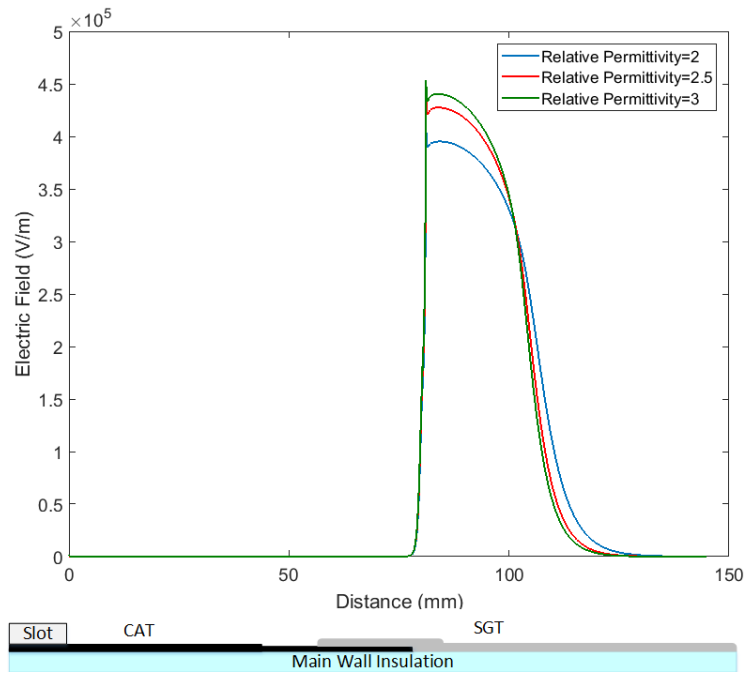
Figure 3-45: The electric field distribution along the stress grading system 15 µs (in the DC part of the pulsed voltage) for three different relative permittivity of MW insulation.
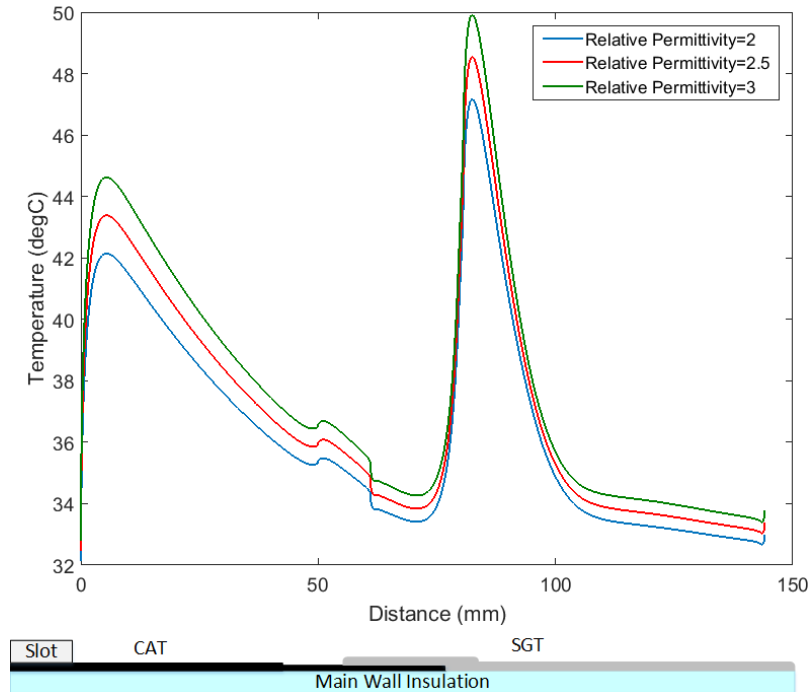
Figure 3-46: The temperature profile along the stress grading system for three different relative permittivity of MW insulation.

3.7.6 Effect of CAT Builds

Three different thicknesses of CAT are considered, and the effect of thickness on the surface electric field distribution and the temperature is investigated. The possible thickness of CAT is limited by the width of the slots; therefore, it must be in an acceptable range. Although the conductivity of CAT is changed by the number of CAT layers (thickness) [15], in this section, the conductivity is considered fixed to check only the effect of thickness. Figure 3-47 shows the electric field distribution along the surface of the stress grading at the end of the pulsed voltage rise time. It is clear that the electric field in the CAT region is reduced by the increment of the CAT thickness. On the other hand, the electric field in the SGT region is slightly increased with an increase in the thickness.
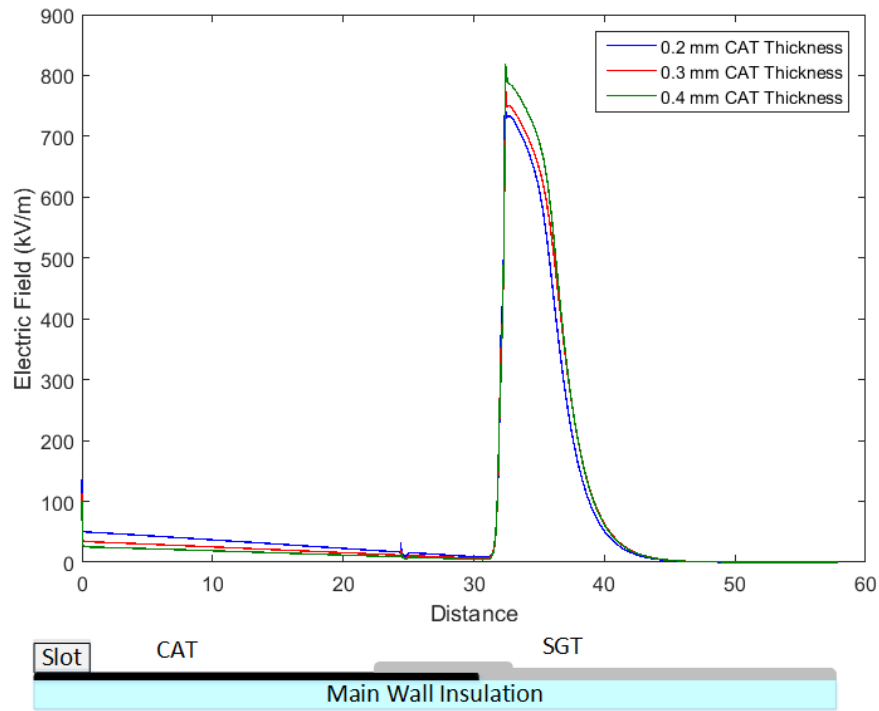
Figure 3-47: The electric field distribution along the surface of the stress grading system at the end of rise time for three different CAT thickness.

The temperature profile along the stress grading system is shown in Figure 3-48. The temperature in the CAT region drops when the CAT thickness is increased. Although the electric field in the SGT region slightly increases at the end of the pulsed voltage rise time due to the increment of CAT thickness, the temperature in this region is reduced. Although, increasing the CAT thickness produces a slight increase in the electric field in the SGT at the rise time, it reduces the electric field in this region

81

during the flat portion of the pulsed voltage, thus decreasing the temperature in SGT region. Figure 3-49 illustrates the electric field on the surface of the stress grading system during the DC portion of the pulsed voltage.
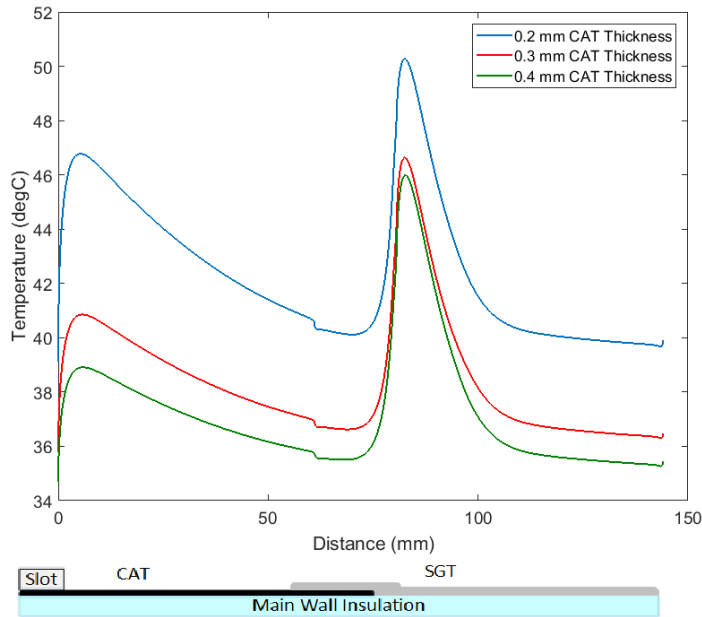
Figure 3-48: The temperature profile along the surface of the stress grading system for three different CAT thickness.
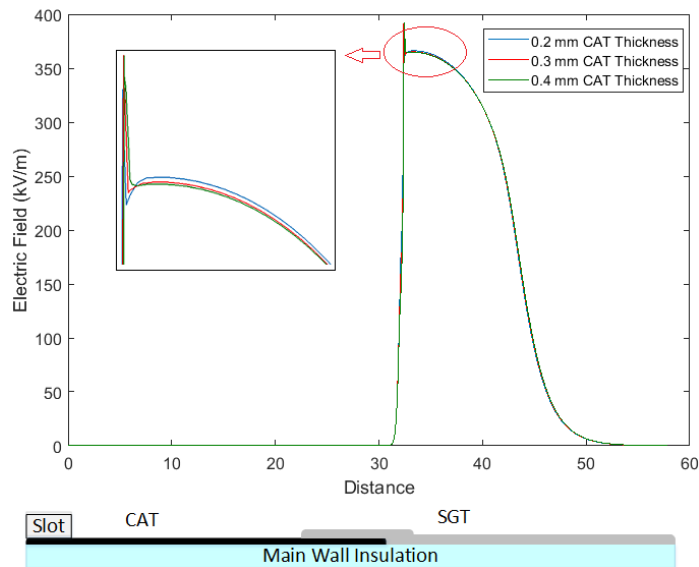
Figure 3-49: The electric field distribution along the surface of the stress grading system during the DC portion of the pulsed voltage for three different SGT thickness.

Samples with different builds were also prepared to experimentally investigate the effect of the CAT builds on the temperature of the stress grading system under pulsed voltage. The three samples were energized by the unipolar pulsed generator for more than two hours to stabilize the temperature, and the IR camera was used to capture the temperature. Figure 3-50 shows that the temperature profiles along the three samples verify the simulation results.
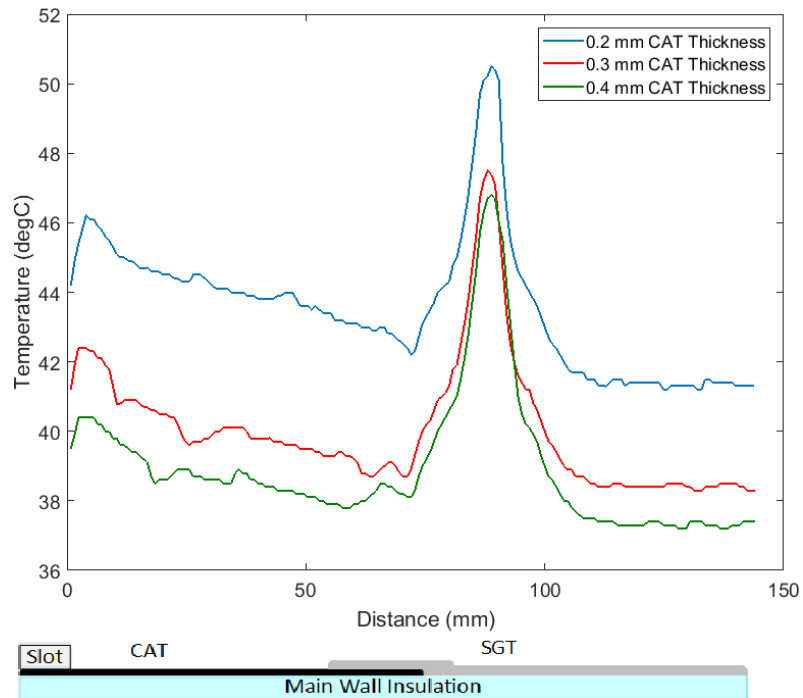
Figure 3-50: The measured temperature profile along the surface of the stress grading system for three different CAT thickness.

3.7.7 Effect of SGT Builds

To evaluate the effect of SGT thickness, three values are considered. The number of the SGT layer (thickness) effects the conductivity of the SGT [18], but for evaluating only the effect of thickness, the conductivity is fixed in this investigation. Figure 3-51 displays the electric field distribution along the surface of the end winding for three different SGT thicknesses. The electric field on the surface of the stress grading system in the SGT region is reduced by increasing the thickness of the SGT. The electric field in the CAT region is almost fixed, and SGT thickness has no effect on it.
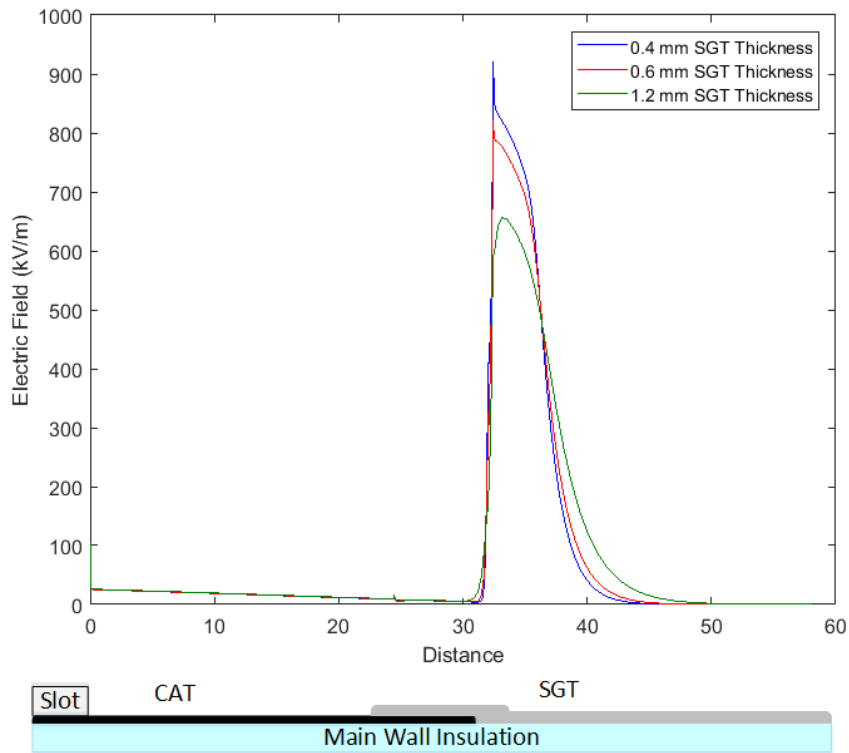
Figure 3-51: The electric field distribution along the surface of the stress grading system at the end of rise time for three different SGT thickness.

The temperature profile along the stress grading system under three different SGT thicknesses is shown in Figure 3-52. Although the increment of the SGT thickness reduces the electric field on the surface of the SGT region during the rise time, the temperature in the SGT region is increased by this increment. The electric field on the surface of the SGT is reduced by increasing the thickness, because the distance between the SGT surface and the high voltage is greater. However, the electric field underneath the SGT is slightly altered. Figure 3-53 depicts the electric field underneath the SGT at the rise time. In addition, the temperature in the CAT region is also increased moderately.
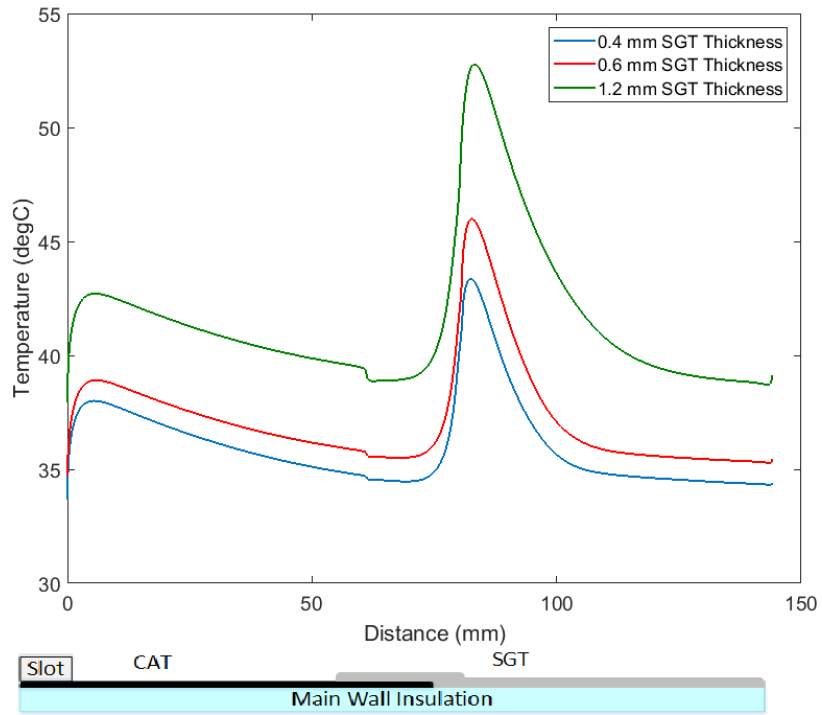
Figure 3-52: The temperature profile along the surface of the stress grading system for three different SGT thickness.
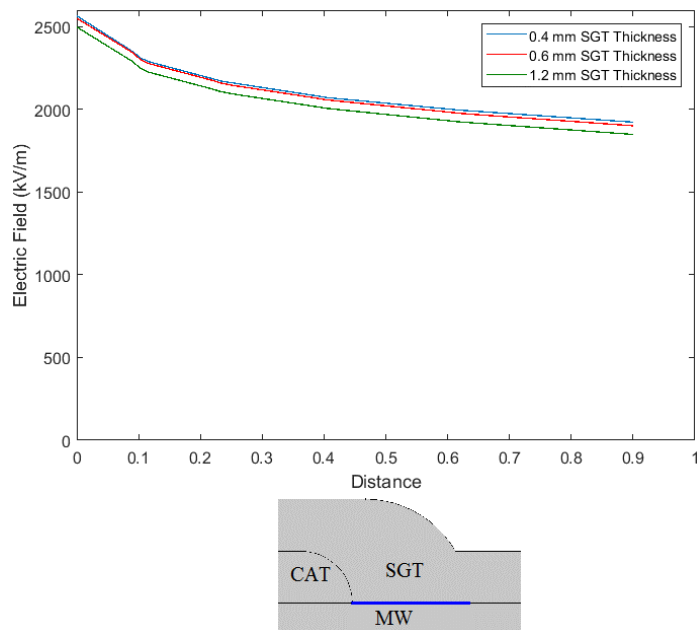
Figure 3-53: The electric field distribution along underneath the SGT at the end of rise time for three different SGT thicknesses.

Samples with different SGT builds were also prepared to experimentally test how the SGT build affects temperature under pulsed voltage. Pulsed voltage was applied to the three samples for more than two hours to stabilize the temperature, and the IR camera was used to capture the temperature. Figure 3-54 shows the temperature profiles along the three samples, again confirming the verification of the simulation results.
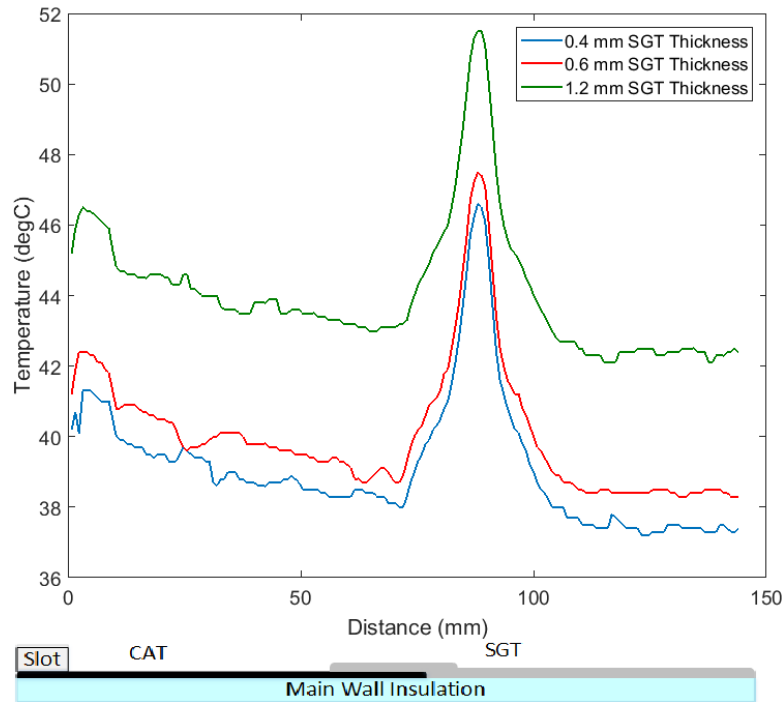
Figure 3-54: The measured temperature profile along the surface of the stress grading system for three different SGT thicknesses.

3.7.8 Effect of CAT Length

The CAT length, measured from the slot exit, was altered to check the effect of this parameter on the performance of the stress grading system. Four lengths of CAT (40, 60, 80 and 100 mm) were considered to examine the effect of the CAT length on the electric field and temperature. Figure 3-55 shows the electric field distribution at the end of the pulsed voltage rise time along the stress grading system. The electric field in the CAT region is reduced with the shorter CAT lengths. For instance, reducing the CAT length from 100 mm to 40 mm reduces the electric field in the CAT region by half. The peak of the electric field in the SGT region is slightly increased by this reduction in CAT length. Figure 3-56 shows the electric field distribution along the stress grading system at 15 µs (in the flat

86

portion of the pulse voltage). After any fast transient and during the low frequency part of the voltage, voltage drop occurs only in the SGT region at the end of the CAT; therefore, changing the CAT length has no effect on the electric field in this region. On the other hand, the peak of the electric field in the SGT is slightly decreased by reducing the CAT length, due to reduced resistance between the SGT and the ground.
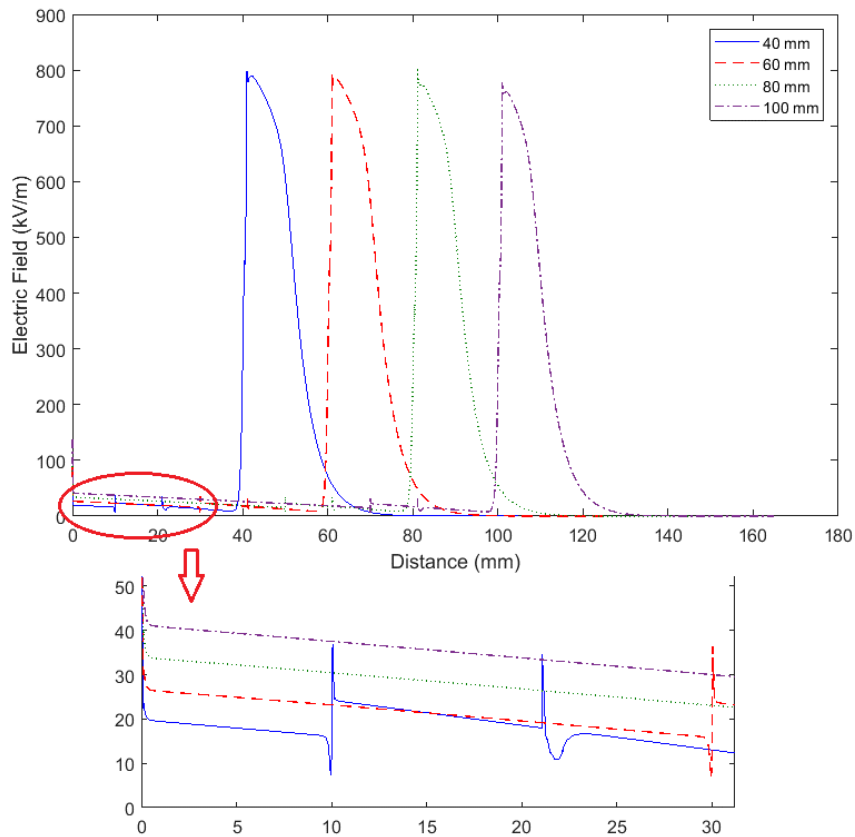
Figure 3-55: Electric field along the stress grading system at the end of rise time at different CAT lengths.
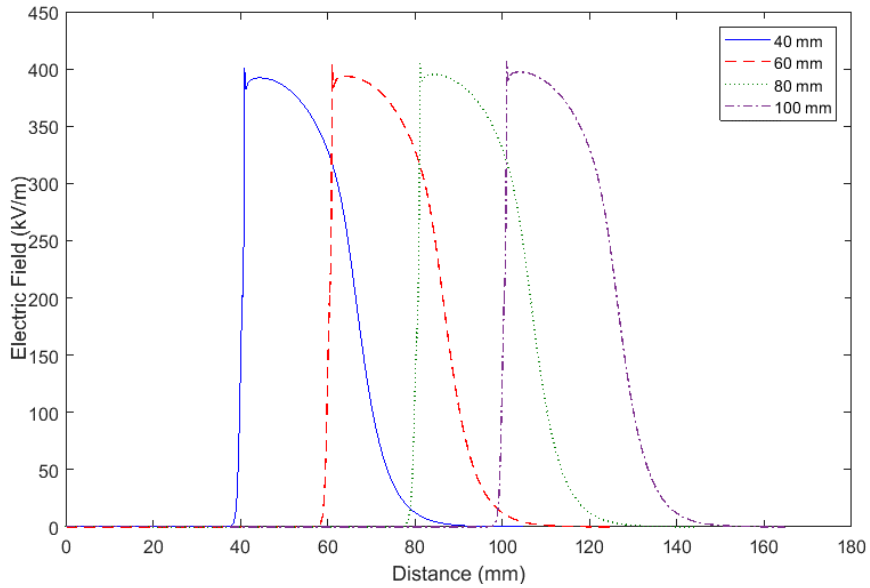
Figure 3-56: The electric field distribution along the stress grading system at 15 µs (in the flat portion of the pulse voltage) at different CAT lengths.

The temperature profile along the stress grading system is illustrated in Figure 3-57. The temperature profile declines as the length of the CAT decreases. The temperature in the CAT region is significantly reduced due to the decreased electric field in this region; therefore, the temperature in the SGT is also decreased by the reduction in CAT length. But the temperature rise at the end of the CAT region remains the same for the four different CAT lengths considered. Figure 3-58 shows the temperature in a 2D configuration for the four lengths of CAT. The maximum temperature for CAT and SGT are decreased by a reduction in CAT length.
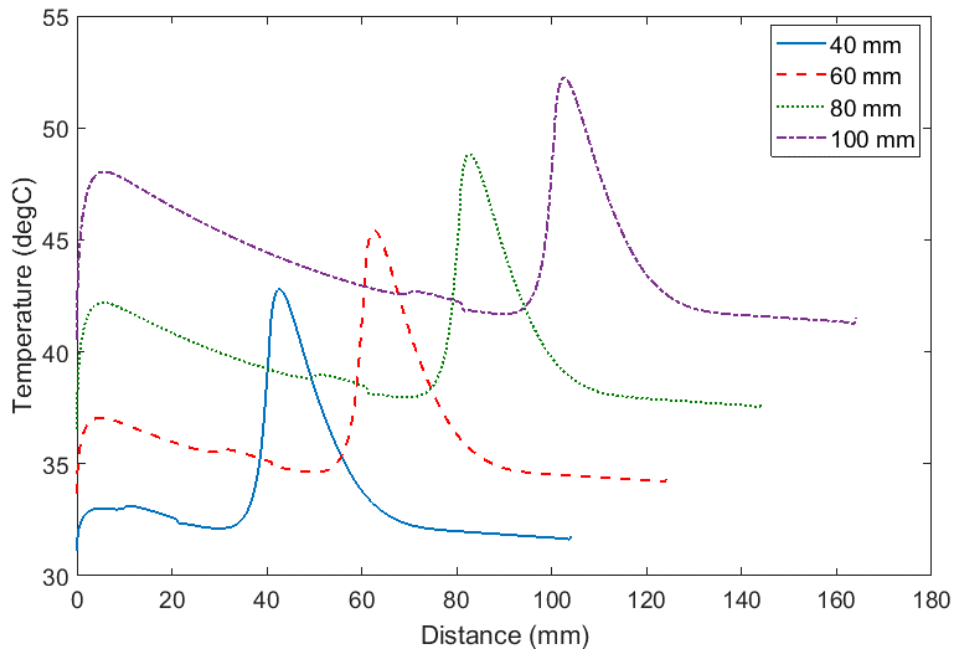
Figure 3-57: Temperature profile along the stress grading system as a function of CAT length.
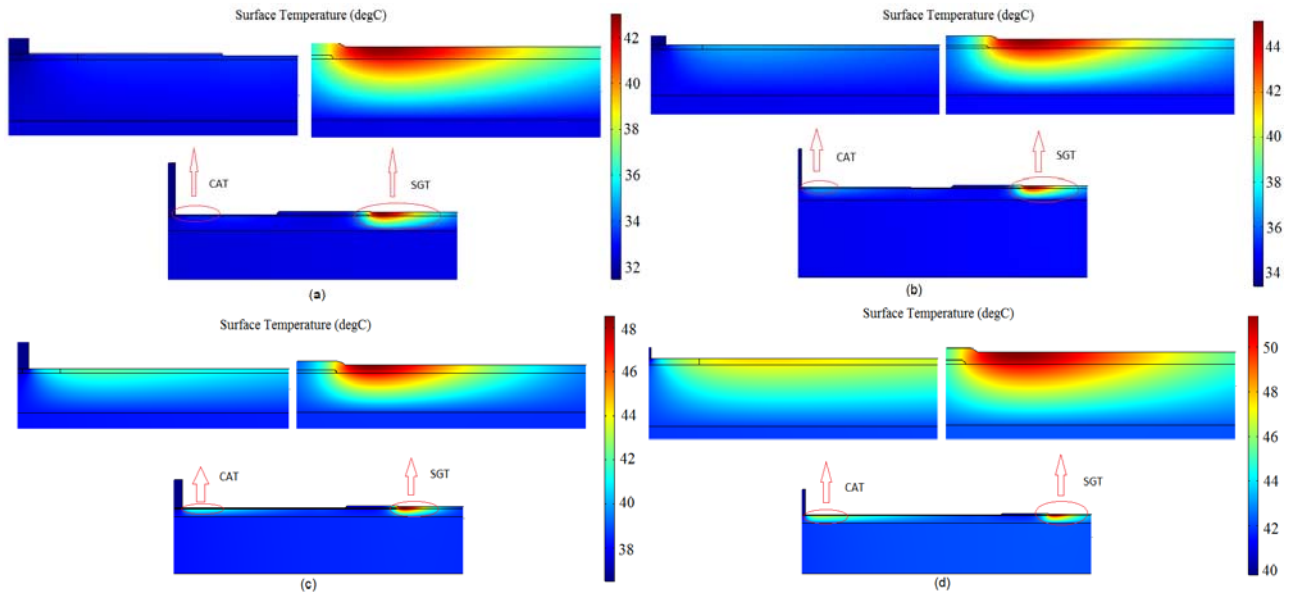
Figure 3-58: Temperature profile in 2D for (a) 40 mm, (b) 60 mm, (c) 80 mm, and (d) 100 mm CAT lengths.

Samples of the end winding having different CAT lengths were also studied under pulsed voltage. The temperature profile was measured at room temperature with and without circulating current, and also at elevated room temperature with circulating current. Figures 3-59 and 3-60 show measured and

simulated temperature profiles without circulating current condition, and at room temperature for 80 and 40 mm CAT lengths, respectively. Results show a reduction on the temperature profile with reduced CAT length.
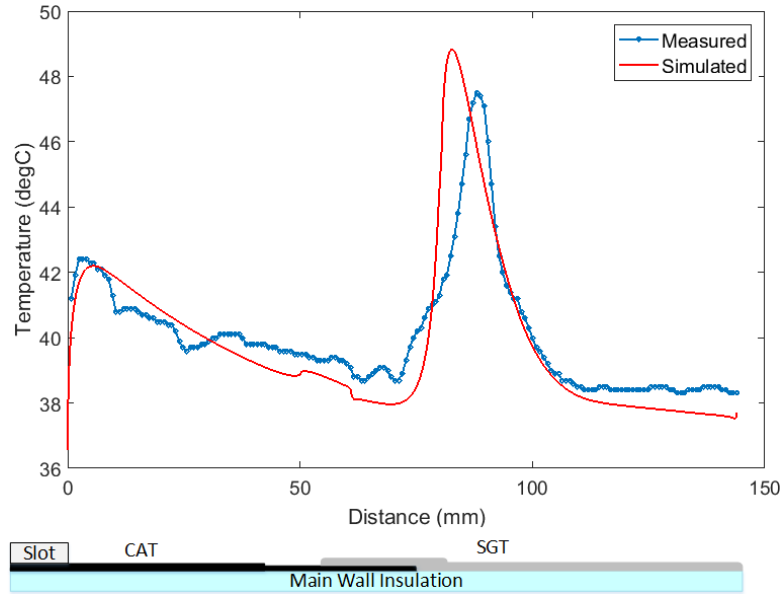
Figure 3-59: The measured and simulated temperature profiles of the stress grading system without circulating current and at room temperature for 80 mm CAT length.
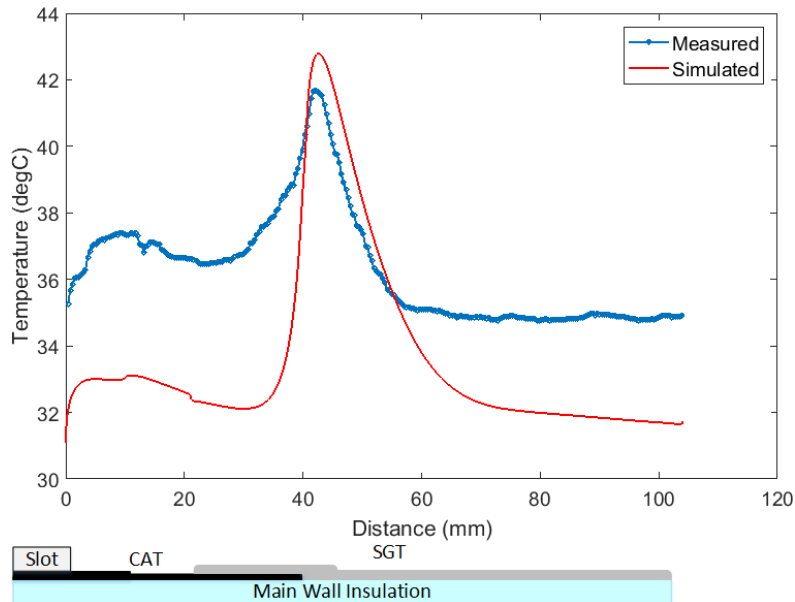
Figure 3-60: The measured and simulated temperature profiles of the stress grading system without circulating current and at room temperature for 40 mm CAT length.

Circulating current was used to increase the temperature of the bar (conductor); pulsed voltage was applied to the sample at the same time. The measured and simulated temperature profiles with circulating current and at room temperature for 80 and 40 mm CAT lengths are shown in Figures 3-61 and 3-62, respectively. Again, results show that maximum temperature is reduced by 5 oC with a reduced CAT length.
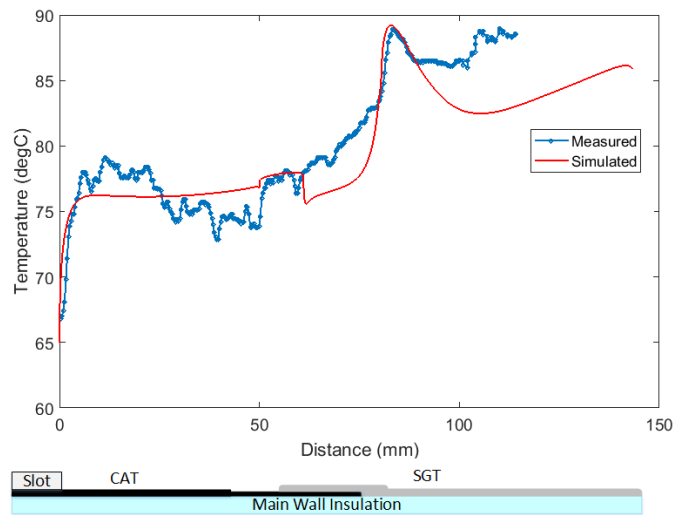
Figure 3-61: Measured and simulated temperature profiles along the stress grading system with circulating current and at room temperature for 80 mm CAT lengths.
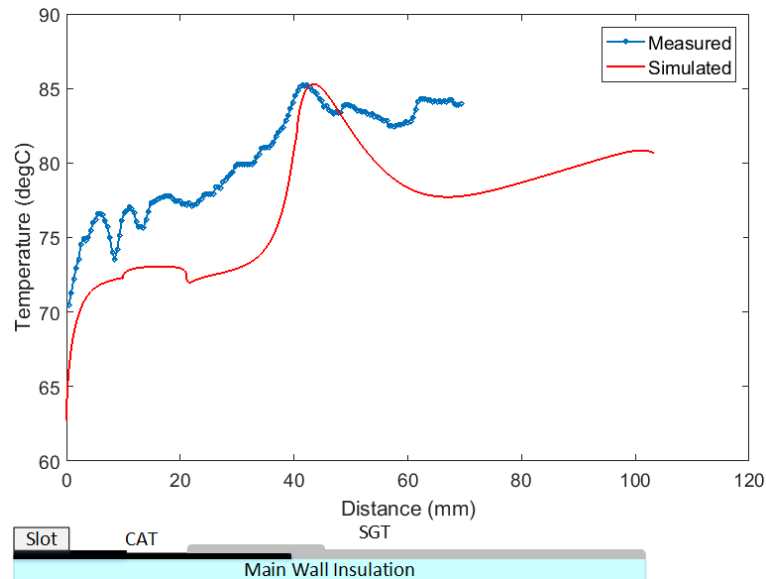
Figure 3-62: Measured and simulated temperature profiles along the stress grading system with circulating current and at room temperature for 40 mm CAT lengths.

The room temperature was increased to 35 °C, and the previous step was run. Figures 3-63 and 3-64 illustrate the measured and simulated temperatures with circulating current and at an elevated room temperature of 35 °C for 80 and 40 mm CAT lengths, respectively. Results show the same trend: the temperature profile is reduced when CAT length is decreased and the maximum temperature is decreased to around 4 oC by this reduction in CAT length.
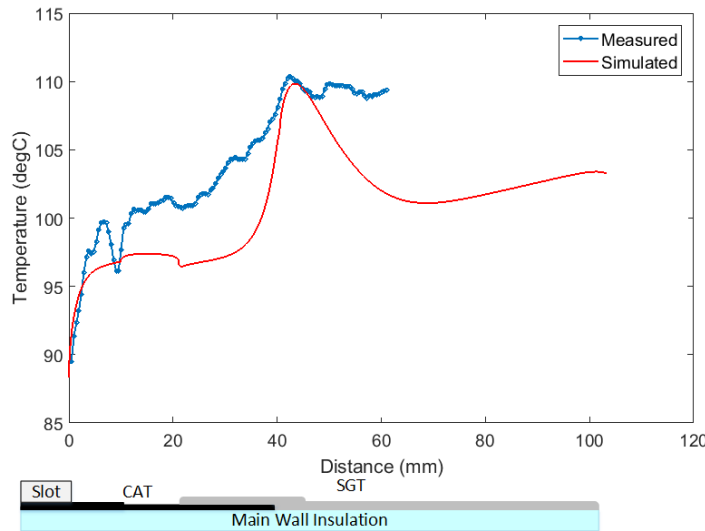
Figure 3-63: The measured and simulated temperature profiles of the stress grading system with circulating current and at elevated room temperature for 80 mm CAT lengths.
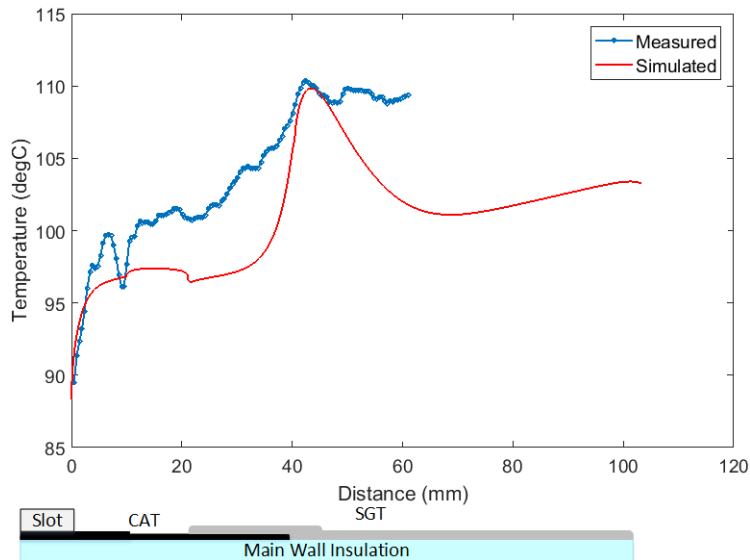
Figure 3-64: The measured and simulated temperature profiles of the stress grading system with circulating current and at elevated room temperature for 40 mm CAT lengths.

92

The trend of reducing CAT length shows that doing so can improve the electrical and thermal performance of a stress grading system. Therefore, performance with minimum CAT length was investigated. This minimum is the length of overlap of CAT-SGT that is equal 20 mm. Figure 3-65 shows measured and simulated temperature profiles for the minimum CAT length (20 mm) at room temperature and without circulating current. As expected, the temperature profile is slightly reduced compared to testing with a 40 mm CAT length.
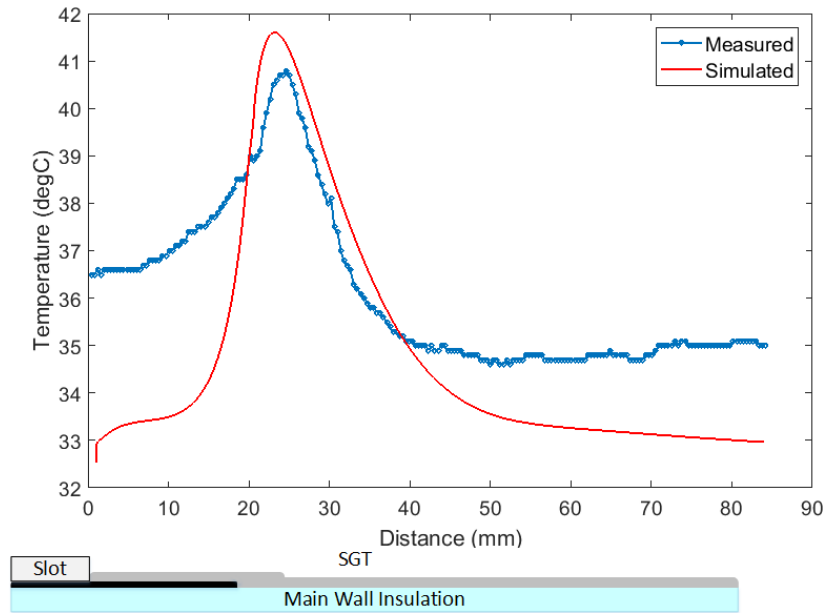
Figure 3-65: Measured and simulated temperature profiles along the stress grading system for 20 mm CAT length (minimum).

3.7.8.1 Presence of Pressure Fingers

With a conventional CAT length, the presence of fingers used to hold core laminations in place in an induction motor has no effect on the electric field distribution along the stress grading system. However, the fingers can change the electric field when CAT length is reduced, because a shorter CAT length brings the SGT layer closer to the pressure fingers than in conventional CAT length design. Therefore, the presence of pressure fingers on electric field distribution was investigated. The fingers' dimensions and distance from the coil are shown in Table 3-6. Figure 3-66 shows the geometry using the 2D axisymmetric module in COMSOL 5.3a for only one side of a coil.

Table 3-6: Dimensions of the pressure fingers.

Finger length	Finger thickness	Distance to coil
38 mm	12 mm	8 mm
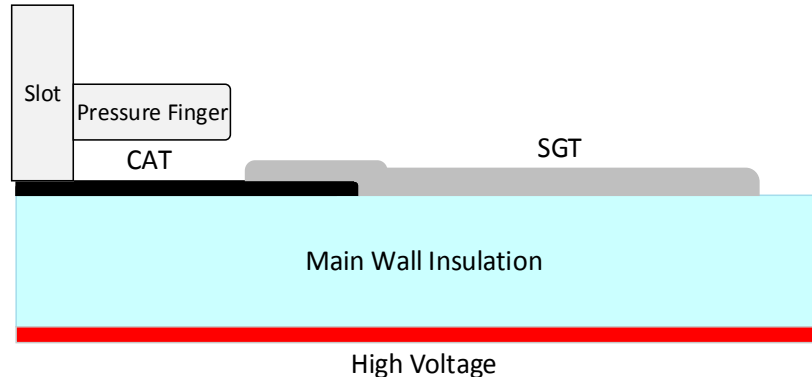
Figure 3-66: Sketch of the stress grading system studies using COMSOL.

The simulation was run for 20 and 40 mm CAT lengths to assess the effect on electric field distribution. Figure 3-67 shows the electric field distribution in the stress grading system region at the end of the pulsed voltage rise time. The maximum electric field on the surface of the finger is approximately 0.8 kV/mm, and increases to 1.8 kV/mm when CAT length is reduced to 20 mm (Figure 3-68), indicating the possibility of PD from the end of the finger. To check for PD, measurements were taken in the laboratory at both power frequency and pulsed voltages.
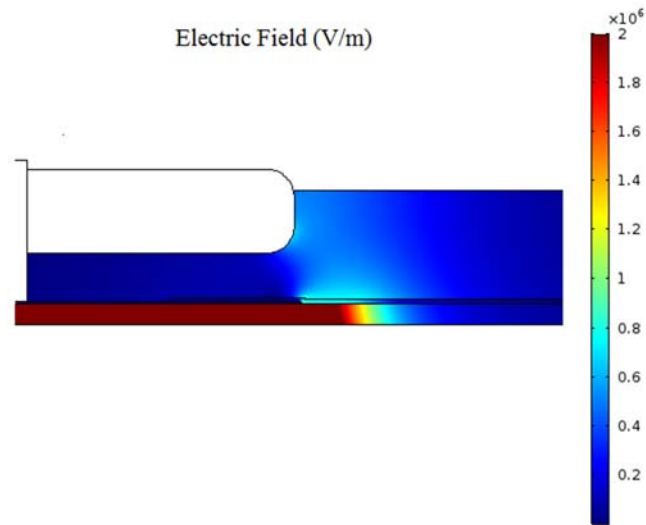
Figure 3-67: Electric field distribution at the end of the rise time of the voltage pulse for a 40 mm CAT length**.**
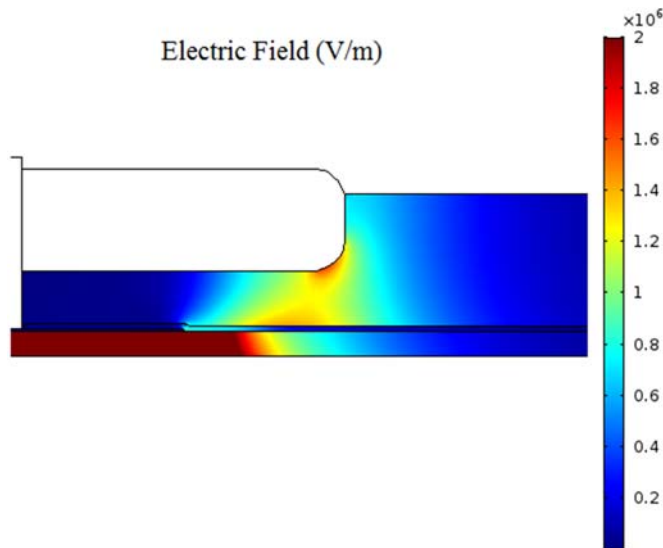
Figure 3-68: Electric field distribution at the end of the rise time of the voltage pulse for a 20 mm CAT length.

3.7.8.2 Measurement of PD

PD measurements were done at power frequency and under pulsed voltages. According to IEC 60270 [85] at power frequency, a coupling capacitor was used to measure PD. Voltage was increased from 0.2 U_n to 1.2 U_n in steps of 0.2 U_n, U_n being the phase-to-ground voltage of the 13.8 kV rotating

machines. At each voltage step, the average of the measured PD during one minute with a sample rate of four measurements per second was considered as the PD at that level. Results are illustrated in Figure 3-69. At the rated voltage, the PD is nearly the same for 40 and 80 mm CAT lengths, but PD is higher for 20 mm CAT length. Also, the measured PDIVs for the three CAT lengths considered in this study were the same: 5.8 ± 0.2 kV.
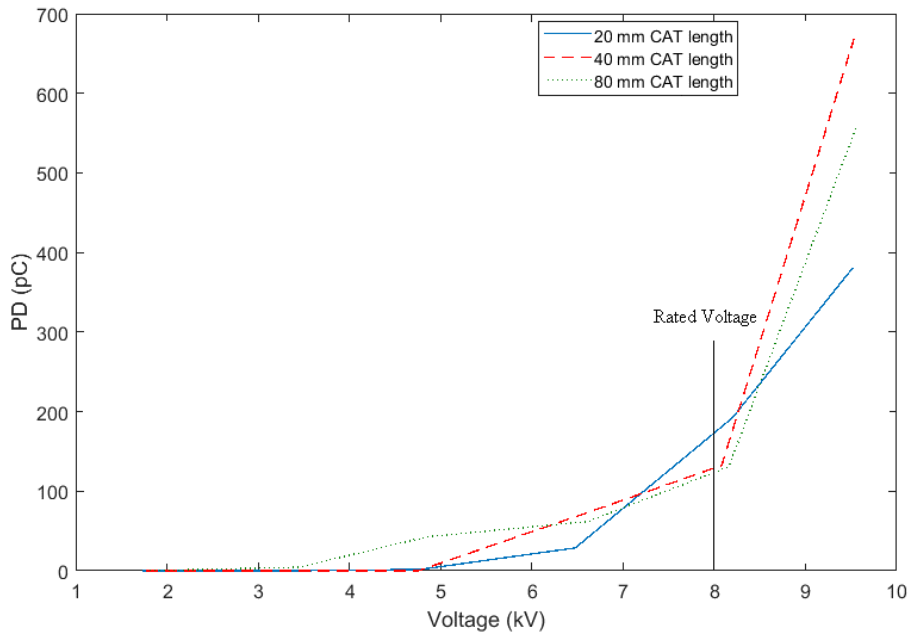
Figure 3-69: Measured PD at power frequency for the three CAT lengths.

As discussed in section 2.2.6, a monopole antenna and a high-pass filter were used for PD measurement under pulsed voltage. The pulsed voltage level for the 13.8 kV coil was taken as 11.3 kV peak and at 2.5 kHz switching frequency. The applied voltage waveform and PD was displayed on a 400 MHz, 5 G s/sec digital oscilloscope. Figure 3-70 shows the measured values for the three CAT lengths. Output from the antenna is voltage and can be used for a relative comparison of the three CAT lengths. To differentiate between the three CAT lengths, captured signals are off-set in time. Results show that the PD levels for the three CAT lengths are essentially the same, although slightly decreased for 80 mm CAT.
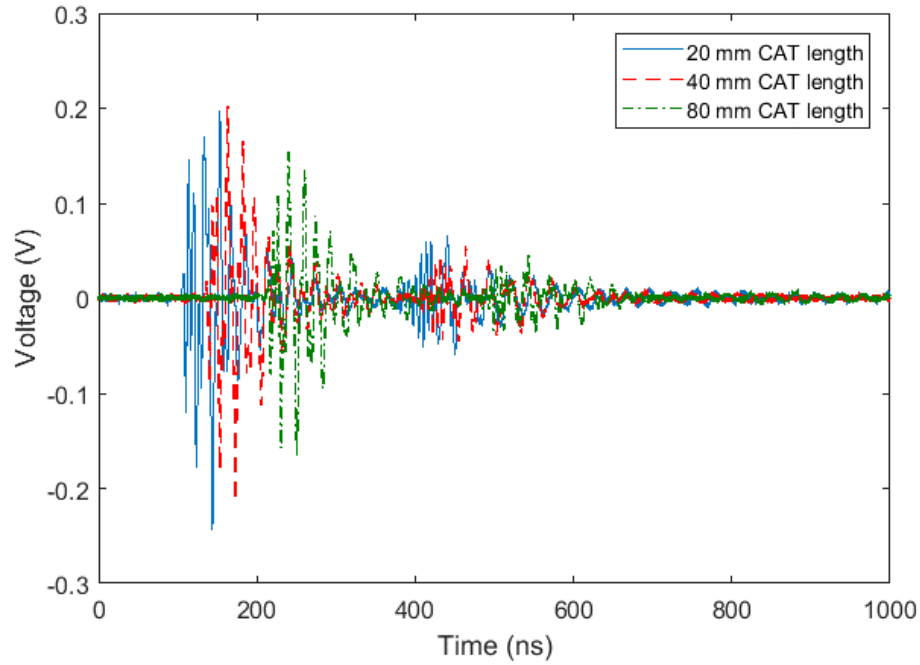
Figure 3-70: Measured PD for pulse voltage for 20, 40 and 80 mm CAT lengths.

3.7.9 SGT Conductivity Based on Micro-varistor

This section examines the effect of the micro-varistor based SGT on electric field and temperature. The conventional SGT conductivity is $3.38 \times 10^{-6} \times e^{6.88 \times 10^{-6} \times E}$ (S/m), and details on the sample preparation and conductivity measurement procedures are described in section 3.2. The conductivity formula for micro-varistor-based SGT comes from [51], in which the conductivity of available commercial stress grading materials was measured and compared. Figure 3-71 shows the resistivity of SiC and micro-varistor materials as a function of electric field. The formula of conductivity for the selected material has been approximated from material number 10 in Figure 3-71b in this source paper.

$$\sigma = 2 \times 10^{-10} \times e^{9 \times 10^{-6} \times E}$$

(3.6)
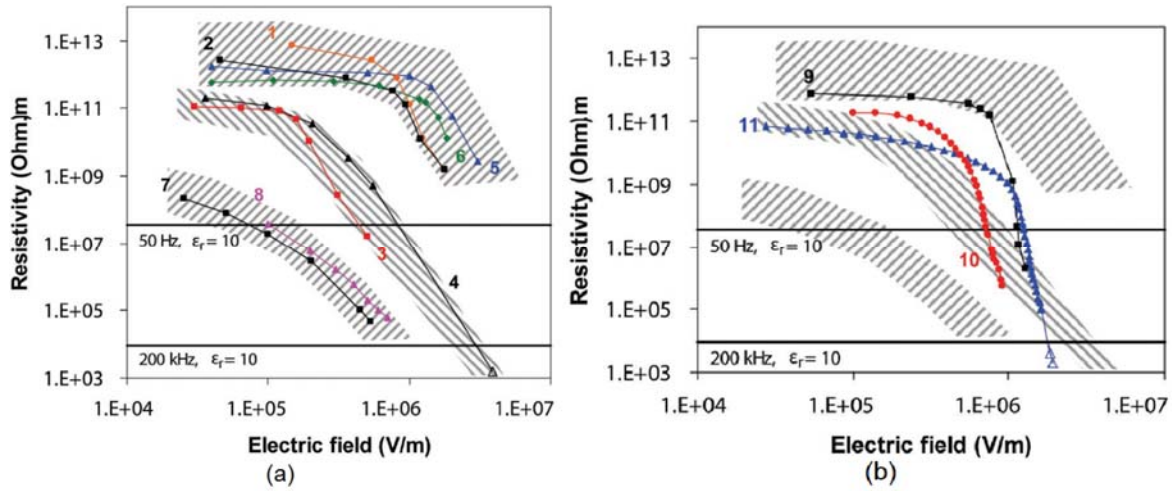
Figure 3-71: Resistivity of (a) SiC (materials 1 to 4 are used in cable terminations, materials 5 and 6 in cable joints, and materials 7 and 8 in stator bars) and (b) three commercially available micro-varistor materials as a function of electric field; reproduced from [51]

The electric field distribution at the end of the pulsed voltage rise time along the stress grading system is shown in Figure 3-72 for the conventional and micro-varistor based SGT. The electric field increases with the use of micro-varistor, with the maximum electric field on the surface of the SGT being almost 2 kV/mm, but the electric field of the CAT region is reduced. Figure 3-73 shows the electric field distribution along the stress grading system at 15 µs (in the flat portion of the pulsed voltage), and confirms that using micro-varistor based SGT enhances the electric field.
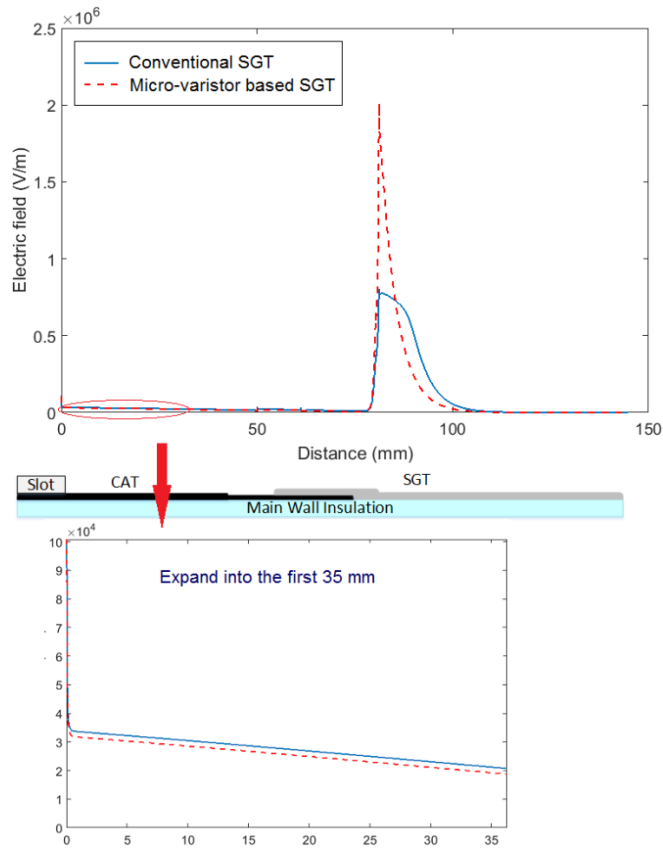
Figure 3-72: Electric field along the stress grading system at the end of rise time for the conventional and micro-varistor based SGT.
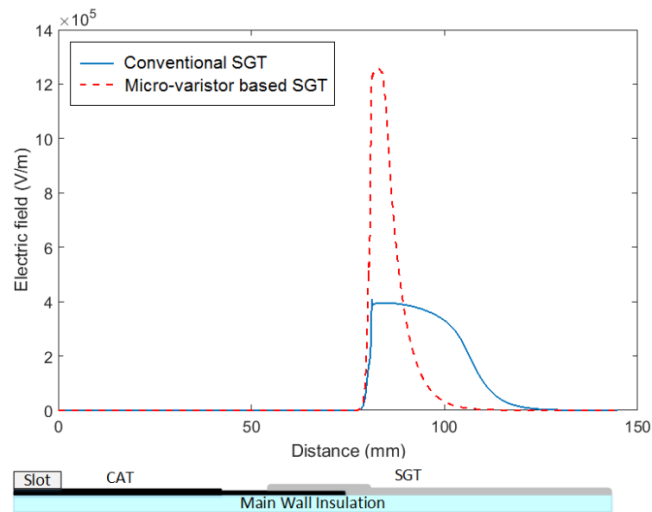
Figure 3-73: Electric field distribution along the stress grading system at 15 µs (in the flat part of the pulsed voltage) for the conventional and micro-varistor based SGT.

The temperature profile along the stress grading system, illustrated in Figure 3-74, declines very well, and almost no temperature rise occurs in the SGT region when the micro-varistor based SGT is used. This temperature reduction is due to the reduced electrical conductivity in the SGT. Although the SGT's electric field doubles, the electrical conductivity is reduced by more than 5 orders of magnitude; therefore, the amount of heat production is less than that in the conventional SGT.
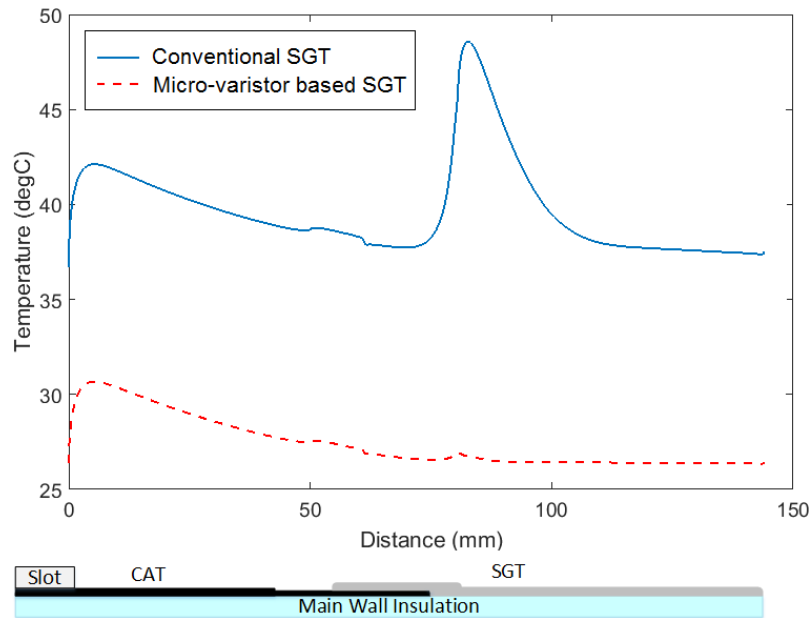
Figure 3-74: Temperature profile along the stress grading system for the conventional and micro-varistor based SGT.

A high electric field on the surface of the stress grading system can lead to PD, which creates ozone and oxides of nitrogen, and additionally, carbonizes insulation, eventually causing it to fail. Therefore, it is necessary to reduce the electric field on a stress grading system's surface. As reported in [13], the electric field can be reduced by increasing the conductivity of the SGT; the conductivity of the micro-varistor based SGT has therefore been selected to $2 \times 10^{-9} \times e^{9 \times 10^{-6} \times E}$ (S/m) without changing the level of nonlinearity. This increase can be achieved by changing the volume, shape and diameter of fillers [19, 46, 48, 51]. Figure 3-75 shows the electric field distribution at the end of the pulsed voltage rise time along the stress grading system for all three SGT conductivities. The maximum electric field reduces to 1.35 kV/mm for the high-conductive micro-varistor based SGT, which can reduce the probability of PD.
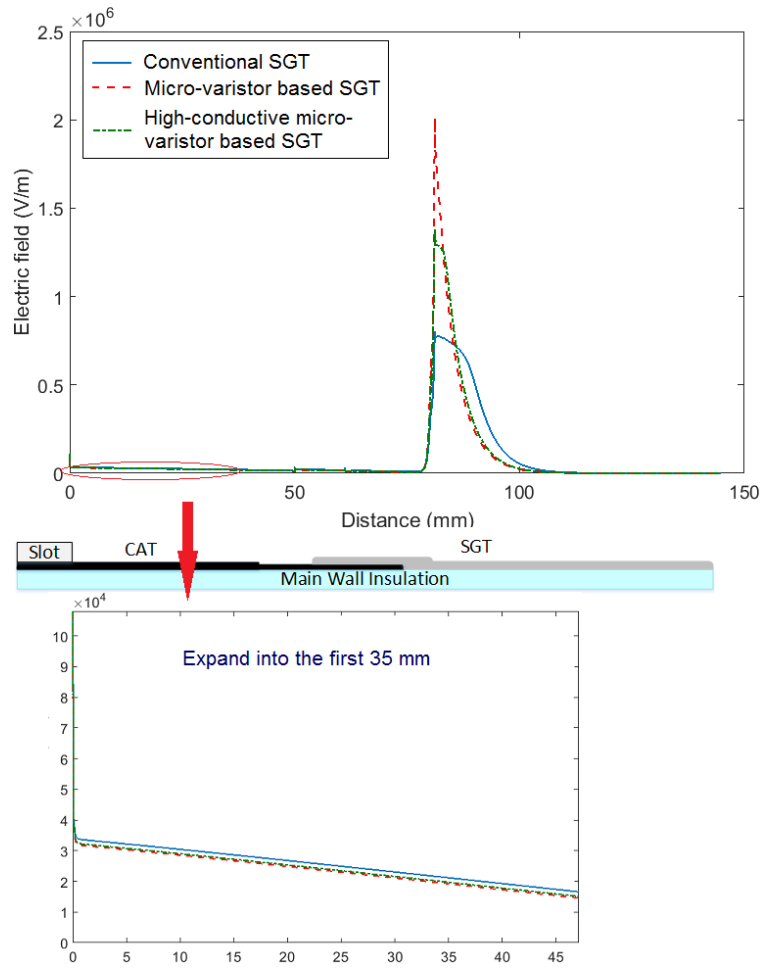
Figure 3-75: Electric field along the stress grading system at the end of rise time for three SGT conductivities.

The temperature profile along the stress grading system is illustrated in Figure 3-76 for the three SGT conductivities. The temperature rise of the SGT region for the high-conductive micro-varistor based SGT is still very low compared to that of conventional SGT, thereby showing the good performance of the high-conductive micro-varistor based SGT.
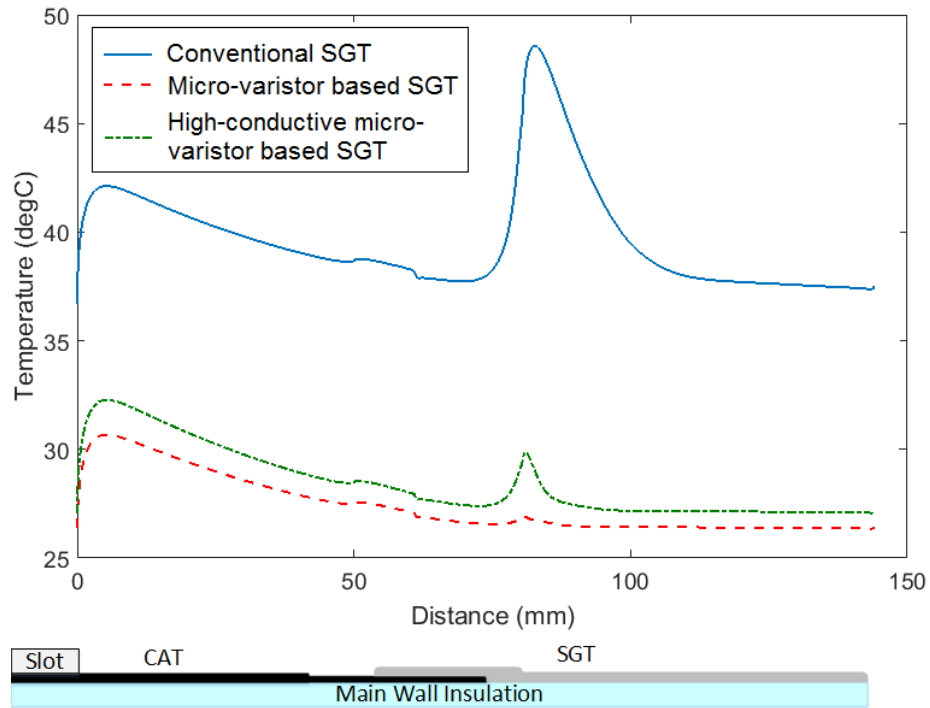
Figure 3-76: Temperature profile along the stress grading system for three SGT conductivities.

3.7.10 Proposed Stress Grading System

The effect of CAT length on the electrical and thermal performances of stress grading systems was investigated in section 3.7.7 and showed the advantages of the reduced CAT length. In this section, the performances of a proposed stress grading system that is combination of both reduced CAT length and the micro-varistor based SGT have been evaluated. Figure 3-77 shows the electric field distribution at the end of the pulsed voltage rise time along the stress grading system for conventional SGT, the high-conductive micro-varistor, and the proposed system with shorter (40 mm) CAT length. The results show that reducing the CAT length reduces the electric field in CAT, whereas the electric field in SGT remains almost the same. The temperature profile along the stress grading is shown in Figure 3-78, in which the combination of these two modifications has a good effect on the thermal performance of the stress grading system. The temperature rise in this proposed system (4 °C) is much less than that in the conventional stress grading system (24 °C).
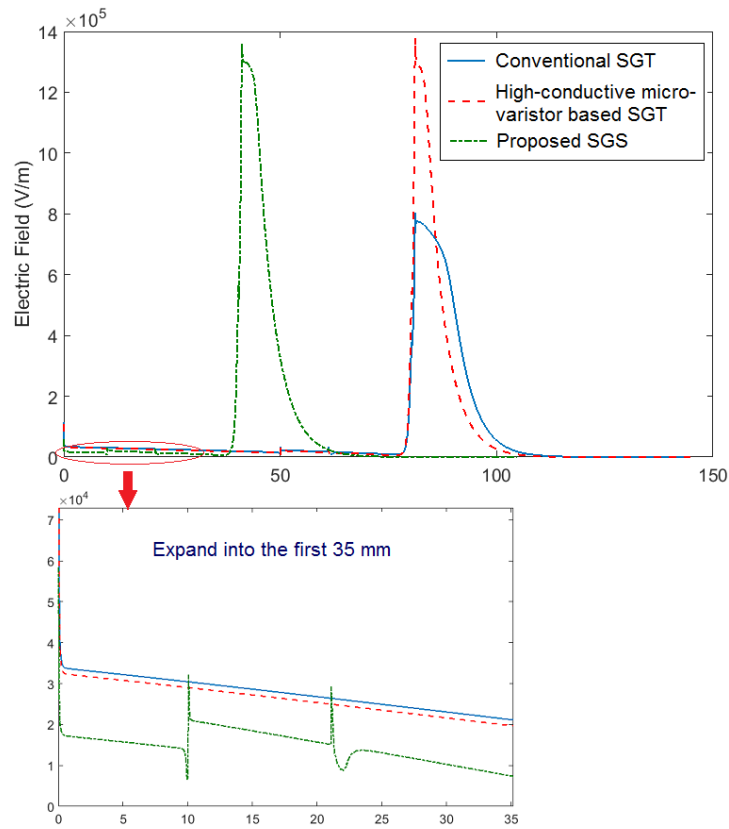
Figure 3-77: Electric field along the stress grading system at the end of rise time for conventional SGT, high-conductive micro-varistor based SGT and the proposed system.
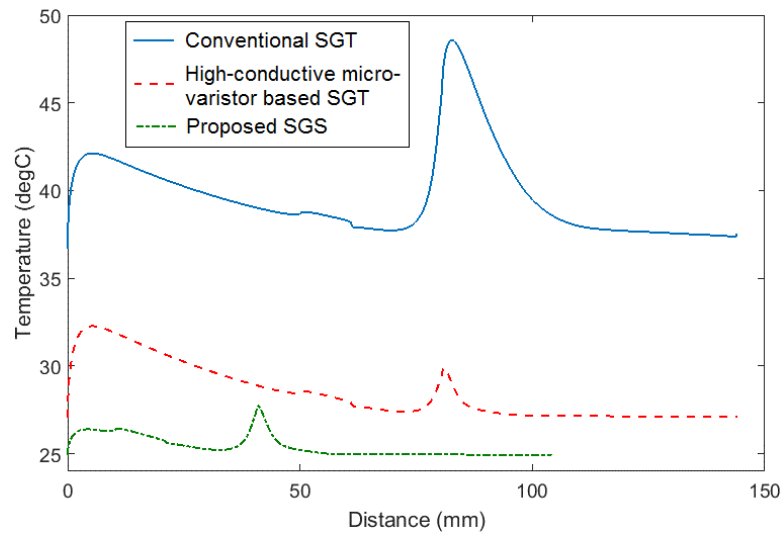
Figure 3-78: Temperature profile along the stress grading system for conventional SGT, high-conductive micro-varistor based SGT and the proposed system.

With a reduced CAT length, the pressure fingers affect the electric field distribution on the surface of the stress grading system and also on the surface of the fingers [25]. Therefore, it is necessary to check the electric field distribution in the overhang region in the presence of the pressure fingers when there is a shorted CAT length. Figure 3-79 illustrates the electric field distribution at the end of the pulsed voltage rise time along the stress grading system in the presence of the pressure fingers for the proposed stress grading system. The maximum electric field on the surface of the pressure finger is around 0.76 kV/m; therefore, the probability of PD occurrence is very low.
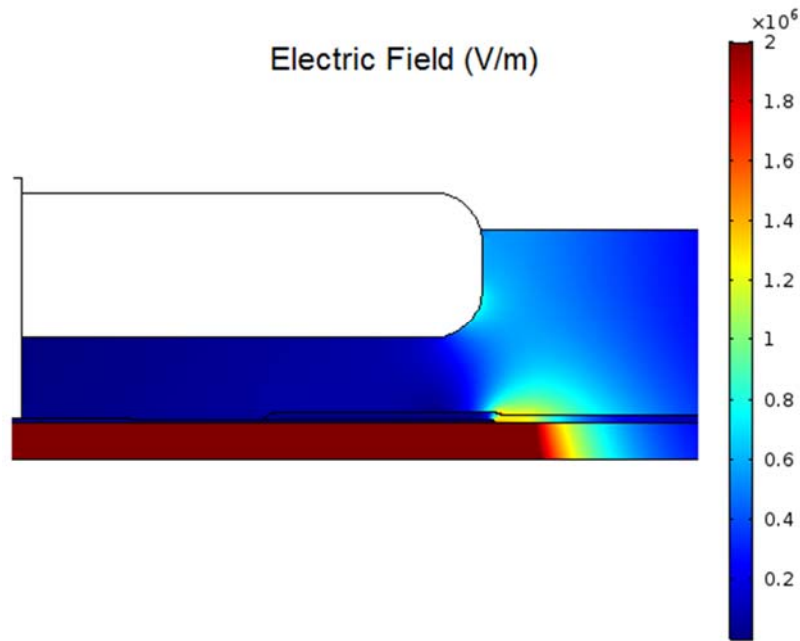
Figure 3-79: Electric field distribution at the end of pulsed voltage rise time for a 40 mm CAT length with a pressure finger.

3.7.10.1 3D Simulation of the Proposed Stress Grading System

To precisely assess the effect of this proposed stress grading system, this system was modeled in a 3D configuration and its electrical and thermal performances were evaluated. The verification of this 3D model is shown in section 3.6.2. The CAT length was reduced to 40 mm and the high-conductive micro-varistor was considered as the SGT in the simulation model. Comparing the results of the conventional and the proposed system clarifies the advantages of this system. Figure 3-80 compares the electric field distribution along the stress grading system at the end of the pulse rise time for the conventional and proposed systems. The electric field distribution is narrowed, and the maximum field

104

is increased from 0.8 kV/mm in the conventional stress grading system to approximately 1.4 kV/mm in the proposed one. The 3D simulation results show the same trend as the 2D ones (Figure 3-77).
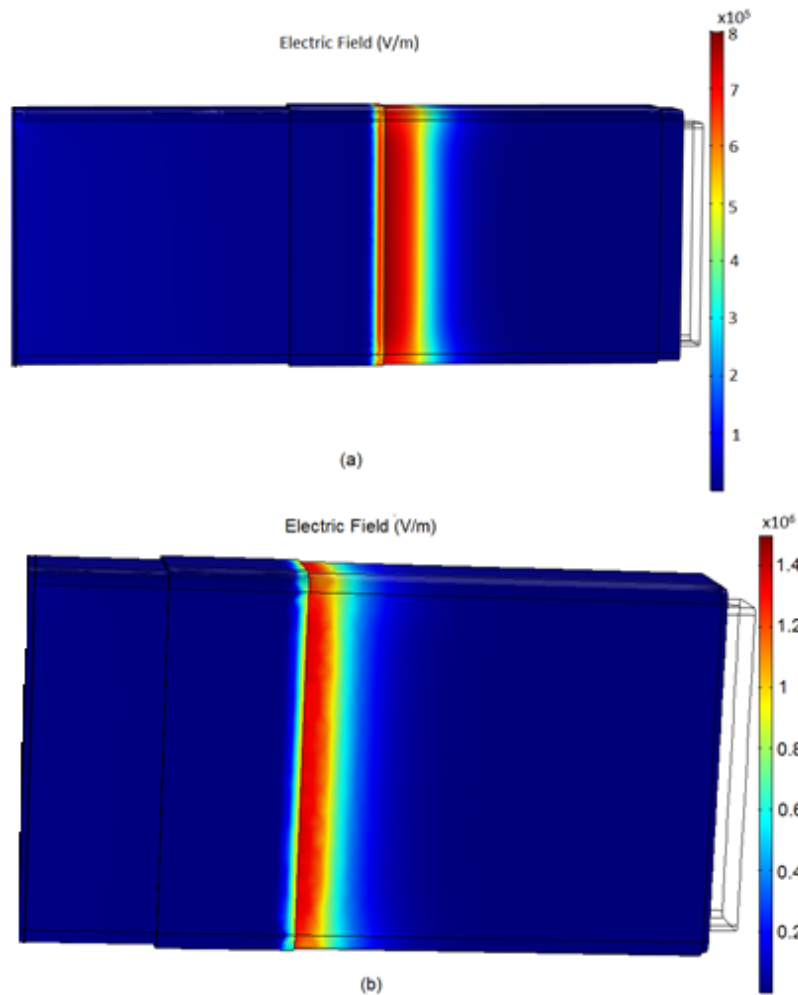
Figure 3-80: Electric field distribution at the end of pulsed voltage rise time for (a) conventional and (b) proposed stress grading system.

Figure 3-81 shows the electric field distribution on the CAT region at the end of the pulse voltage rise time. The maximum range of simulation results was reduced to clearly reveal the differences between these two systems. The electric field on the CAT region decreases in the proposed stress grading system, and the maximum electric field reduces from 0.12 to 0.08 kV/mm. The CAT on the top of actual coils and also in 3D simulation does not connect to the stator; therefore, all surface current on the top of the CAT must go through one point (the top left point in Figure 3-81) to the ground,

increasing the electric field at this point. Thus, the maximum electric field in the 3D simulation is higher than that in the 2D one (Figure 3-78).
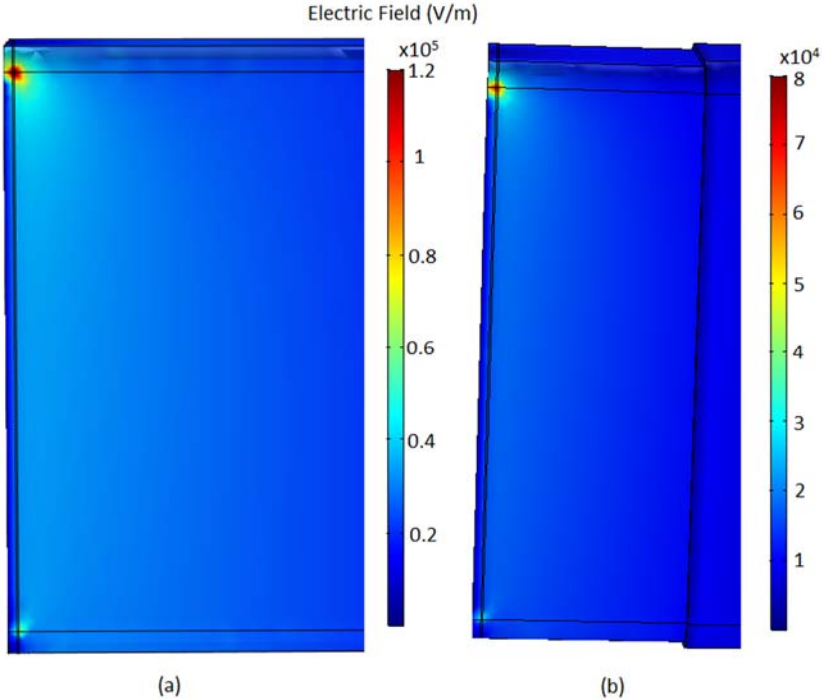
Figure 3-81: Electric field distribution at the end of pulsed voltage rise time in CAT region for (a) conventional and (b) proposed stress grading system.

The temperature profile along the stress grading system under pulsed voltage for both systems is illustrated in Figure 3-82. The temperature significantly reduces with the proposed stress grading system, leading to good performance under pulsed voltage condition. The maximum temperature decreases to 31 °C for the proposed system, compared to approximately 47 °C for the conventional one.
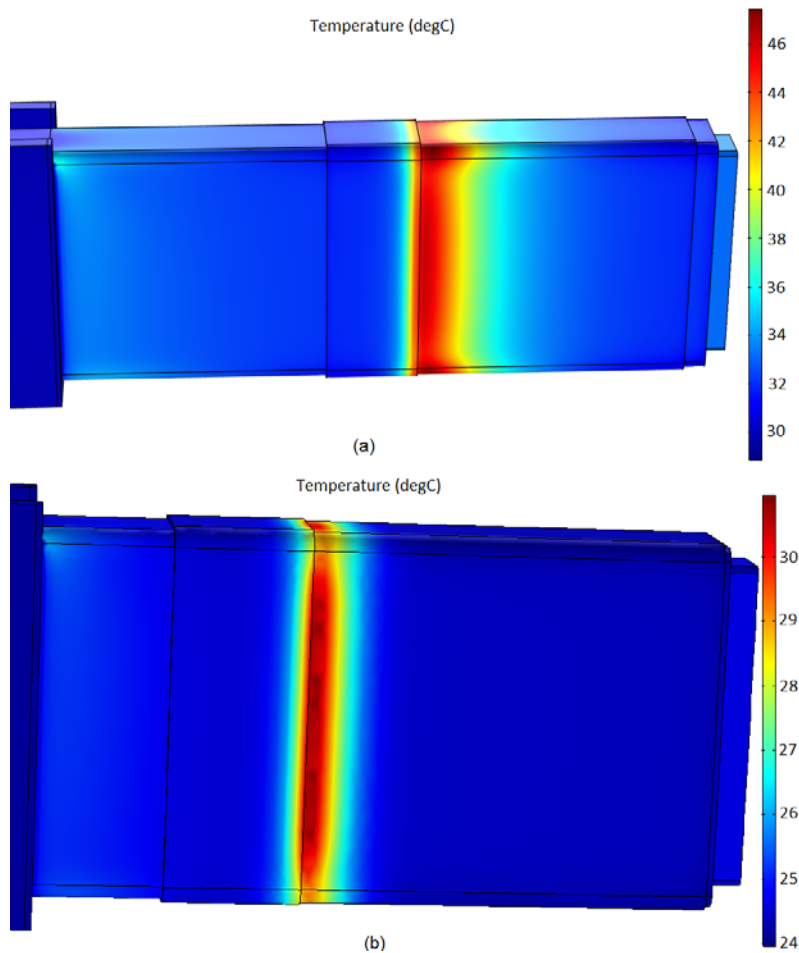
Figure 3-82: Temperature profiles along the stress grading system under pulsed voltage for (a) conventional (b) proposed stress grading system.

3.8 Cable Termination

The thermal performance of the cable termination using micro-varistor- based stress grading was evaluated using an advanced infrared camera. The temperature profile along the cable termination was measured and simulated under a pulsed voltage (a 2.5 kHz, 12 kV peak pulsed voltage). This voltage was applied to the conductor for two hours at room temperature to stabilize the temperature. The measured surface temperature of the cable termination can be seen in Figure 3-83.
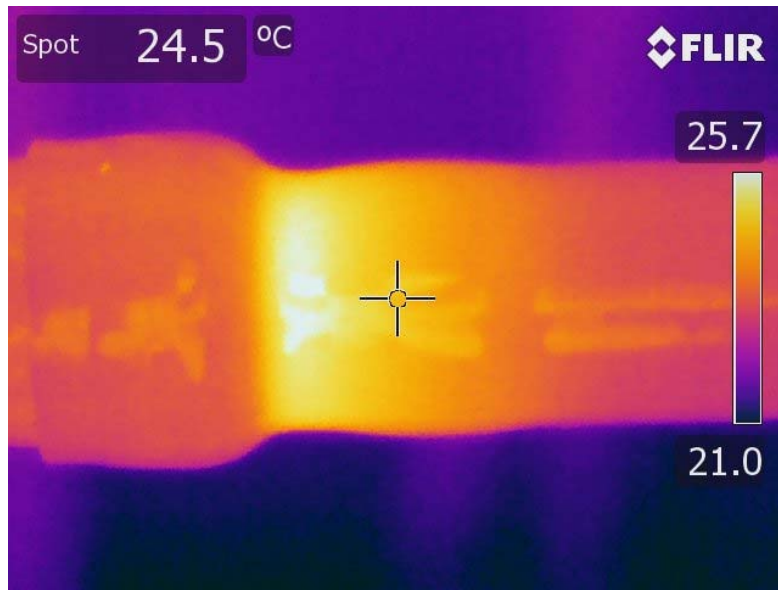
Figure 3-83: Measured temperature profile along the cable termination under pulsed voltage.

As discussed earlier, the actual applied pulsed voltage was implemented as the input voltage for the simulation. Figure 3-84 shows the schematic of cable termination used in simulation. Figure 3-85 illustrates the simulated profile of the temperature on the surface of the cable termination. Figure 3-86 presents the measured and simulated profiles of the temperature along the cable termination under the pulsed voltage. Comparing these profiles verifies the simulated results.
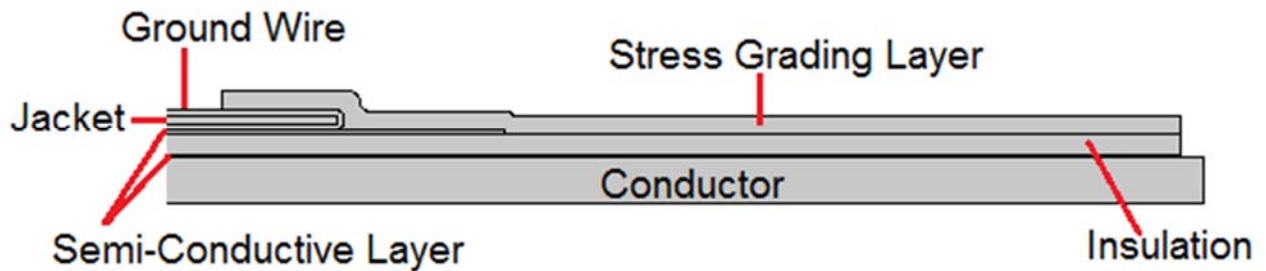
Figure 3-84: Schematic of cable termination used in COMSOL.
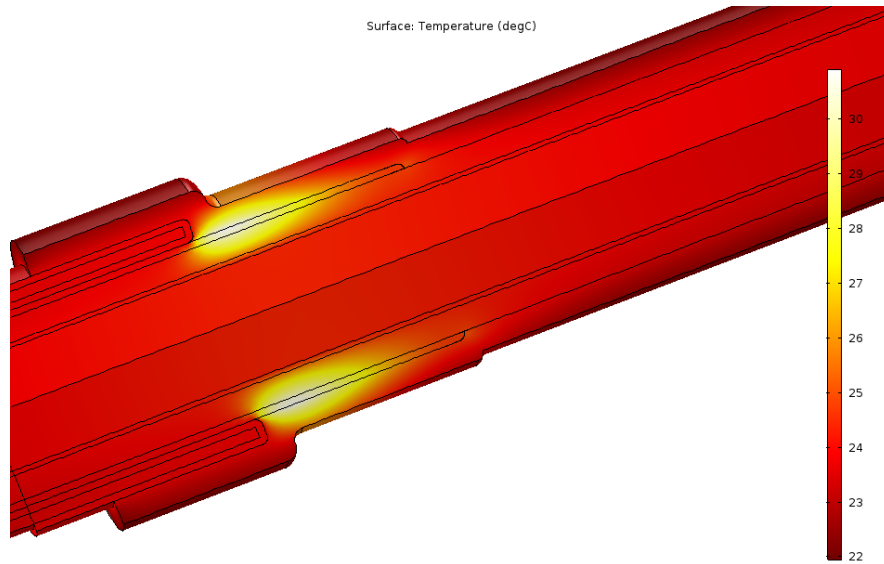
Figure 3-85: Simulated temperature profile along the cable termination under pulsed voltage.
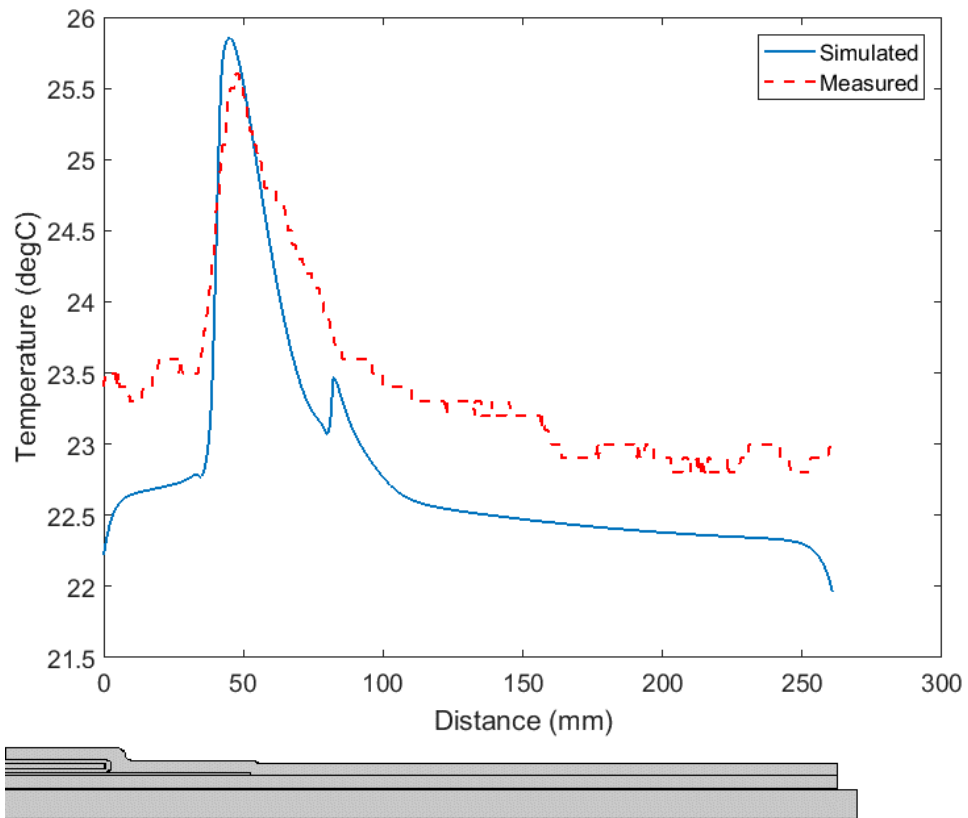
Figure 3-86: The measured and simulated temperature profiles along the surface of the cable termination under pulsed voltage.

109

The electric field distribution at the end of the rise time and the flat portion of the pulsed voltage along the cable termination is shown in Figure 3-87. The 2D electric field distribution along the cable termination at the end of the rise time and the DC portion of the pulsed voltage are shown in Figure 3-88.
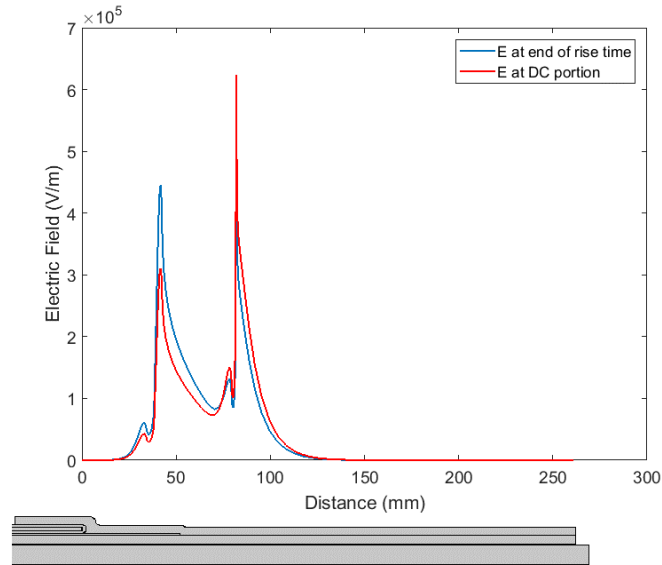
Figure 3-87: The electric field distribution along the cable termination at the end of rise time and DC portion of pulsed voltage.
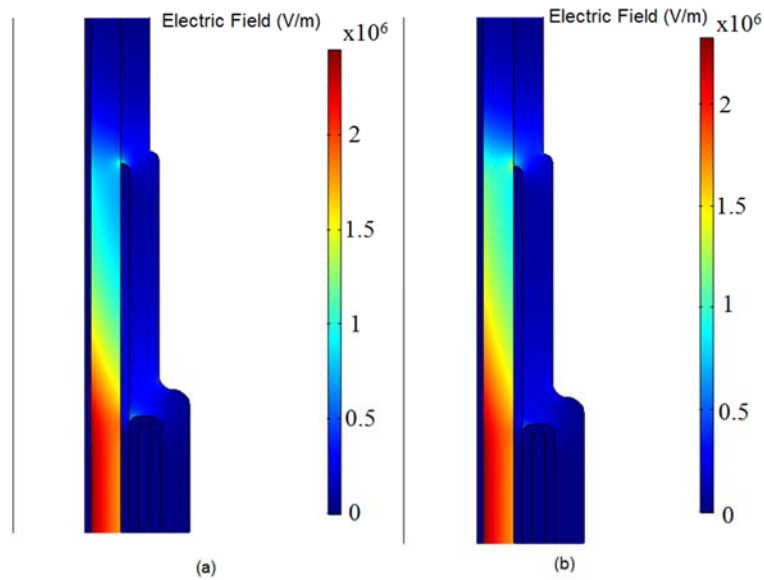
Figure 3-88: The 2D electric field distribution along the cable termination (a) at the end of rise time and (b) at the DC portion of pulsed voltage.

110

Chapter 4

Discussion

4.1 Introduction

This chapter discusses the findings presented in Chapter 3. The electrical conductivity of the CAT and SGT are analyzed, and their dependence on the electric field, temperature, and vacuum pressure impregnation (VPI) are discussed. Experimental and simulation works are used to evaluate the performance of a conventional stress grading system under pulsed width modulation (PWM) voltages. The influence of material properties and stress grading builds on the electrical and thermal performances of stress grading system is summarized. The coupled electro-thermal simulation model is developed by using appropriate material properties measured in situ to simulate accurate electrical and thermal analyses. The advantages of reducing CAT length are investigated, and SGT conductivity is optimized to improve electrical and thermal performances. A proposed stress grading system that combines an optimized SGT conductivity and minimum CAT length is evaluated, summarizing the effect on temperature and electrical performances under pulsed voltage. It is essential to note that the worst case scenario of output voltage (output voltage of three-level drivers without LC filters) are considered in this study.

4.2 Electrical Conductivity of CAT and SGT

The manufacturer's specified electrical conductivity, usually given for room temperature, does not represent the conductivity that follows VPI of the tapes. As the electrical conductivity can be altered by the VPI process, simulation studies must be performed using conductivity values measured after VPI. An additional factor is that normal motor operating temperature is well above the room temperature; thus, accurate analysis requires the use of electrical conductivity at those operating temperatures.

In addition to using the appropriate operating temperature, because the electric field at the SGT region can exceed 1 kV/mm, SGT electrical conductivity must be measured under a high electric field. Since the temperature rises excessively in the SGT during these measurements above 0.6 kV/mm under DC conditions, it is recommended the measurement is carried out under pulse conditions. The excellent match between the simulated and measured temperature profiles is possibly due to use of the material properties under operating conditions.

111

A class F motor insulation system is designed for continuous operation below 155 °C, for example, with an 80 °C temperature rise in a 40 °C temperature environment. The profile of the temperature along the stress grading system at a high temperature exhibits a temperature rise of approximately 8 °C in the SGT region for continuous operation under a pulsed voltage. As a consequence, the temperature of the insulation system design must be decreased, in turn reducing system efficiency. Otherwise, a higher insulation class will be needed.

Increasing the CAT electrical conductivity reduces the electric field at the rise time and temperatures in the CAT region. Raising the CAT electrical conductivity also slightly increases the electric field in the SGT region. The CAT electrical conductivity is limited by the eddy currents inside the slot, so one solution is to increase the CAT electrical conductivity only outside of the slot [50]. This solution is complicated for manufacturing because coils are prepared outside and then inserted into the slots, which means the location of the slot exits is not fully clear during coil preparation. On the other hand, increasing the CAT electrical conductivity could also increase the electric field in the SGT above the threshold so that PDs occur in this region. The key consideration should be that CAT electrical conductivity can be increased only as long as the eddy current and electric field in the SGT region remain within acceptable margins.

Although increase in the SGT electrical conductivity reduces the electric field in this region, the temperature of the end winding is increased, and the extent of a high electric field in the SGT region is also expanded; which creates an area of increased heat production in the SGT. Additionally, increased SGT electrical conductivity slightly increases the electric field in the CAT under a pulsed voltage leading to a rise in the temperature of the CAT region. On the other hand, reducing the SGT electrical conductivity increases the electric field in this region, which can produce PDs. The use of other non-linear tape materials for SGT might be needed for the effective reduction of the temperature rise and the electric field in the SGT.

Increasing the level of the nonlinearity of the SGT conductivity expands the region of the SGT having a high electric field; therefore, the SGT is more efficiently used. Additionally, the peak of the electric field in the SGT region is reduced significantly with an increase in the level of the nonlinearity. But the thermal performance corresponding to the high level of the nonlinearity is unacceptable as the temperature rise is increased.

The thermal performance with a low level of nonlinearity of the SGT conductivity is acceptable but the peak of the electric field is very high in SGT, which might lead to PD inception in the SGT region

112

under certain operating temperatures and field conditions. It is therefore concluded that changing only the level of the nonlinearity of the SGT conductivity cannot improve both electrical and thermal performances. Therefore, an alternative SGT material is necessary to improve the electrical and thermal performances of stress grading systems.

4.3 Stress Grading Builds

The CAT length was optimized to minimize both the temperature and maximum electric field along the stress grading system. The temperature profiles of samples with different CAT lengths were measured under pulsed voltage at room temperature and at elevated room temperature (Figures 3-22, 3-23, and 3-24). A coupled electro-thermal finite element method (FEM) simulation of two CAT lengths was verified by measuring the temperature profiles under certain conditions (described in Chapter 3). The simulation results show the profile of the temperature and electric field in the overhang region of a form wound medium voltage coil. In addition, the partial discharge (PD) were measured under power frequency voltage and pulsed voltage for the samples with different CAT lengths.

Maximum temperature for insulation materials is specified by the insulation class. Thermal life expectancy of an insulation system, when operated continuously at the maximum temperature rating of the insulation system, is approximately 20,000 to 25,000 hours under ideal environmental conditions [1]. However, a three-year operation is not sufficient for the MV motor, therefore, the manufacturer must consider an operating temperature much lower than the maximum temperature. For example, for class F (used mostly in MV motors) the allowable maximum temperature is 155 $^{\circ}$C; but the recommended operating temperature is 110 $^{\circ}$C to increase the life of insulation system. As illustrated in Figure 3-57, the maximum temperature can be decreased if the CAT length is reduced. As a consequence, the temperature specified in the insulation system design can remain unchanged when the motor is fed by an adjustable speed drive, with no reduction in the motor's life.

Reducing the length of the CAT significantly reduces the electric field in the CAT region, which leads to a reduction in Joule heat and temperature at the slot exit of the machine. The electric field is reduced by half if the CAT length is decreased from 100 to 40 mm. During the rise time of the pulse voltage, the electric field on the SGT increases slightly but decreases slightly during the DC portion of the pulse. Therefore, average heat production in SGT region is almost fixed.

In MV motor designs where pressure fingers are used, the fingers alter the electric field distribution along the stress grading system. The CAT length cannot be reduced without considering the effect of

the pressure finger on the electric field distribution. For the case considered with 13.8 kV motor coil, the electric field on the surface of the finger is modified by the location and shape of the fingers and it is increased to 1.8 kV/mm for the 20 mm CAT length; a high electric field also can give rise to PDs. Optimization of the shape and location of the pressure finger to reduce and unify the electric field along the stress grading system is essential.

If the electric field on the surface of the stress grading system exceeds a threshold that is related to the temperature and pressure, PD will occur that will eventually erode the main wall insulation. IEC standard 60034-18-42 describes Type II insulation systems that can be subjected to PD during operation, but PD must not significantly increase in the proposed configuration. PD measurement under pulsed voltage is essential for motors fed by ASDs and can provide critical information on the insulation system that cannot be obtained with a conventional PD measurement with power frequency voltage. For the proposed stress grading system, it is important to note that PD measurement under power frequency and pulsed voltages are not significantly impacted by a change in CAT length.

Increasing CAT thickness by increasing the number of CAT layers reduces the electric field and temperature in this region. Although the electric field in the SGT region is slightly increased by this change, the temperature in the SGT region is reduced. Generally, increasing the CAT thickness has good effects on the electrical and thermal performances of the stress grading system, but has limitations due to the width of the slots. In addition, CAT conductivity is also increased by enhancement of the CAT thickness, which also improves performance.

The electric field in the SGT region is reduced with increased SGT thickness. On the other hand, the electric field in CAT is almost fixed and does not change with a change in SGT thickness. Although an increase in SGT thickness leads to better electrical performance of the stress grading system during the rise time, the temperature in the SGT and CAT regions increases slightly.

4.4 Proposed Stress Grading System

The electrical conductivity of SGT is an important parameter influencing the electric field distribution and temperature profile along stress grading systems. Increasing the electrical conductivity of the SGT decreases the space charge limited field (SCLF), resulting in uniform voltage and electric field distributions, but the temperature rise increases, leading to hot spots and eventual material degradation in the stress grading system [16, 18, 86]. On the other hand, changing the level of nonlinearity of the SGT conductivity cannot improve the electric field and temperature rise together, and an increase of

this level reduces the electric field along the stress grading system, but increases the temperature rise and vice versa [16]. Therefore, optimized SGT conductivity is essential to improve both the electric field distribution and temperature rise along stress grading systems.

The micro-varistor-based SGT is more nonlinear than the SiC-based ones that are commonly used for the SGT of motor winding, although according to [51], some SiC-based stress grading materials are used in cable terminations, and have nonlinear conductivity that depends on an electric field, much like micro-varistor ones (Figure 3-71). These highly nonlinear conductivities for SGT significantly reduce the temperature rise of stress grading systems, but can increase the electric field more than a threshold, leading to PD on the stress grading system's surface. Therefore, optimization was done on the conductivity characteristic to reduce the electric field to an acceptable level where the temperature rise is still much lower than that generated in conventional stress grading systems. The conductivity of the micro-varistor-based SGT was increased to achieve both good electrical and temperature performances.

The proposed stress grading system combines two approaches: reduced CAT length and high-conductive micro-varistor-based SGT. The results confirm the desired improvements in electrical and temperature performances of the proposed system. The maximum electric field on the surface of this system may still be high enough to create PD under certain operating conditions, but it can easily be reduced by increasing the conductivity of SGT. The conductivity formula is considered as an exponential function. Thus,

$$\sigma = \sigma_0 * exp^{k*E} \qquad (S/m)$$

$$(4.1)$$

where σ_0 is the initial conductivity, and k is the level of nonlinearity in the SGT conductivity. Without changing the level of nonlinearity, $k = 9 \times 10^{-6}$ for the micro-varistor, increasing the initial conductivity reduces the electric field in the SGT region. For various initial conductivities, the electric field and temperature distribution along the stress grading system with 40 mm CAT length are shown in Figures 4-1 and 4-2, respectively. The maximum electric field and temperature, as functions of the initial conductivity (σ_0), are illustrated in Figure 4-3; the maximum electric field is reduced by increased initial conductivity, but the temperature rise is slightly enhanced. An optimized initial conductivity must be selected to achieve the desirable electrical and thermal performances.
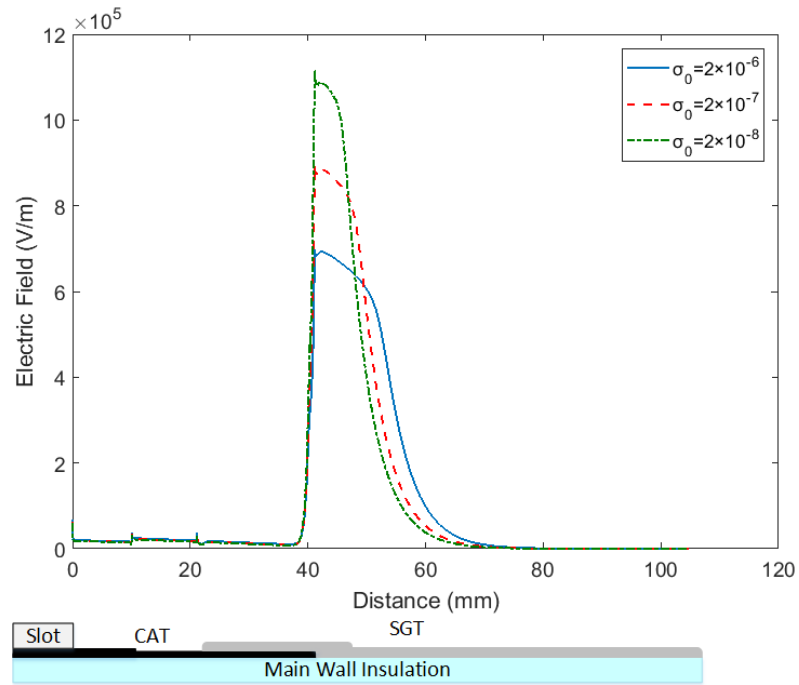
Figure 4-1: Electric field distribution at the end of pulsed voltage rise time for three different initial conductivity of micro-varistor based SGT with 40 mm CAT length.
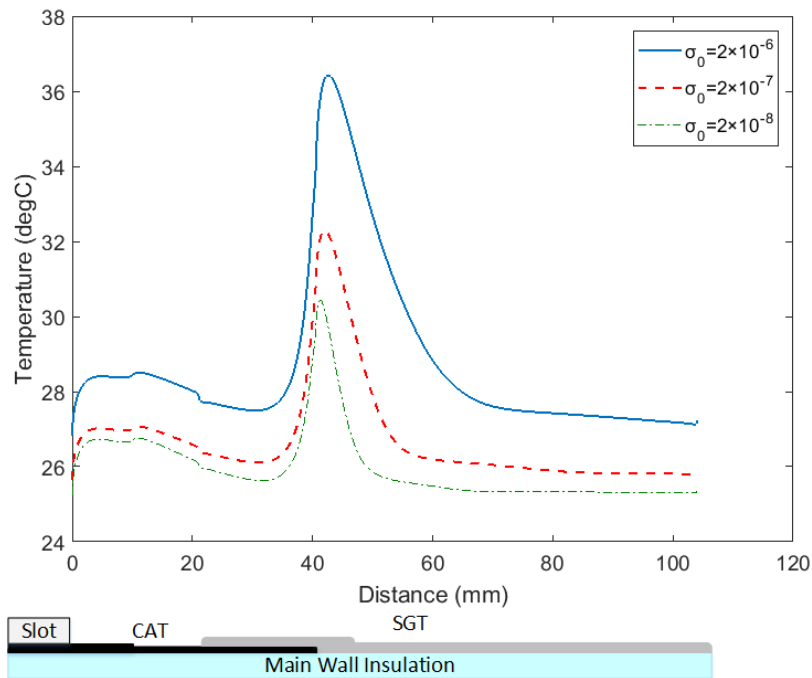
Figure 4-2: Temperature profiles along the stress grading system for three different initial conductivity of micro-varistor based SGT with 40 mm CAT length.
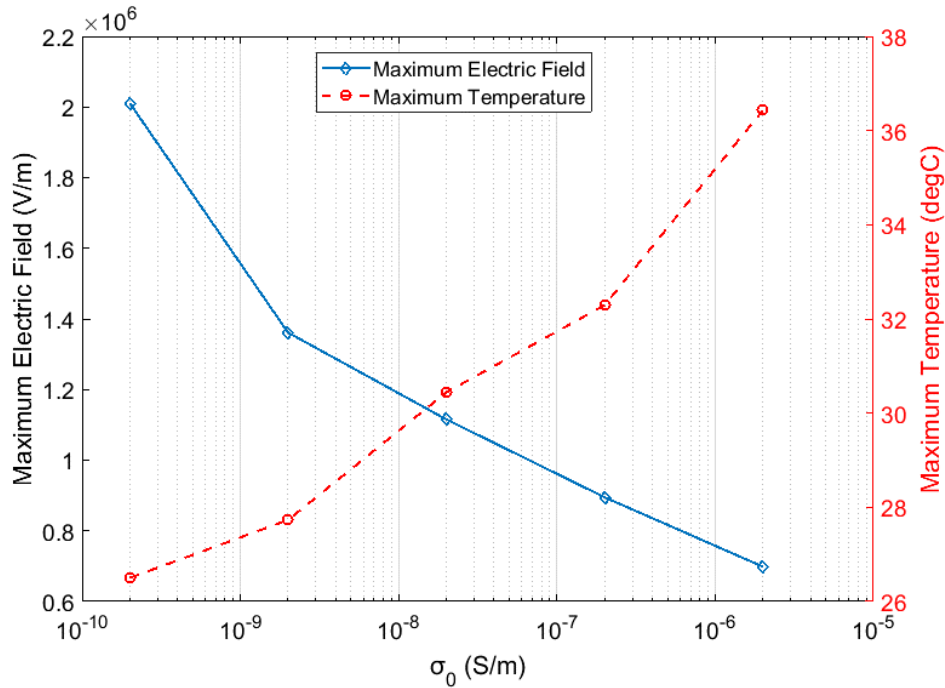
Figure 4-3: Maximum electric field and temperature of the stress grading system as a function of initial conductivity of micro-varistor based SGT with 40 mm CAT length.

According to Figure 4-3, the best value for initial conductivity of the SGT is 2×10^{-8} S/m, which leads to maximum electric field less than 1.2 kV/mm and temperature rise of 32 ºC. The proposed stress grading system with the desired SGT conductivity reduces the temperature rise under repetitive impulse voltages leading to maintain the lifetime of insulation system without any de-rating of the output power of MV motors. Additionally, the maximum electric field is not high enough to produce PDs.

4.5 Cable Termination

The repetitive impulse voltage is applied to the commercial cable termination used micro-varistor based stress grading and temperature rise associated to this type of voltage is measured. The cable termination is also modelled in COMSOL to deeply evaluate the micro-varistor based stress grading system. The measured and simulated results confirm the desire electrical and thermal performance of micro-varistor materials that can be used in the form wound coils of MV motors and improve the performance of the stress grading system under repetitive impulse voltage.

Chapter 5

Conclusions and Suggestions for Future Work

5.1 Summary

The trend of using medium voltage (MV) motors with adjustable speed drives (ASD) has increased recently because this type of drive can precisely control the speed of industrial processes. The conventional materials of conductive armor tape (CAT) and stress grading tape (SGT) and their builds on form-wound motor coils are suitable for power frequency. However, under repetitive fast impulse voltages from pulse-width modulated (PWM) drivers, they are exposed to severe electrical and thermal stresses that may lead to premature insulation failure. Only a few previous studies have focused on the problems associated with stress grading systems of MV motors subjected to repetitive fast impulse voltages. Therefore, this thesis has carried out a comprehensive study of the problems associated with the stress grading systems in drive-fed motors and proposes an effective stress grading system under repetitive fast impulse voltages.

The study measured the material properties after VPI and under operating conditions by using actual samples made by GE Power Conversion of the end winding region of a 13.8 kV motor. In addition, repetitive impulse voltages with an 11.3 kV peak at 2.5 kHz and 300 ns rise time were applied to samples for two hours to stabilize the temperature profile. The surface temperature was measured by using an IR camera to verify the simulation models. The same dimensions as the actual sample were used to simulate the stress grading system in the COMSOL simulation, along with the accurate material properties. The pulsed voltage used in the experimental study was also captured by oscilloscope and then digitized and used in the simulation, to provide the same input data. The verified numerical simulation was used to investigate the effects of materials' properties and the builds of stress grading systems on the electrical and thermal performance of this system under repetitive fast impulse voltages.

For high rated voltage motors, three-level drivers with a large LC filters or higher level drivers are commonly used to reduce the stress on the insulation systems. Using three-level drivers without LC filters has economic advantages and reduce the weight and size of drivers; therefore, the worst case scenario (three-level drivers without LC filters) was considered in this study. The comprehensive study of effect of material properties and builds on the electrical and thermal performance of the stress grading system was carried out in this condition and the proposed stress grading system works well under the

output voltage of three-level drivers that can open a new window to future development of three-level drivers.

A high voltage pulse generator and an antenna-based PD detector were implemented to investigate the effects of pressure fingers on the PD levels of form-wound coils under reduced CAT length. By conducting measurements and finite element method (FEM) simulations on different builds and materials' properties of stress grading systems, a new system is proposed, and provides the desired electrical and thermal performance under repetitive fast impulse voltages.

5.2 Conclusions

The conductivity measurements and simulations on the electrical and thermal performances of stress grading systems with different CAT and SGT conductivities led to the following conclusions:

- The surface and volume conductivities of the CAT layer are greatly affected by the VPI process, particularly in the transverse direction. The VPI process changes the conductivity of the top layer, because of the resin rich layer, but under this layer the volume conductivity in the longitudinal direction is only marginally affected.

- Temperature and tape build can alter electrical conductivity. CAT conductivity is increased when both the number of layers and the temperature are raised. On the other hand, the SGT conductivity elevates with an increase in the number of layers and a decrease in the temperature.

- Increasing CAT conductivity reduces the electric field in this region. Although this increment leads to a slight increase in the electric field in the SGT region, the temperature and heat production are decreased.

- Increasing the SGT electrical conductivity decreases the electric field in this region, thus creating a uniform electric field distribution. On the other hand, it increases the temperature and heat production of the stress grading system. SGT conductivity has less effect on the electric field distribution in the CAT under pulsed voltage conditions.

Investigating the effects of stress grading system builds on its performance led to the following conclusions about builds and desired CAT length:

- Increasing the CAT thickness by increasing the number of layers reduces the electric field and heat production in this region. It has good effects on the electrical and thermal

119

performances of the stress grading system, but has limitations due to the width of the slots. In addition, CAT conductivity increases with enhanced CAT thickness, and also improves stress grading system performances. Although the electric field in the SGT region was slightly increased with the greater CAT thickness, the heat production in the SGT region was reduced.

- The electric field in the SGT region was reduced by the increase in SGT thickness. On the other hand, the electric field in the CAT was almost fixed and did not change with changes to the SGT thickness. Increasing the SGT thickness leads to improved electrical performance of the stress grading system during the rise time, but the average heat production in the SGT and CAT regions increased.

- Decreasing the CAT length significantly reduces the electric field in the CAT region, leading to decreased heat production and a lower temperature profile for the stress grading system. Reduced CAT length slightly increases the electric field in the SGT region during the rise time of the pulsed voltage and reduces moderately during the flat portion of the pulsed voltage. The jump in the temperature profile in the SGT region for different CAT lengths confirms that the average heat production and temperature profile in the SGT region are almost fixed for a given CAT length.

- Minimizing the CAT length leads to good electrical and thermal performances of the stress grading system under pulsed voltage and reduces the temperature rise of the stress grading system. Therefore, the design temperature for the insulation system can remain unchanged when the system is fed by an adjustable speed drive, without any reduction in the life of the motor.

- The pressure finger limits the minimum CAT length, and it is important to evaluate the effect of the pressure finger on the electrical and thermal performances of the stress grading system.

- PD measurement under pulsed voltage is important for motors fed by ASD. PD measurement results under power frequency and pulsed voltages show that CAT length has no effect on the PD of the stress grading system, and the PD is almost fixed for different selected CAT lengths.

Based on the simulation studies on the effect of the SGT nonlinearity on the electrical and thermal performance of stress grading system, the following conclusions are drawn:

120

- Increasing the level of the nonlinearity of the SGT conductivity expands the region of high electric field in SGT; therefore, the SGT is more efficiently used. Additionally, the peak of the electric field in the SGT region is reduced by increasing the level of nonlinearity. On the other hand, the thermal performance with a high level of the nonlinearity is unacceptable, and the maximum temperature rise is increased.

- The thermal performance with a low level of the nonlinearity is acceptable, but the peak of the electric field is very high, thus increasing the partial discharges on the stress grading system.

Simulation results show that changing only the level of the nonlinearity of the SGT cannot simultaneously improve electrical and thermal performance, nor can changing the SGT conductivity. Therefore, new SGT material is necessary to improve the electrical and thermal performances of the stress grading system. Investigating the use of micro-varistor-based stress grading materials led to following conclusions and a proposed stress grading system:

- Using the conductivity characteristic for SGT based on a micro-varistor improves the temperature profile of the stress grading system, and significantly reduces the temperature rise in this system under PWM voltages. On the other hand, the maximum electric field in the SGT region increases to approximately 2 kV/mm, probably leading to localized PD.

- Optimized SGT conductivity reduces the maximum electric field to an acceptable value by increasing the initial conductivity (σ_0). This value must be selected according to both the temperature rise and maximum electric field.

- The proposed stress grading system (a combination of an optimized SGT conductivity and minimum CAT length) performs well both electrically and thermally, making this system effective under PWM voltages.

- The practical usage of micro-varistor based material as a stress grading system in cable termination shows desirable electrical and thermal performance with this type of materials.

5.3 Contribution

Motivated by the aim of designing an improved stress grading system with the ability to withstand the severe stresses created by repetitive fast impulse voltages, this thesis has presented a comprehensive overview of the effects of high frequency fast rise stresses on the stress grading systems of form-wound

coils in MV motors. The results of this project expand the understanding of how the material properties and builds of the stress grading systems influence their electrical and thermal performances. An additional important finding is that both electrical and thermal performances are not improved by changing the conductivity of conventional SGT under three-level drivers; therefore, new SGT material is necessary to improve the electrical and thermal performances of stress grading systems. This research carried out a comprehensive study of the stress grading systems that also contributes to the development of a standard for the qualification of the stress grading systems of MV motors fed by ASDs.

The test equipment developed during this research, including high voltage pulse generators and a PD measurement system under repetitive impulse voltages, will contribute to further research in the high voltage engineering laboratory.

This comprehensive study of the effects of different materials' properties and the builds of stress grading systems on their performance can be employed by manufacturers to improve the design of these systems. In addition, the proposed stress grading system can be used by manufacturers to improve the performance of stress grading systems under the output voltage of three-level drivers.

Another important part of this research is the numerical simulation model can be used to evaluate the effect of any changes in the stress grading systems on both electric field distribution and temperature profiles. Additionally, any changes in the output voltages of modern drivers with the new generation of power switches based on SiC power switches can be incorporated.

5.4 Suggestions for Future Work

Practical implementation of the proposed stress grading system for the end winding of form-wound coils will require close cooperation with a manufacturer of motors in order to evaluate the possibility of manufacturing the system. The implementation will require the development of suitable tapes of good quality to ensure a long useful life.

After preparing the proposed stress grading system, long-term full monitoring of this system proposed in this study is suggested as an extension of this work. Accelerated tests, with temperature and voltage, can be used to compare the system's performance with that of conventional ones. During these long-term evaluations, measurements of temperature along the stress grading system and PD measurements under repetitive impulse voltage are recommended as additional parameters to be monitored.

One suggestion for future work is to improve the thermal conductivity of materials used in the stress grading systems by adding high thermal conductive Nano-fillers into insulation systems. Higher thermal conductivity, not only in the stress grading systems' materials but also in the main wall insulations, would be beneficial in minimizing hot spots in the system.

Another suggestion for future work, to evaluate the effects of pulse's parameters, such as rise time and switching frequency, on the performance of a stress grading systems, could be used in designing a suitable ASD for MV motors. More work is required to find the desire switching frequency and rise time needed to achieve an efficient combination of motors and drives.

The simulation study of the stress grading system with field-dependent composites can also be extended to other applications in high voltage devices where a high electric field represents a problem. The design of the stress grading systems for high voltage cable termination is one potential area.

Bibliography

[1] G. C. Stone, E. A. Boulter, I. Culbert, and H. Dhirani, "Electrical Insulation for Rotating Machines," IEEE Press, 2004.

[2] Hiller M., Sommer R. and Beuermann M., "Medium-Voltage Drives," IEEE Industry Applications Magazine, vol. 16, no. 2, pp. 22-30, Feb. 2010.

[3] S. Ul Haq, PhD thesis, "A Study on Insulation Problems in Drive Fed Medium Voltage Induction Motors," University of Waterloo, Waterloo, Ontario, Canada, 2007.

[4] Emad Sharifi-Ghazvini, PhD thesis, "Analysis of Electrical and Thermal Stresses in the Stress Relief System of Inverter Fed Medium Voltage Induction Motors," University of Waterloo, Waterloo, Ontario, Canada, 2010.

[5] D. Krug, S. Bernet, S. S. Fazel, K. Jalili, and M. Malinowski, "Comparison of 2.3-kV medium-voltage multilevel converters for industrial medium-voltage drives," IEEE Trans. Ind. Electron., vol. 54, no. 6, pp. 2979–2992, Dec. 2007.

[6] J. K. Steinke, "Use of an LC filter to achieve a motor-friendly performance of the PWM voltage source inverter," IEEE Trans. Energy Convers., vol. 14, no. 3, pp. 649–654, Sep. 1999.

[7] S. Pöhler, A. Mertens, and R. Sommer, "Optimization of output filters for inverter fed drives," in Proc. IEEE Annu. Conf. Ind. Electron. Soc., Paris, France, 2006, pp. 1082–1088.

[8] M. Veenstra and A. Rufer, "Control of a hybrid asymmetric multilevel inverter for competitive medium-voltage industrial drives," IEEE Trans. Ind. Appl., vol. 41, no. 2, pp. 655–664, Mar./Apr. 2005.

[9] Y. Shakweh, "Power Devices for Medium Voltage PWM Converters," Power Engineering Journal, vol. 13, no. 6, pp. 297-307, Dec. 1999.

[10] Qualification and Acceptance Tests for Type II Electrical Insulation Systems used in Rotating Electrical Machines Fed from Voltage Converters, IEC/TC 60034-18-42, Ed. 1.0, 2017.

[11] R.H. Rehder, R.E. Draper, and B.J. Moore, "How good is your motor insulation systems," IEEE Electrical Insulation Magazine, vol. 12, no. 4, pp. 8-13, July-Aug. 1996.

[12] T. Weege, "Basic Impregnation Techniques," Electrical Insulation Conference, and Electrical Manufacturing & Coil Winding Conference, pp. 709-715, September 1997.

[13] Emad Sharifi, Edward. A. Cherney, Shesha H. Jayaram, "Anisotropic Dielectric Properties of Stress Grading Materials used in Medium Voltage Form-Wound Motor Coils to Study Thermal Effects of Repetitive Fast Pulses", 2009 IEEE

Electrical Insulation Conference, Montreal, QC, Canada, pp. 333-337, 31 May - 3 June 2009.

[14] Steven A. Boggs, Akiko Kumada, and Tetsuo Yoshimitsu, "Analytical Approximations for the Rotating Machine End-Turn Field Distribution", IEEE Transactions on Dielectrics and Electrical Insulation, vol. 22, no. 6, Dec. 2015.

[15] Alireza Naeini, Edward. A. Cherney, Shesha H. Jayaram, Saeed Ul Haq, "Effect of Vacuum Pressure Impregnation Process on Electrical Conductivity of Conductive Armor Tape having various Tape Builds and Constructions", in 2017 Electrical Insulation Conference (EIC), Baltimore USA, pp. 451-454, June 2017.

[16] Alireza Naeini, Edward A. Cherney, Shesha H. Jayaram, "Effect of Conductivity on the Thermal and Electrical Properties of the Stress Grading System of an Inverter-Fed Rotating Machine," IEEE Trans. Dielect. Elect. Insul., vol.23, no. 1, pp. 29‑35, Feb. 2019.

[17] F. P. Espino Cortés, PhD thesis, "A Study of Field-Dependent Stress Grading Systems Working under Fast Rise Time Pulses," University of Waterloo, Waterloo, Ontario, Canada, 2006.

[18] Alireza Naeini, Edward A. Cherney, Shesha H. Jayaram, "Effect of Stress Grading Tape Conductivity on the Electric Field Distribution in Stress Grading System of an Inverter-Fed Rotating Machine", in 2018 Electrical Insulation Conference (EIC), San Antonio USA, pp. 14-17, June 2018.

[19] C. Onneby, E. Martensson, U. Gafvert, A. Gustafsson, and L. Palmqvist, "Electrical Properties of Field Grading Materials Influenced by the Silicon Carbide Grain Size," in IEEE 7th International Conference on Solid Dielectrics, pp. 43-45, 2001.

[20] A. Merouchi, E. David, F. Baudoin, D. Mary and I. Fofana, "Optimization of the Electrical Properties of Epoxy-SiC Composites for Stress-Grading Application", in 2015 IEEE Conference on Electrical Insulation and Dielectric Phenomena (CEIDP), pp. 713-716, Oct. 2015.

[21] F.T. Emery, "The Application of Conductive and Stress Grading Tapes to Vacuum Pressure Impregnated, High Voltage Stator Coils," IEEE Electrical Insulation Magazine, vol. 12, Issue 4, pp. 15-22, July/August 1996.

[22] J. C. G. Wheeler, A. M. Gully, A. E. Baker, and F. A. Perrot, "Thermal Performance of Stress Grading Systems for Converter-Fed Motors", IEEE Electrical Insulation Magazine, vol. 23, no. 2, pp. 5 – 11, March/April 2007.

[23] Alireza Naeini, Edward. A. Cherney, and Shesha H. Jayaram, "Effectiveness of Stress Grading System Builds on the Heat Production in a Form-Wound Coil of an Inverter-fed Rotating Machine," Annu. Rep. Conf. Electr. Insul and Dielectric Phenomena (CEIDP), pp. 330-333, Oct. 2018.

[24] Emad Sharifi, Shesha H. Jayaram and Edward A. Cherney, "Analysis of Thermal Stresses in Medium-voltage Motor Coils under Repetitive Fast Pulse and High-frequency Voltages", IEEE Trans. Dielectr. Electr. Insul., vol. 17, no. 5, pp. 1378 – 1384, Oct. 2010.

[25] Alireza Naeini, Edward A. Cherney, and Shesha H. Jayaram, "Modified Stress Grading System for a 13.8 kV Inverter-Fed Rotating Machine," IEEE Trans. Dielect. Elect. Insul., vol. 26, no. 4, pp. 1227‑1234, Aug. 2019.

[26] Jeremy C. G. Wheeler, "Effects of Converter Pulses on the Electrical Insulation in Low and Medium Voltage Motors," Elect. Insul. Mag., vol. 21, pp. 22-29, Mar./Apr. 2005.

[27] R. H. Engelmann and W. H. Middendorf, Handbook of Electric Motors. Marcel and Dekker NY. 1995.

[28] B.R. Andersen, L. Xu, and K.T.G. Wong, "Topologies for VSC transmission," Seventh International Conference on AC-DC Power Transmission, pp. 298-304, Nov. 2001.

[29] Mohan, Undeland and Robbins, Power Electronics: Converters, Applications, and Design, 3rd Edition, John Wiley & Sons, Inc., 2003.

[30] Nguyen Nhat Nam, and Satoshi Matsumoto, "Operation Analysis of Stress Grading System in Inverter-Driven Medium Voltage Motors," 48th International Universities' Power Engineering Conference (UPEC), pp. 1-6, Sep. 2013.

[31] Y. Shakweh, "MV Inverter Stack Topologies," IEE Power Engineering Journal, vol. 15, no. 3, pp 139-149, June 2001.

[32] E.I. Carroll, "Power electronics for very high power applications," Power Engineering Journal, vol. 13, no. 2, pp. 81-87, April 1999.

[33] E. Persson, "Fast switching adjustable speed drives-an overview," Power Engineering Journal, vol. 14, Issue 4, pp. 148-157, Aug. 2000.

[34] H. Zois, L. Apekis, and M. Omastova, "Electrical Properties and Percolation Phenomena in Carbon Black Filled Polymer Composites," in International Symposium on Electrets (ISE), pp. 529-532, Sept.1999.

[35] S. Nakamura, K. Saito, G. Sawa, and K. Kitagawa, "Percolation Threshold of Carbon Black-Polyethylene Composites," Japanese Journal of Applied Physics, vol. 36, no. 8, pp. 5163-5168, 1997.

[36] M.K.W. Stranges, J.E. Hayward, R. Omranipour, and J.H. Dymond, "Comparative Evaluation of Glass Conducting Armour Materials for Form-Wound Stator Coils," in IEEE International Symposium on Electrical Insulation, pp. 216- 221, Sept. 2004.

[37] T. Nakamura, A. Kumada, H. Ikeda, K. Hidaka, S. A. Boggs, Y.Tsuboi and T. Yoshimitsu, "Transient Potential Measurement on Stress Grading under Multi-

level PWM", 2015 Electrical Insulation Conference (EIC), Seattle, Washington, USA, pp. 161-165, June 2015.

[38] A. Kumada, T. Nakamura, H. Ikeda, K. Hidaka, Y. Tsuboi, T. Kisakibaru, and T. Yoshimitsu, "Transient Potential Distribution on Stress Grading System of Rotating Machines under Repetitive Impulse Voltages", 2014 Electrical Insulation Conference, Philadelphia, Pennsylvania, USA, pp. 368-372, June 2014.

[39] Takahiro Umemoto, Takao Tsurimoto, Tomohito Kisakibaru, Takayuki Sakurai, Toshihiro Tsuda and Kazunari Karasawa, "Novel evaluation methods of end-turn stress grading materials for converter fed high voltage rotating machines", 2016 IEEE Conference on Electrical Insulation and Dielectric Phenomena (CEIDP), Toronto, On, Canada, pp. 307-310, Oct. 2016 .

[40] A. Kumada, T. Nakamura, K. Hidaka, Y. Tsuboi and T. Yoshimitsu, "Potential Distribution on the Stress Grading System of High-Voltage Rotating Machines – I. Measuring System", IEEE Transactions on Dielectrics and Electrical Insulation, vol. 22, no. 6, pp. 3163-3169, Dec. 2015.

[41] Fermín P. Espino-Cortés, Tomás I. Asiain-Olivares and Pablo Gómez "Simulation of the Effect of Armor Coating Conductivity on the Stress Grading Coating Performance under PWM Multilevel Waveforms" in 2015 Electrical Insulation Conference (EIC), Washington, USA, pp. 172-175, June 2015.

[42] A. Roberts, "Stress Grading for High Voltage Motor and Generators Coils," IEEE Electrical Insulation Magazine, vol. 11, no. 4, pp. 26-31, July-Aug. 1995.

[43] Emad Sharifi, Shesha H. Jayaram and Edward A. Cherney, "Capacitive Grading of 13.8 kV Form-Wound Motor Coil Ends for Pulse Width Modulated Drive Operation", in Electrical Insulation, 2008 Conference, pp. 632-635, June 2008.

[44] E. Martensson, B. Nettelbled, U. Gafvert, and L. Palmqvist, "Electrical Properties of Field Grading Materials with Silicon Carbide and Carbon Black," in IEEE 6th International Conference on Conduction and Breakdown in Solid Dielectrics, pp. 548-552, June 1998.

[45] B.R. Varlow, K. Li, "Non-linear AC Properties of Filled Resins," IEE Proceedings on Science, Measurement, and Technology, vol. 150, no.2, pp. 75-82, March 2003.

[46] L. S. Schadler, X. Wang, J. K. Nelson and H. Hillborg, "Non-linear Field Grading Materials and Carbon Nanotube Nanocomposites with Controlled Conductivity," Chapter 9, Dielectric Polymer Nanocomposites, Springer US, pp. 259-284, 2010.

[47] Xiao Yang, Jun Hu, and Jinliang He, "Adjusting nonlinear characteristics of ZnO-silicone rubber composites by controlling filler's shape and size," IEEE International Conference on Dielectrics (ICD), pp. 313 – 317, July 2016.

[48] C. Vanga-Bouanga, T.F. Heid, E. David, M. F. Fréchette, S. Savoie, "Tailoring of the Electrical Properties of Silicon Carbide for Field Grading Application," in IEEE Electrical Insulation Conf. , pp.263-266, June 2013.

[49] E. Martensson, U. Gäfvert, and C. Önneby, "Alternate Current Characteristics of SiC Powders," Journal of Applied Physics, vol. 90, no. 6, pp. 2870-2878, 2001.

[50] F.P. Espino-Cortes, E.A. Cherney, and S. Jayaram, "Effectiveness of Stress Grading Coatings on Form Wound Stator Coil Groundwall Insulation Under Fast Rise Time Pulse Voltages," IEEE Transactions on Energy Conversion, vol. 20, no. 4, pp. 844- 851, Dec. 2005.

[51] Lise Donzel, Felix Greuter, and Thomas Christen, "Nonlinear Resistive Electric Field Grading Part 2: Materials and Applications," IEEE Electrical Insulation Magazine, vol. 27, no. 2, pp. 18-29, March/April 2011.

[52] X. Qi, Z. Zheng, and S. Boggs, "Engineering with Nonlinear Dielectrics," IEEE Electrical Insulation Magazine, vol. 20, No. 6, pp. 27-34, 2004.

[53] T. Okamoto, I. Yoshiyuki, M. Kawahara, T. Yamada, and S. Nakamura, "Development of Potential Grading Layer for High Voltage Rotating Machine," in IEEE International Symposium on Electrical Insulation, pp. 210- 215, Sept. 2004.

[54] H. El-Kishky, R. Hebner, and M. Abdel-Salam, "Minimization of Local Field Enhancement Along Stress-Grading Systems of HV Large Rotating Machines," in IEEE Conference on Electrical Insulation and Dielectric Phenomena, pp. 214 – 217, Oct. 2006,.

[55] R. Malamud and I. Cheremisov; "Anti-Corona Protection of the High Voltage Stator Windings and Semi-Conductive Materials for its Realization" in IEEE Electrical Insulation Conference (EIC), pp. 32-35, April 2000.

[56] L. Yingyan, and X. Chuanxiang, "Optimal Design on Anti-corona Coating of High Voltage Generator Coil Ends", in 6th International Conference On Properties and Applications of Dielectric Materials, pp. 967-969, 2000.

[57] L. Shangchun, R. Xiuhua, L. Jingfu, "Optimization of Anti-corona Construction for HV Generators and its Verification Test", in IEEE, Second International Conference on Properties and Applications of Dielectric Materials, pp. 662-666, Sept. 1988.

[58] F. P. Espino-Cortés, P. Gómez and J. D. Betanzos Ramírez "Modeling of Heat Generated on Stress Grading Coatings of Motors Fed by Multilevel Drives" IEEE Transactions on Dielectrics and Electrical Insulation vol. 18, no. 4, pp. 1328 - 1333, Aug. 2011.

[59] F. P. Espino-Cortes, E. A. Cherney and S. H. Jayaram "Impact of Inverter Drives Employing Fast-Switching Devices on Form-Wound AC Machine Stator Coil

Stress Grading" IEEE Electrical Insulation Magazine, vol. 23, no. 1, pp. 16 - 28, January/February 2007.

[60] T. Nakamura, Y. Morita, A. Kumada, H. Ikeda, K. Hidaka, Y. Tsuboi, T. Kisakibaru, T. Sakurai, and K. Karasawa, "Optimal Resistance of Stress Grading System in Converter-fed Rotating Machines," IEEE Electr. Insul. Conf. (EIC), pp. 15-18, Oct. 2016.

[61] Steven A. Boggs, A. Kumada, K. Karasawa, and T. Kisakibaru, "Power Dissipation in Stress Grading as a Function of CAT-SG Interface Topology," Electr. Insul. Conf. (EIC), pp. 294-297, June 2017.

[62] Rolf Schmerling, Frank Jenau, Christian Staubach, and Friedhelm Pohlmann, "Investigations of modified nonlinear electrical materials for   end   corona protection in large rotating machines," in International Universities Power Engineering Conference (UPEC), pp. 1-5, 2012.

[63] Alireza Naeini, Edward A. Cherney, Shesha H. Jayaram, "Temperature and Electric Field under Pulse Voltage along the Stress Grading System of a Form-Wound Coil", in 2019 Electrical Insulation Conference (EIC), Calgary Canada, June 2019.

[64] V. Tucci and M. Vitelli, "On the Effect of Anisotropy in Nonlinear Composite Materials for Stress Grading Applications- A Numerical Study," IEEE Transaction on Dielectrics and Electrical Insulation, vol. 7, no. 3, pp. 378-393, June 2000.

[65] Takahiro Nakamura, Akiko Kumada, Hisatoshi Ikeda, Kunihiko Hidaka, Steven A. Boggs, Yuichi Tsuboi, Tomohito Kisakibaru, Sakurai Takayuki & Tetsuo Yoshimitsu, "Potential distribution on stress grading of inverterfed rotating machines under DC biased voltage", Journal of International Council on Electrical Engineering, vol. 6, no. 1, pp. 36–42, 2016.

[66] L. Engiziano, V. Tucci, C. Petrarca, and M. Vittelli, "A Galerkin Model to Study the Field Distribution in Electrical Components Employing Nonlinear Stress Grading Materials", IEEE Transactions on Dielectrics and Electrical Insulation, vol. 6 , no. 6 , pp 765-773, Dec. 1999.

[67] G. Jiang, J. Kuang, S. Boggs, "Evaluation of High Field Conduction Models of Polymeric Dielectrics" in IEEE Conference on Electrical Insulation and Dielectric Phenomena, pp. 187 – 190, Oct. 2000.

[68] Z. Zheng and S. A. Boggs, "Efficient Solution of Transient Nonlinear Field Problems", in IEEE Conference on Electrical Insulation and Dielectric Phenomena, pp. 130 – 133, Oct. 2002.

[69] S.A Boggs, A. Kumada, and T. Yoshimitsu. "Measurement of stress grading conductivity to 1.6 MV/m and 155 °C and Computation of grading power density

and temperature rise for PWM waveforms" in Proceedings of 2014 International Symposium on Electrical Insulating Materials, pp. 54-56, June 2014.

[70] Standard Test Methods for DC Resistance or Conductance of Insulating Materials, ASTM International D257 – 14, Approved April 1, 2014.

[71] Determination of thermal conductivity and thermal diffusivity-Part 2: Transient plane heat source (hot disc) method, ISO 22007-2:2015, 2015-08.

[72] Operator's Manual, Agilent E4980A, RC meter.

[73] Operator's Manual, Treck Model 341A, Electrostatic Voltmeter.

[74] Operator's Manual, FLIR T650sc, Portable Thermal Imaging Camera.

[75] Standard Test Method for Detection and Measurement of Partial Discharge (Corona) Pulses in Evaluation of Insulation Systems, ASTM D1868, 2007.

[76] Rotating Electrical Machines- Part 27: Off-line Partial Discharge Measurements On the Stator Winding Insulation of Rotating Electrical Machines, IEC/TS 60034-27, Ed. 1.0, 2006.

[77] D. Fabiani, G. C. Montanari, A. Cavallini, and G. Mazzanti, "Relation between space charge accumulation and partial discharge activity in enameled wires under PWM-like voltage waveforms," IEEE Trans. Dielectr. Electr. Insul., vol. 11, no. 3, pp. 393–405, June 2004.

[78] B. Florkowska, J. Roehrich, P. Zydroń, and M. Florkowski, "Measurement and analysis of surface partial discharges at semi-square voltage waveforms," IEEE Trans. Dielectr. Electr. Insul., vol. 18, no. 4, pp. 990–996, Aug. 2011.

[79] Peng Wang, A. Cavallini, G. C. Montanari, and Guangning Wu, "Effect of rise time on PD pulse features under repetitive square wave voltages," IEEE Trans. Dielectr. Electr. Insul., vol. 20, no. 1, pp. 245–254, Feb. 2013.

[80] Sang Bin Lee, Alireza Naeini, Shesha Jayaram, Greg Stone, Mladen Sasic, "Impulse Voltage-based Test Method for Identifying the Stator Insulation Component with PD Activity for Low Voltage AC Motors", in 2019 Electrical Insulation Conference (EIC), Calgary Canada, June 2019.

[81] Y. Luo, G. N. Wu, P. Wang, K. J. Cao, and Y. Cui, "Insulation failure of inter-turn insulation in inverter-fed traction motor," Annu. Rep. - Conf. Electr. Insul. Dielectr. Phenomena, CEIDP, pp. 831–834, Oct. 2012.

[82] M. Hikita et al., "Development of repetitive voltage impulse generator and automatic repetitive PD inception voltage measurement system for testing inverter-fed motor insulation," Annu. Rep. - Conf. Electr. Insul. Dielectr. Phenomena, CEIDP, pp. 145–148, Oct. 2012.

[83] Y. Yu, "High Voltage Square-Wave and SPWM-Wave Generator Design and Application," MACs Thesis, University of Waterloo, Waterloo, Ontario, Canada, 2009.

[84] Yunis A. Cengel and Michael A. Boles, Thermodynamics an engineering approach, sixth edition, McGraw Hill.

[85] High-voltage test techniques – Partial discharge measurements, IEC 60270, Third Edition, 2000-12.

[86] Weijun Yin, Lionel Durantay, Lili Zhang, Saeed Ul Haq, and François Vannay, "End Winding Protections Improvements Helping To Downsize dV/dt Filter For Medium Voltage Machine Fed By NPP Multi-Levels VSI Drive," IEEE 2nd International Conference on Dielectrics (ICD), pp. 1-4, July 2018.

Appendix A: PMW Switching Procedure [29]

For PMW-based inverters, a constant control signal has been compared with a triangular carrier signal to generate the switch control signals. The switching frequency was defined by the carrier signal frequency. The magnitude of the output voltage was controlled and was proportional to the control signal. The information about the fundamental component of the output voltage is modulated in the widths of the output voltage pulses. The demodulation takes place in the output low-pass filter, where the switching harmonics are separated from the fundamental component, or in the inductive load, where the pulsed voltage waveform is transformed into a sinusoidal voltage at the fundamental frequency.

The full-bridge inverter used is composed of two legs, each having two switches and two anti-parallel diodes. The output terminals are formed by the middle of the converter legs, and there is no need for the center-tapped dc voltage source arrangement, unless a neutral point is required. The two switches in each leg receive complementary switching signals to avoid short circuiting of the dc voltage source. Furthermore, due to the finite time that it takes for a switch to turn on and turn off, the turn-on signal of the in-coming switch is delayed behind the turn-off signal of the out-going switch to make sure the ON periods of the two switches in the same leg do not overlap. Figure A-1 shows the schematic of a full bridge inverters.
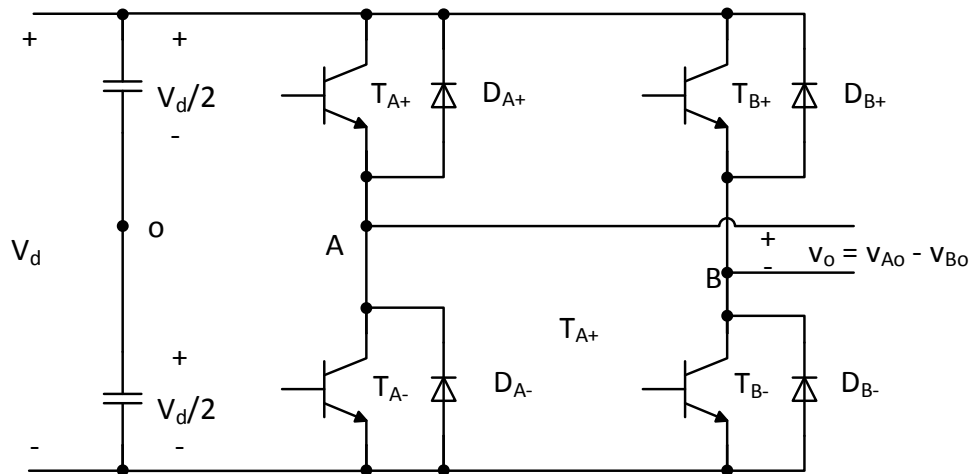

Figure A-1: Schematic of a full bridge inverters.

In bipolar voltage switching, the diagonal switches are treated as a pair and are turned on and off together. A sinusoidal control signal with the same frequency and phase shift angle of the fundamental

component of the desired output voltage is compared with a triangular carrier signal. The intersection points of the two signals define the beginning of the ON and OFF periods of the switches. Figure A-2 shows the control signal and the output signal.
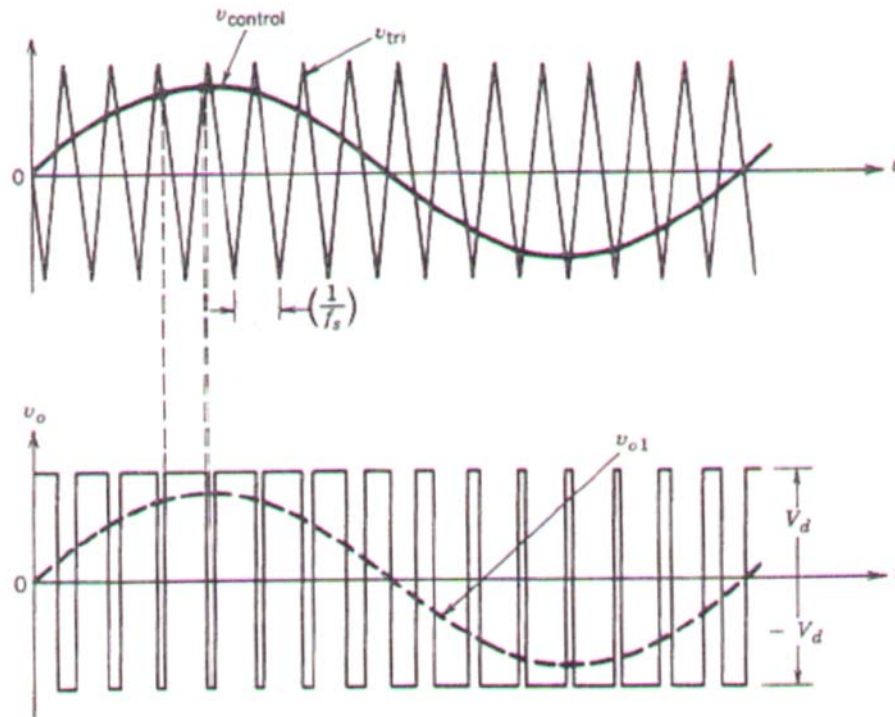

Figure 0-2: Switch control signal and output voltage waveforms.

The common rule of comparison and the resulting output voltages are as follows:

- If the control signal is larger than the carrier signal, T_{A+} and T_{B-} are turned on and T_{B+} and T_{A-} are turned off. This results in $v_{AN} = V_d$ and $v_{BN} = 0$.

- If the control signal is smaller than the carrier signal, T_{A+} and T_{B-} are turned off and T_{B+} and T_{A-} are turned on. This results in $v_{AN} = 0$ and $v_{BN} = V_d$.

The output voltage is $v_o = v_{AB} = v_{AN} - v_{BN}$. This voltage is equal to V_d or $-V_d$ depending on the positions of switches. The term bipolar has been assigned to this method since the output voltage has two possible polarities.